Modeling and Simulation the Impacts of STATCOMs on Distance Protection and Developing a Microgrid Energy Management Scheme for a Pacific Northwest City

A Thesis

Presented in Partial Fulfillment of the Requirements for the

Degree of Master of Science

with a

Major in Electrical Engineering

in the

College of Graduate Studies

University of Idaho

by

Husam Sameer Samkari

Major Professor: Brian K. Johnson, Ph.D.

Committee Members: Herbert Hess, Ph.D.; Ahmed Abdel-Rahim, Ph.D.

Department Administrator: Mohsen Guizani, Ph.D.

June 2016

Authorization to Submit Thesis

This thesis of Husam Sameer Samkari, submitted for the degree of Master of Science with a major in Electrical Engineering and titled "Modeling and Simulation the Impacts of STATCOMs on Distance Protection and Developing a Microgrid Energy Management Scheme for a Pacific Northwest City," has been reviewed in final form. Permission, as indicated by the signatures and dates given below, is now granted to submit final copies to the College of Graduate Studies for approval.

Major Professor: _____ Date: _____
Brian K. Johnson, Ph.D.

Committee Members: _____ Date: _____
Herbert Hess, Ph.D.

_____ Date: _____
Ahmed Abdel-Rahim, Ph.D.

Department Administrator: _____ Date: _____
Mohsen Guizani, Ph.D.

Abstract

This thesis has two research topics. The larger focus of this thesis is the development of a microgrid model as a testbed for control design. However, the first topic studies the impact of a static synchronous compensator (STATCOM) on distance protection in a transmission line. A power system and a STATCOM device are modeled and simulated by using an EMTP-type program. A distance relay model is used to determine the effective impedance seen by the relay with and without the presence of the STATCOM. The results show that the distance relay performance is affected by the fault location relative to the location of the STATCOM. During capacitive current injection by the STATCOM, the simulation results show that the mho relay underreaches for faults applied beyond the STATCOM location on the line.

The second topic is the development of a microgrid energy management scheme for a Pacific Northwest City. An EMTP-type model is used to represent the power system and the control systems of the microgrid. The microgrid model includes hydroelectric generators, a photovoltaic (PV) system, a storage system, and variable loads. Several cases examine the microgrid during both seasonal and hourly variation. Generation and load profiles are compared with a storage system profile in order to characterize the shortage during islanded mode. Simulation results are presented. Suggested solutions and planning considerations are discussed for managing the power and energy inside the microgrid.

Acknowledgements

I would like to start by thanking God for the unlimited and continuous blessings in my life. I sincerely thank my major professor, Dr. Brian Johnson for his guidance and support through my Master's program. His inspirations, suggestions, kindness, and enthusiasm have been invaluable to help me complete my degree.

Also, I'm thankful to Dr. Herbert Hess and Dr. Ahmed Abdel-Rahim for their valuable time, insightful suggestions and questions, which motivated me to improve my thesis.

I am thankful to the utility sponsor, and the team that I worked with for their supports, time, and guidance.

I am also thankful to my fellow students, faculty, and staff of the ECE department who have been part of my Master's Degree completion.

Last but not the least, I would like to thank my family and friends for their sincere prayers, and believing in me throughout my academic life. I would like also to express my sincere gratitude to my dear wife Hala for her supports, help, and kindness.

Table of Contents

List of Figures

List of Tables

Acronyms

αβ – Two Axis Stationary Reference Frame

abc – Positive Sequence Three Phase Stationary Reference Frame

AC – Alternating Current

ATP-EMTP – Alternate Transients Program - Electromagnetic Transients Program

DC – Direct Current

DG – Distributed Generation

DLG – Double Line to Ground

dq – Two Axis Synchronous Direct-Quadrature Reference Frame

DR – Distributed Resources

DS – Distributed Storage

DT – District

DN – Downtown

EMS – Energy Management System

FACTS – Flexible AC Transmission Systems

H1 – Hospital 1

H2 – Hospital 2

H3 – Hospital 3

HYD 1 – Hydroelectric Generators 1

HYD 2 – Hydroelectric Generators 2

HYD 3 – Hydroelectric Generators 3

IEEE – Institute of Electrical and Electronics Engineers

JC – Jail and Courthouse

kV – kilovolt

MVA – Megavolt-Ampere

MVAR – Megavolt-Ampere Reactive

MW – Megawatts

NREL – National Renewable Energy Laboratory

PANW – Pacific Northwest

PCC – Point of Common Coupling

PLL – Phase Locked Loop

PMS – Power Management System

PV – Photovoltaic

SCADA – Supervisory Control and Data Acquisition

SLG – Single Line to Ground

STATCOM – Static Synchronous Compensator

STR – Storage System

USGS – United States Geological Survey

VSC – Voltage Sourced Converter

Chapter 1: Introduction

This chapter presents a brief introduction to this thesis, and defines each chapter. The thesis is divided into two main topics: 1) "Modeling and Simulation the Impacts of STATCOMs on Distance Protection." 2) "Developing a Microgrid Energy Management Scheme for a Pacific Northwest City."

1.1 Impacts of STATCOMs on Distance Protection

The first topic is a study on the impacts of a static synchronous compensator (STATCOM) on transmission line distance protection. An EMTP-type model is developed in order to simulate the power system and a STATCOM device. A simulated distance relay model with supervisory elements is used. The effective impedance seen by the distance relay is investigated and evaluated both with and without the presence of the STATCOM. This topic characterizes the impact of the performance of a STATCOM on distance relay elements and on supervisory elements during a capacitive current injection. The performance of the distance relay is evaluated when faults locations are changed relative to the location of the STATCOM. Chapter 2 addresses this topic and presents study cases and simulation results.

1.2 Forming Microgrids in a Pacific Northwest City

The second topic is a microgrid energy management scheme for a Pacific Northwest City. The study is based on an ongoing research project. At the request of the sponsor, the

name of the city and the sponsor will not be mentioned and, in this thesis, the city will be called PANW City. The purpose of the project is to form a microgrid in part of the city. This thesis provides study on the city's energy resources and the power consumption of the critical loads. Moreover, a model of the microgrid based on real data has been developed using an EMTP-type program. The potential of adding a photovoltaic (PV) system and a storage system is also investigated in order to manage the power and energy inside the microgrid. The objective of the second topic is to study the feasibility of enhancing the PANW city microgrid by adding a PV system, load shedding plans, capacitor banks, and an energy storage system.

This second topic is covered in six chapters starting from Chapter 3. The topic is introduced, along with background in microgrid concepts and microgrid management. Moreover, the chapter reviews basic principles of solar energy generation and technologies. Chapter 4 describes the power system which existed in the PANW city at the time this project started. The chapter analyzes data from the generation resources and critical load profiles of the PANW city. In Chapter 5, a hydroelectric generator model, a PV system model, and a variable load model are discussed. The chapter also provides validation procedures along with some validation results.

Chapter 6 presents and examines simulation results from the microgrid model. The chapter describes results from different case studies and tests. In Chapter 7, planning considerations to form microgrid in the PANW city are characterized. The chapter discusses some of the important considerations relative to loads, generation, and control systems. Chapter 8 briefly summarizes the topic, and provides conclusions, and recommends future work.

Chapter 2: Impacts of STATCOMs on Distance Protection

This chapter is drawn from a paper published at the 2015 North American Power Symposium [1]. It is written by author Husam Samkari with co-authors Mohammed Allehyani and Dr. Brian K. Johnson. The chapter will characterize the impact of a shunt-connected STATCOM on the performance of distance relay elements and on supervisory elements.

2.1. Introduction

Flexible AC transmission systems (FACTS) devices are sometimes used as a solution to allow stable increase in power transfer through existing transmission lines. FACTS devices can be connected in series, shunt, or both. Transmission lines are typically protected by distance protection schemes as either primary or back up protection. FACTS devices can impact the response of protective devices for faults, at least those that are not so close as to cause a FACTS device to go into self-protection mode. This chapter will characterize the impact of the performance of a shunt-connected STATCOM on distance relay elements and on supervisory elements.

A STATCOM is a shunt-connected voltage source converter (VSC) based controller [2]. This application can exchange reactive power with the power system by injecting reactive current to achieve different goals. Some benefits of applying STATCOMs are: increasing the line power transferred, regulating the voltage magnitude and enhancing stability [3]. A STATCOM is capable of supplying or absorbing reactive power to fulfill the desired control [4]. One of the most commonly used control schemes is a controlled DC-

voltage power port where the AC voltage is measured at the point of common coupling (PCC). The DC bus voltage is controlled to obtain the desired operation. The STATCOM is usually magnetically connected to the PCC through a transformer. The DC bus of the VSC is terminated to the DC bus capacitors with no additional source or load on the DC link [2].

Although the presence of a STATCOM could achieve several performance advantages, it also could raise some issues for line protection relays.

Transmission lines – typically 69 kV and higher – are mostly protected by distance relays because of their effectiveness and reliability. Supervisory directional overcurrent elements are used to improve security [4]. Communication aided distance schemes such as permissive underreaching transfer trip (PUTT), direct underreaching transfer trip (DUTT), and directional comparison unblocking (DCUB) schemes are typically used to improve response time. The basic principle of the distance relay is applying Ohm's Law by calculating the apparent impedance seen by the relay. The relay measures the voltage and current and then computes the effective impedance. The effective impedance is compared to the threshold impedance setting. If the calculated impedance is less than the line impedance threshold setting, the relay will send a trip command. The reach point for this element is set according to the line impedance. A minimum two zones are needed where zone 1 is typically set from 70% to 90% of the actual line impedance, and zone 2 is set with time delay to overreach the protected line. Zone 2 is typically set to reach 120% of the line impedance [5]. Most distance relays are represented in an impedance R-X diagram. The relay characteristic can be a circle, which is known as a mho distance element, or it can have a polygon shape, which is known as a quadrilateral distance element. The mho distance element is a widely used element for line protection in North America [6]. In order to

increase reliability, a polarizing reference quantity is needed. The mho element can be self-polarized, taking measurements from the phase from which it measures current. Self polarization has some issues, such as poor fault-resistance coverage and seeing very low voltage for close-in faults in front of or behind the relay. Cross polarization can solve the fault-resistance coverage issue since it uses the phase voltages from other phases, and has a dynamic mho characteristic. The circle of the cross-polarized mho element can expand for forward faults increasing coverage of the line during faults with fault resistance. The memory-polarized element uses stored voltages from a memory filter in order to avoid zero-voltage faults. It also expands the mho characteristic, improving coverage for high fault-resistance forward faults [5]. The major task of the distance relay is to operate when needed and not operate when the protected line is not the one faulted. Distance relays should not trip for out-of-zone faults. However, a distance relay could be affected and missoperate under certain circumstances such as during the presence of a current infeed source.

A shunt-connected STATCOM behaves as a weak infeed source at the transmission line midpoint. The objective of this study is to present the impact of STATCOM on distance protection. An ATP-EMTP model (ATP stands for alternate transients program which is in the EMTP family – Electromagnetic Transients Program) is built to simulate and examine the behavior of the system with and without adding a STATCOM. The system is tested with different fault locations and conditions. The results from the model are analyzed and evaluated to show the impacts of STATCOM on distance protection.

2.2. Protection Issues

Employing a STATCOM on a transmission line could undesirably affect distance relay performance. The presence of the STATCOM may cause a transient trajectory in the measured effective impedance. This transient behavior could result in a delayed operation for the distance relay or multiple pickups and drop offs. As a result, the speed of operation time could be longer. With the presence of the STATCOM in the fault loop, the distance relay could give a wrong fault type selection especially for unsymmetrical faults. The fault resistance (R_f) coverage also could be impacted. The higher the R_f, the bigger is the effective impedance seen by the relay. The infeed current can increase the effective resistance. This increase on the impedance would cause the distance relay to either misoperate or trip in zone 2 for some faults in zone 1 or to fail to pick up some faults in zone 2. Therefore, pilot distance schemes that depend on zone 2 such as PUTT and DUTT would be affected. In addition, the reach accuracy is another concern for a distance relay when we use a STATCOM on transmission lines [7].

Depending on the existence and operating state of a STATCOM on the system, a distance relay may behave differently. A STATCOM could be used to supply or absorb reactive power. For the two cases, the effective impedance is influenced by the STATCOM current injection. In the case of a fault in zone 1 beyond the location of a STATCOM that provides reactive power, relay measurements will result in a larger measured impedance [8]. This larger impedance will cause the relay to underreach and potentially missoperate. If the STATCOM is absorbing reactive power, the measured impedance is going to be lower. Thus, the relay will overreach and operate when it should not [9]-[10]. See Appendix A.4 for more explanation. Similar behavior would result for faults in zone 2 [4]. Using

communication aided schemes can provide better performance. However, it fails to provide reliable operation for all types of faults [7]. This issue could be faced for faults between the relay and the STATCOM location. The results of a study case simulations will demonstrate this particular issue and show how it affects the distance relay decision.

2.3. Study Case

The focus of this study is to show an aspect of the behavior of a distance element when a STATCOM is connected to a transmission line. In order to examine the problem, different scenarios have been studied and compared to a base case for the simulated experiment. The first case has faults before the connected STATCOM (20% of the line out from BUS 1; see Figure 2.1). The second case has faults after the connected STATCOM, (80% from BUS 1). The results from both cases are compared with cases when the STATCOM is not connected (breaker M is open). The power system model is described in Appendix A.1.

Three fault types are applied for each case: single line to ground (SLG), three phase, and double line to ground faults (DLG). Phase A is chosen for SLG faults, and phases B and C for DLG. Zero fault resistance ($R_f = 0$) is assumed for the three fault types.

The power system and the STATCOM models are created and simulated in the ATP-EMTP program as described in Appendix A.2. Then, the three phase voltages and currents, and the zero sequence currents are imported from the ATP-EMTP program to a Mathcad file. The distance relay is modeled in the Mathcad file described in Appendix A.3 to show the behavior and the impact of the STATCOM.

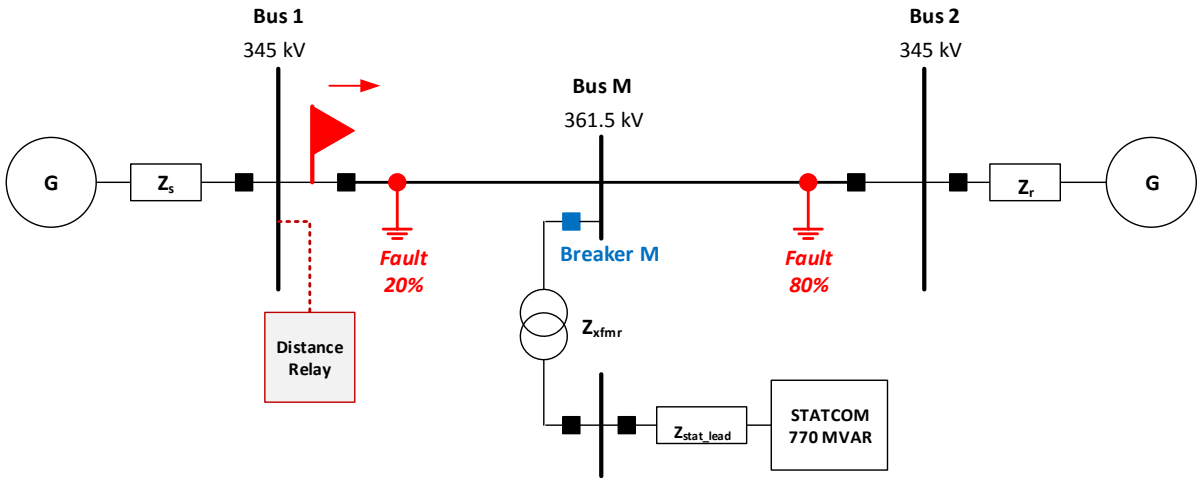

Figure 2.1. Power system diagram with STATCOM

2.3.1. Model Description

In this section, a brief description of the ATP-EMTP and Mathcad models are presented to give an overview of the study case. The models can be divided in three main parts.

1. Power model (ATP-EMTP model)
2. STATCOM model (ATP-EMTP model)
3. Digital filter and distance relay model (Mathcad model)

The following sections describe each model. More detail is provided in Appendix A.

2.3.1.1 Power Model (ATP-EMTP Model)

The model consists of a 345 kV three phase system with two equivalent source impedances and a transmission line (Appendix A provides more details) [10]. As shown in Figure 2.1, the transmission line is between BUS 1 and BUS 2. The transmission line transfers a maximum power of 500 MW without the STATCOM (breaker M is open). The STATCOM is connected to the midpoint of the transmission line through a 1:10 power transformer and bus work. The maximum rating of the STATCOM is ±770 MVAR and 0 MW. The transmission line is able to transfer 530 MW when the STATCOM is connected and operates on its full rating. Different types of faults are applied at 20% of the line and 80% of the line. The voltage and current measurements are imported from BUS 1 with positive current looking in to the transmission line. Then, the imported measurements are used in the distance relay model to calculate the effective impedance.

2.3.1.2 Distance Relay Model (Mathcad Model)

Figure 2.2 shows the steps of processing data starting from the ATP-EMTP simulation results. The imported data is converted from time domain to discrete time. The Mathcad file takes the imported data from the ATP-EMTP and resamples them to 16 samples per cycle as a first step. Then, an averaging low pass filter is applied with a cutoff frequency at 1/2 the sampling frequency. A full cycle cosine filter is applied and combined with virtual sine filter to calculate magnitude and phase of the line to ground voltages, line currents, and zero sequence currents at BUS 1.

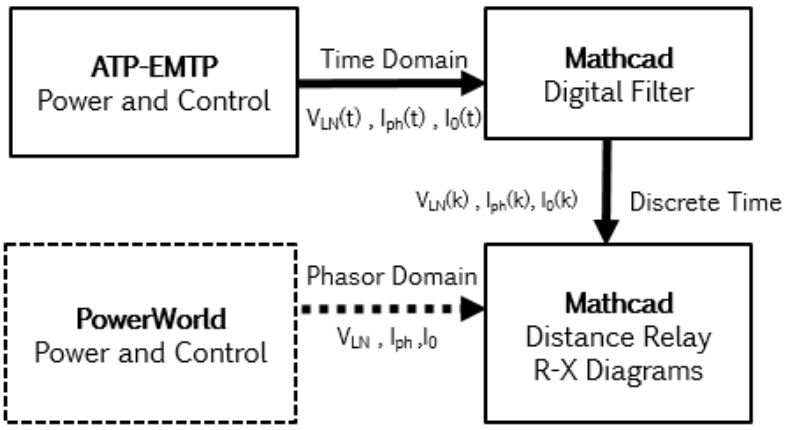

Figure 2.2. Steps of processing data

The next step is taking the phasor-domain measurements and applying them to a mho element (with CTs and VTs before filtering). In this model, the mho element has one zone that reaches 85% of the total line impedance. For simplicity, a self-polarized mho element is assumed since the fault resistance is zero and no close-in faults are applied. The mho element uses both voltage and current measurements from the faulted phase to calculate the effective impedance seen by the relay at BUS 1. An assumption is that the relay has successfully selected the fault type. Since fault resistance is neglected, only two loops of the six standard fault loops are calculated and displayed. For the SLG and the three phase faults, phase A to ground loop is chosen. For the DLG faults, phase C to ground loop is used for demonstration since $R_f = 0$ in this study case. However, other fault loops were examined for validation. The responses of the six fault loops are consistent, so the others are not shown. Equation (2.1) has the equation for the AG fault loop, and equation (2.2) shows the CG fault loop.

$$Z_{AG} = V_{AG} / (I_A + (3*I_0*K_0)) \quad (2.1)$$

Z_{AG}: effective impedance-phase A to ground loop

V_{AG}: phase A line to ground voltage

I_0: zero sequence current

K_0: zero sequence compensation factor

$$Z_{CG} = V_{CG} / (I_A + (3*I_0*K_0)) \quad (2.2)$$

Z_{CG}: effective impedance-phase C to ground loop

V_{CG}: phase C line to ground voltage

Equations (2.1) and (2.2) show how the effective impedance has been calculated. Both equations account for zero sequence impedance effects. The K_0 factor [11] has been calculated from line data by using equation (2.3) where K_0=0.597+0.13i. For this reason, the zero sequence current effect has been calculated and applied for each case. The effective impedance and the digital filter behavior from each case are shown in an impedance plane characteristic. When the effective impedance enters zone 1 (the mho circle), the distance relay will send a trip signal to trip BUS 1 circuit breaker. On the other hand, the relay will not trip when the effective impedance is out of zone 1.

$$K_0 = (Z_0-Z_1)/Z_0 \quad (2.3)$$

Z_0: zero sequence impedance

Z_1: positive sequence impedance

2.3.1.3 STATCOM Model (ATP-EMTP Model)

The STATCOM model has two main parts. The first part is the three phase DC/AC VSC average model. Reference [3] proves that using the VSC average model will give a decent approximation to represent the STATCOM dynamic behavior. The model has two capacitors connected to the DC bus as shown in the diagram in Figure 2.3.

The second part of the model is the STATCOM control system. In this paper, the control system will not be discussed in detail. The main point in the STATCOM control system is to both regulate the DC bus voltage and to maintain the desired AC voltage Vs at the PCC. The desired AC voltage and the DC bus voltage references are assumed constant for this analysis. The measurements from the DC bus are used to regulate the DC bus voltage V_{DC} using a DC-bus voltage controller in order to maintain the specified voltage. The output from the controller will be the reference power set point P_{sref} which is zero in steady-state in the STATCOM case when losses are neglected. In order to regulate the PCC to the desired AC voltage, the voltage measurements have been taken from the PCC, which is at the midpoint of the line in this case. After converting the measurements from the sequence three phase stationary reference frame (abc) to a two axis synchronous direct-quadrature reference frame (dq), the measured direct voltage V_{sd} is compared with the desired voltage V_{td}.

The STATCOM control will try to achieve this desired setpoint voltage and will supply or absorb reactive power to or from the power system to do this. In this study case, the STATCOM is supplying the power system with capacitive current to raise the voltage magnitude at the midpoint of the line.

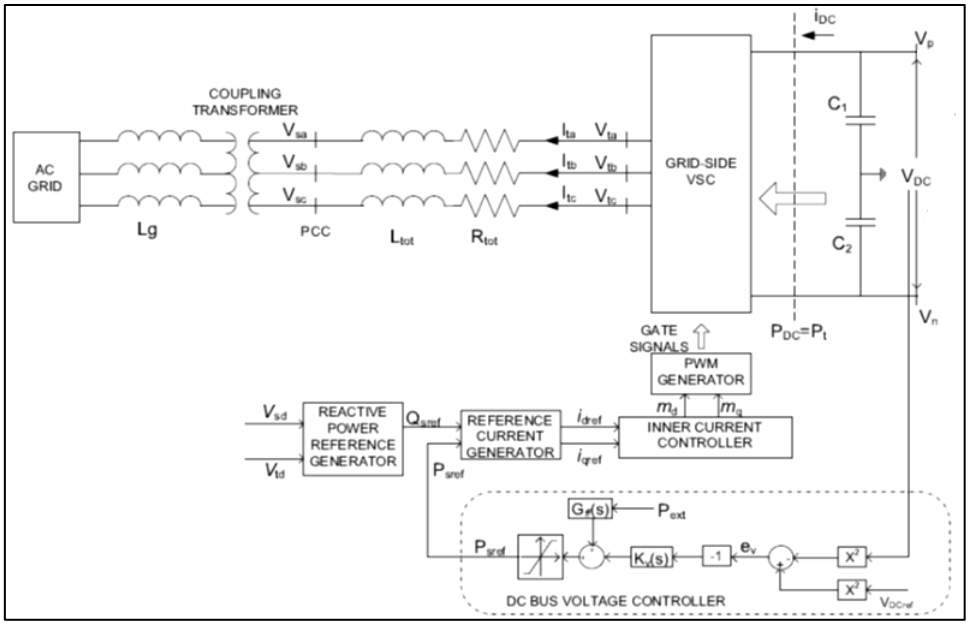

Figure 2.3. Schematic diagram of controlled DC-voltage power port

2.2.3 Model Validation

Since the ATP-EMTP model is a complicated model and consists of power and control parts, a validation process is needed. A Powerworld model is created in order to measure the magnitude and phase voltages, currents and zero sequence currents at BUS 1 for each case for comparison to the ATP results. Powerworld performs phasor solutions, there is no need for using digital filter. Moreover, the model uses an ideal source to represent the STATCOM behavior. The data have been imported from the Powerworld model and used to calculate the effective impedance by using equations (2.1) and (2.2). The results for each case are shown in the same impedance plane that is used to show the effective impedance from the ATP model through the Mathcad model.

2.4. Results

In this section, the distance relay impedances are shown in Figures 2.4, 2.5, 2.6, 2.7, 2.8, and 2.9 in order to state the impact of the STATCOM on the distance relay at BUS 1 for different fault cases. Figures 2.4, 2.5 and 2.6 show the results when the faults are applied at 20% of the line, and Figures 2.7, 2.8 and 2.9 show the results when the faults are applied at 80% of the line. The fault resistance is zero ohms for all cases. Each figure has two impedance planes to compare between the simulation results when the STATCOM is not connected and when the STATCOM is connected. A power flow of 530 MW from Bus 1 to Bus 2 is used, when the STATCOM is connected, to load the system in each case. However, a power flow of 500 MW is used when the STATCOM is not connected.

2.4.1 Faults at Twenty Percent of the Line

2.4.1.1 Single Line to Ground Fault

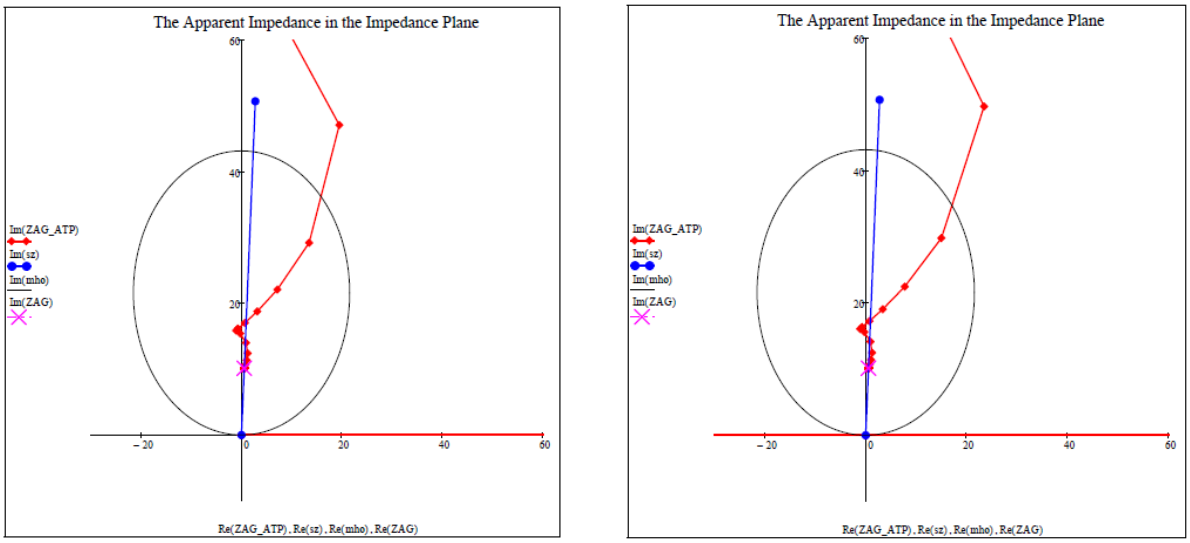

(a) Without STATCOM (b) With STATCOM

Figure 2.4. Apparent impedance seen by the relay for a SLG fault at 20% of the line

2.4.1.2 Double Line to Ground Fault

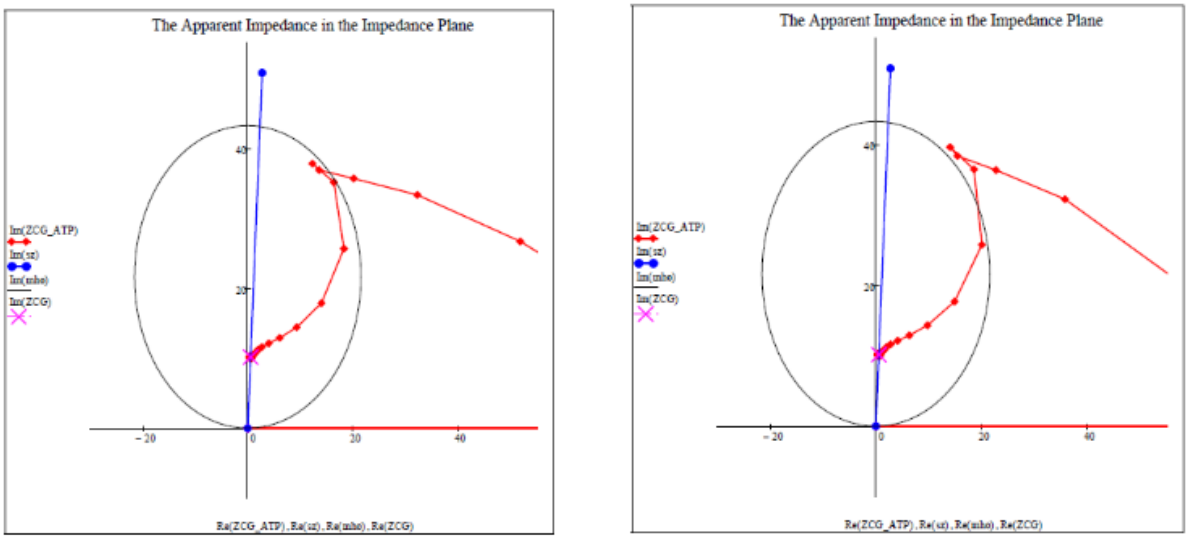

(a) Without STATCOM (b) With STATCOM

Figure 2.5. Apparent impedance seen by the relay for a DLG fault at 20% of the line

2.4.1.3 Three Phase Fault

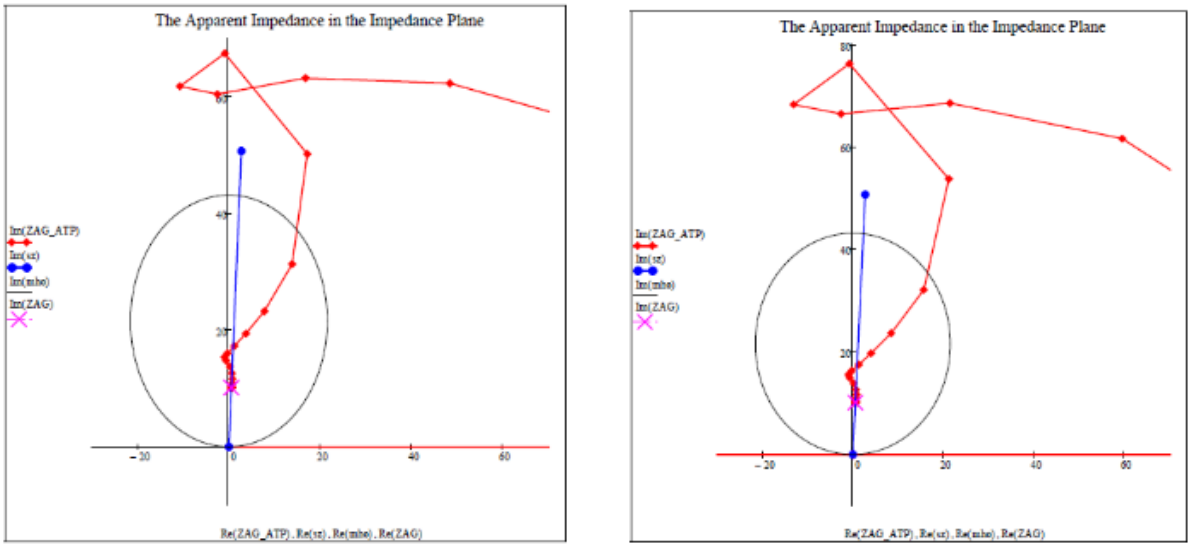

(a) Without STATCOM (b) With STATCOM

Figure 2.6. Apparent impedance seen by the relay for a three phase fault at 20%

2.4.2 Faults at Eighty Percent of the Line

2.4.2.1 Single Line to Ground Fault

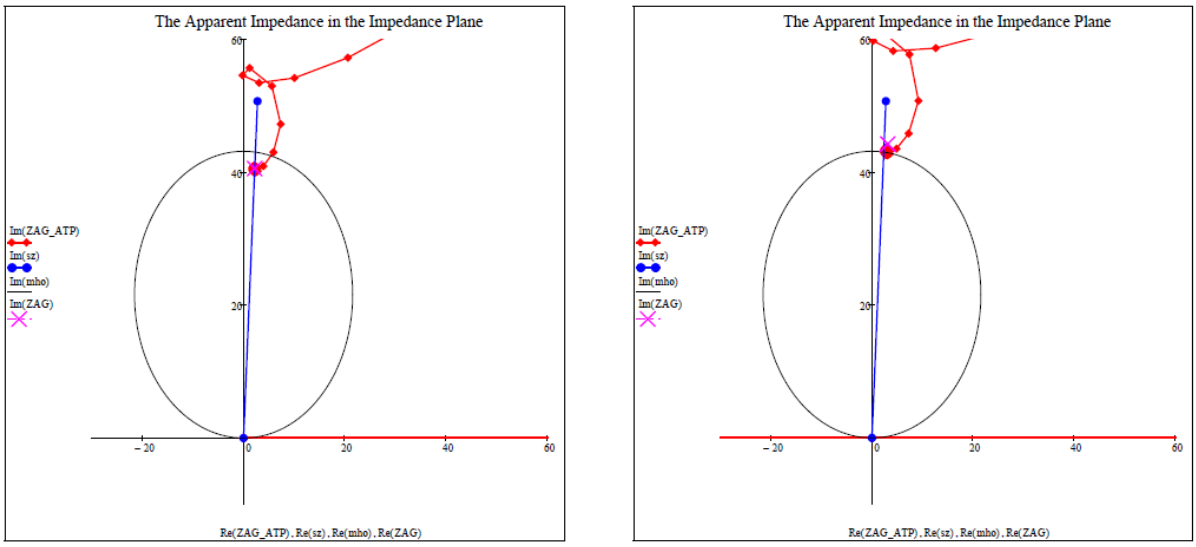

(a) Without STATCOM (b) With STATCOM

Figure 2.7. Apparent impedance seen by the relay for a SLG fault at 80% of the line

2.4.2.2 Double Line to Ground Fault

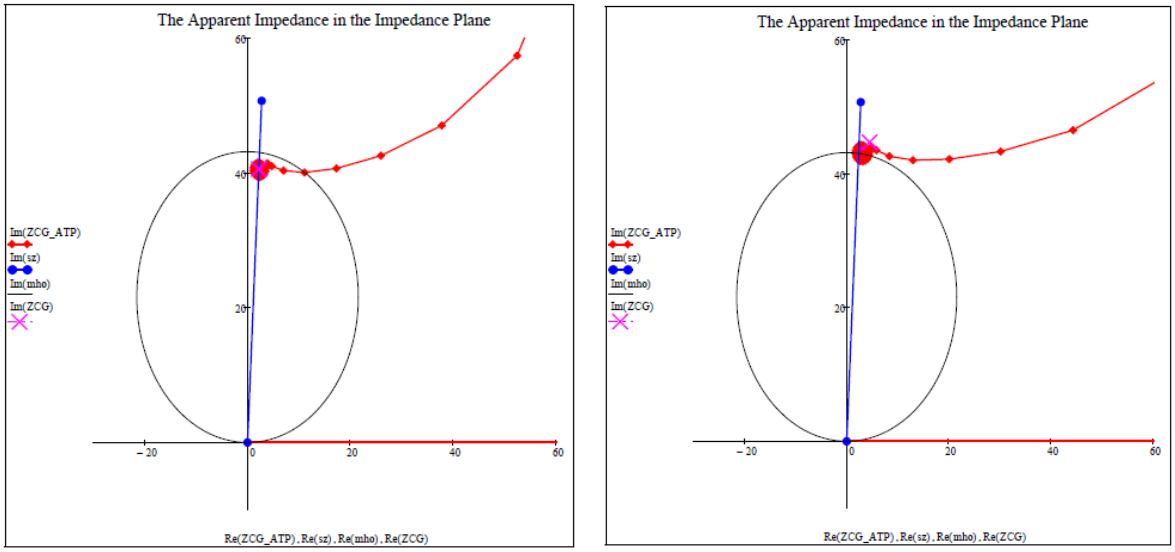

(a) Without STATCOM (b) With STATCOM

Figure 2.8. Apparent impedance seen by the relay for a DLG fault at 80% of the line

2.4.2.3 Three Phase Fault

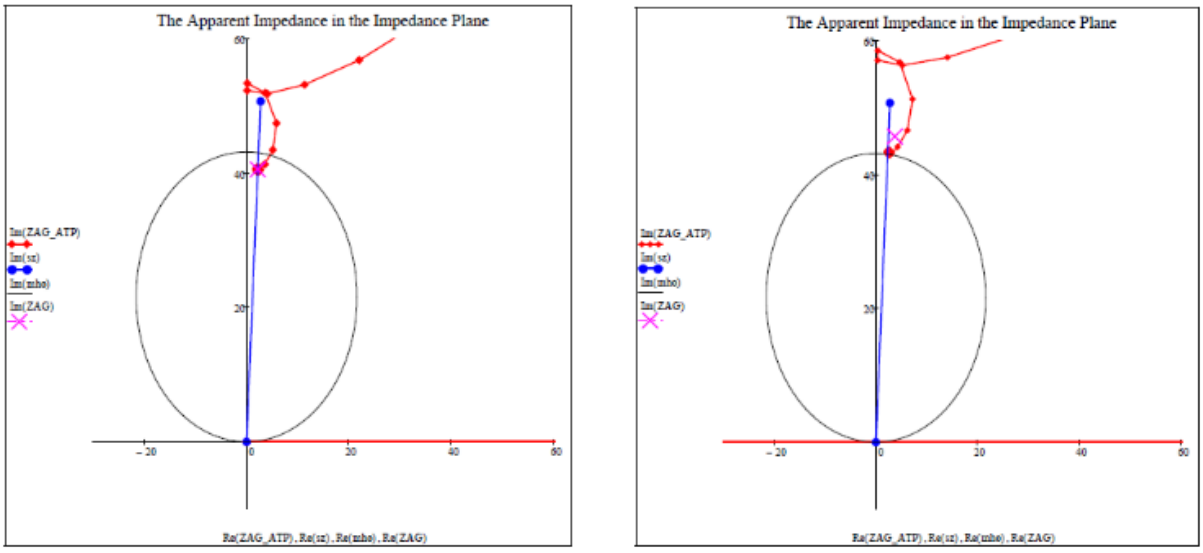

(a) Without STATCOM (b) With STATCOM

Figure 2.9. Apparent impedance seen by the relay for a three phase fault at 80%

2.4.3 Evaluation of Results

The key results are summarized as:

- The distance relay will underreach when the faults applied at 80% of the line (STATCOM is connected) as shown in Figures 2.7 (b), 2.8 (b), and 2.9 (b). The reasons are:
    - The voltage support provided by the STATCOM is between the fault location and the distance relay in this case.
    - The fault currents measured by the distance relay are reduced.
    - The effective impedance calculated by the distance relay is increased.
- There is no significant effect on the distance relay when the faults applied at 20% of the line (STATCOM is connected) as shown in Figures 2.4 (b), 2.5 (b), and 2.6 (b).
    - There is no supported voltage since the STATCOM is not between the fault location and the distance relay.
    - The measured current by the distance relay is not significantly affected.
- Both ATP-EMTP simulation and steady state fault current calculated from Powerworld simulation show similar results (red dots are from the ATP-EMTP model, and pink crosses are measured from the Powerworld model).
- The supervisory element will be effected as well. The minimum fault current is changed since the presence STATCOM will reduce the fault current seen by the relay for faults at 80%.
- The supervisory element will not be significantly affected for faults at 20%.

2.5 Potential Solutions

One approach for solving the distance relay issue is using an adaptive offset for the measured impedance. A solution is proposed in [10] to overcome the underreaching and overreaching problem for STATCOMs and static VAR compensators (SVC). The basic function of this method is removing the STATCOM-associated impedance based on synchrophasor current measurements from the STATCOM outputs that causes the problem from the relay measured impedance. In other words, the relay effective impedance is going to be the impedance seen by the relay to the fault location minus the STATCOM impedance (the error impedance).

2.6 Conclusions and Future Work

This paper presents a focused study on a power system transmission line protection challenge that involves a STATCOM at a line's midpoint. Simulation results reveal the impacts of the STATCOM depends on the fault location relative to the STACOM. When the fault happens before the STATCOM location, the distance relay is able to successfully detect the fault, and therefore will give the right decision. However, if the fault occurs after the STATCOM location, the relay could misoperate. The resulting maloperation is due to the relay underreach (at the case of STATCOM injecting capacitive reactive current).

Some interesting cases were beyond paper's scope such as testing a phase to phase faults and using phase to phase elements. Variable fault resistance and different power flow directions are need to be examined to evaluate the impacts of STATCOMs. The case when STATCOM absorbs reactive power is also an important study.

Chapter 3: Background Relative to Microgrids

This chapter provides background on current research on microgrid concepts and their management, additionally presenting a brief introduction to pertinent parts of the Institute of Electrical and Electronics Engineers (IEEE) Standards 1547 and 2030. Application of solar energy generation and voltage source converters to power systems are also reviewed in this chapter.

3.1. Microgrid System

Microgrid systems, as the U.S. Department of Energy explains, are a localized power and control grid which can be connected and disconnected from the traditional power system [12]. Microgrids can continue work while the main power system is down, which can strengthen grid resilience and mitigate grid outages. Microgrids support the use of local renewable sources of energy such as solar and wind to serve local loads. As a result, energy losses in transmission and distribution systems are reduced, producing a flexible and efficient electric grid [12]. Microgrids "can be thought of as a controlled cell of the power system" [13]. Each cell has its own generation sources, storage system, control system, and load demand.

3.1.1. Microgrid Concepts

Microgrids are designed to operate completely independent from the power system where necessary. In this case, the microgrid system is in "islanded mode." Microgrid

systems also operate in parallel with the power system when they are grid connected. This operation is called “non-islanded mode” or “connected mode.” For islanded and non-islanded modes, load demand has to be maintained, and the local power system controlled. Connections and disconnections are achieved through one or more interconnection switches at the PCC. PCCs are typically located at the distribution feeder breakers in substations (Figure 3.1).

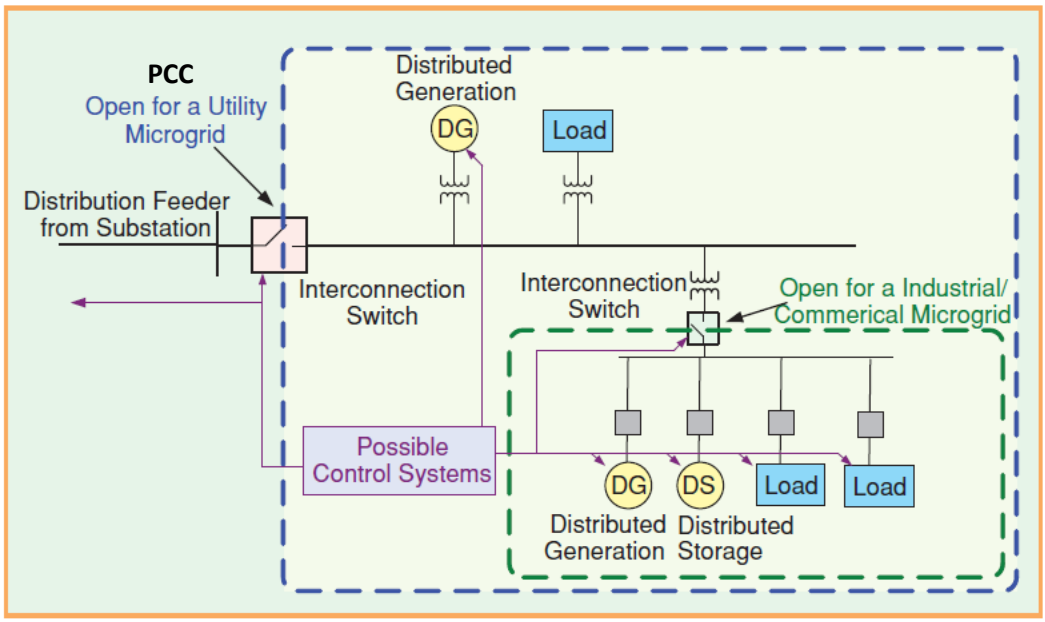

Figure 3.1. Microgrid main components [14]

The distributed generation (DG) and distributed storage (DS) are located near the loads. The term distributed resources (DR) is used for both DGs and DSs. A microgrid’s main components are shown in Figure 3.1. Microgrids can include:

- DG
- DS

- Control system
- Loads
- Interconnection switches

DGs can be any type of small generation resources such as small hydroelectric units, PV systems, gas turbines or microturbines to name a few. DGs are the only power generation sources available during islanded mode. Since many microgrids have renewable energy resources with variable availability, DSs can be used to manage the energy inside the microgrid with exception of larger hydroelectric. Most renewable energy generation resources have variable output power [14].

DSs are sized depending on the need to match load and generation with both peak power transfer and total energy stored considered in sizing the DS.

Reference [14] mentions some of the benefits of having DSs:

- Enabling DG units to run at a constant and stable output, despite variable load profiles
- Providing ride-through capability when there are dynamic variations of primary energy sources such as those of sun, wind, and hydropower sources
- Enabling renewable resource DGs to operate as a dispatchable unit

DSs are often considered to be critical when renewable energy generation resources are used. Despite the high cost of DSs, they can solve most renewable resources issues. For example, PV systems depend on solar irradiation. When the output of the PV systems are reduced unpredictably because of variable clouds, DS systems can support the PV systems to overcome this shortage and supply the load.

Controlling voltage, frequency, and balancing active and reactive power are the goals for operating microgrids. Dispatchable units (for example, diesel generators) can be fully controlled. On the other hand, nondispatchable units are usually operated to extract the maximum possible power from a resource (for example, PV systems). For example, DC-to-AC power converters are used for DSs and PV systems have peak power tracking algorithms. AC-to-AC or AC-DC-AC power converters also are used for some types of wind turbines [15]. For controlling loads' demand response schemes, or in the worst case, load shedding with breaker schemes are used.

Reference [16] has an overview of some of real-world microgrids. Here is a list of some of the microgrids which exist in North America at the time of this writing:

- The Consortium for Electric Reliability Technology Solution (CERTS) Microgrid at the Dolan Technology Center's Walnut Test Site
- Mad River Microgrid - by Northern Power Systems (NPS)
- The British Columbia Hydro Boston Bar

3.1.2. Microgrid Management

Control and operation of microgrids can be significantly different than for traditional power systems. Microgrids may use more renewable energy resources which are electronically coupled, and possibly storage systems [17]. For these reasons and more, power and energy management approaches are important factors for forming microgrids. Reference [17] discusses existing microgrid controls and power/energy management strategies. Fast responses of a power management system (PMS) and an energy management

system (EMS) are recommended since microgrids with renewables often will include multiple small DGs with electronically coupled sources and have no dominant stiff source.

PMS and EMS can be thought of as the decision makers that manage the microgrid based on forecasting and real-time data. Figure 3.2 shows the function of a real-time PMS/EMS. The PMS/EMS receives weather forecast-based predictions and present data from variable sources and loads, and collects information from the electricity market when grid connected (however, the PANW city does not have an electricity market at a level relevant for microgrids; as a result, the PANW PMS/EMS may not use information from an electricity market). The output from the real-time power/energy management is to be able to control utility power level, DER level, and load level. For example, during high load demand, the PMS/EMS can increase the set point of the power at DGs and DSs, or can apply a planned demand response or load shedding scheme. The decision depends on many factors such as the availability of the DGs and DSs, and the forecasting data.

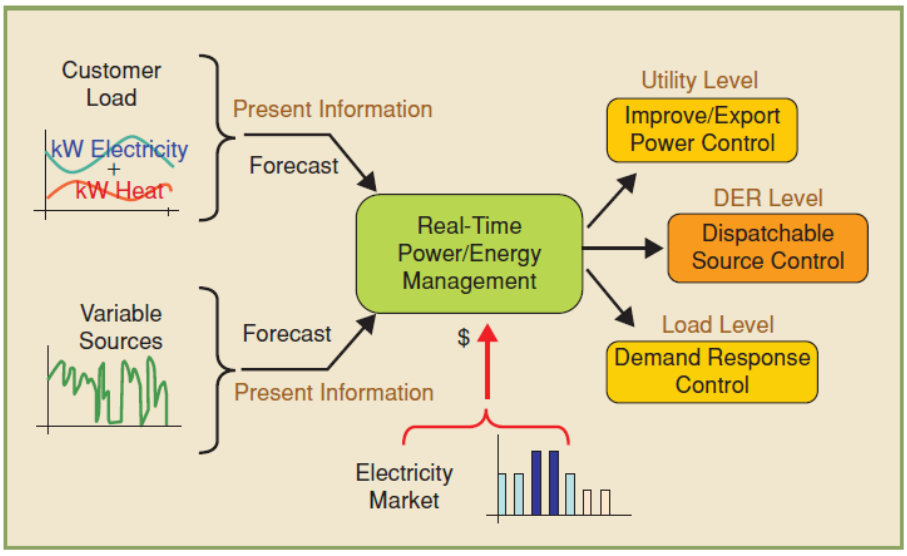

Figure 3.2. The role of real-time PMS/EMS [17]

3.1.3. IEEE Standards 1547 and 2030

IEEE Standard 1547-2003 (Amendment 1, 2014) [18] discusses technical requirements for interconnecting distributed resources with the main electric power grid. Additional standards activities are designated under the IEEE 1547-2003 series of standards [18]:

- 1547.1: Test procedures for interconnecting DRs with electric power systems [19]
- 1547.2: Application guide for IEEE Standard 1547 [20]
- 1547.3: Guide for monitoring, information exchange, and control of DRs interconnected with power Systems [21]
- 1547.4: Guide for design, operation, and integration of DRs - islanded systems [22]
- 1547.6: Interconnecting distributed resources with power systems distribution secondary networks [23]
- 1547.7: Guide for conducting distribution impact studies for DRs [24]
- 1547.8 (draft): Supplemental support for implementation strategies for expanded use of IEEE Standard 1547 (only a draft - not available at the time of this writing)

Standard 1547.4 suggests important tests to be examined in order to operate microgrids, such as:

- Response to abnormal voltage and frequency
- Synchronization
- Unintentional islanding
- Limitation of DC injection
- Harmonics [22]

Moreover, IEEE Standard 1547 advises ranges for abnormal voltages and frequencies. The acceptable range for the voltage on feeder is between 88% and 110%, and the acceptable range of the frequency is between 59.3-60.5 Hz. IEEE Standard 1547 has the potential to be used in federal legislation, and is used by some utilities "in formulating technical requirements for interconnection agreements for distributed generators powering the electric grid" [18]. Some states have created their own interconnection standards.

Additionally, IEEE Standard 2030-2011 provides guidance for smart grid interoperability of energy technology and information technology operation with the electric power system (EPS), end-use applications, and loads [25]. Additional standards activities are designated under the IEEE 2030-2011 series of standards:

- IEEE Std 2030.1-2015 Standard Technical Specifications of a DC Quick Charger for Use with Electric Vehicles [26]
- IEEE Std 2030.2-2015: Guide for the Interoperability of Energy Storage Systems Integrated with the Electric Power Infrastructure [27]
- IEEE Std 2030.3 (Draft): Standard for Test Procedures for Electric Energy Storage Equipment and Systems for Electric Power Systems Applications (only a draft - not available at the time of this writing)

3.2. Photovoltaic Systems

PV systems have many advantages over other renewable sources, which make them a favorite choice for hypothetical microgrids. However, PV systems may eventually be used in many microgrids. PV systems are environmentally friendly when one ignores fabrication

and disposal. The panels are noiseless, and produce no carbon dioxide (CO2) emissions once they are in operation. The systems also have no moving parts, unlike most other generators, and can be installed almost anywhere (for example, on the ground or on the top of buildings) [28]. Since the panels generate power at a low voltage level, the system can easily to be applied at the distribution level. This is can be beneficial to microgrid systems since generating power at the distribution level is one of the microgrid's goals.

3.2.1. Solar Energy Generation Principles

PV systems convert solar energy to electric energy, and consist of several solar panels and other electrical components such as inverters, and meters (Figure 3.3). The output of the panels is a DC current. However, because most of the electrical applications need AC current, PV systems are more likely to have one collector inverter or several inverters in order to convert the DC current to an AC current (Section 3.2.2. presents one of the commonly used classes of inverters).

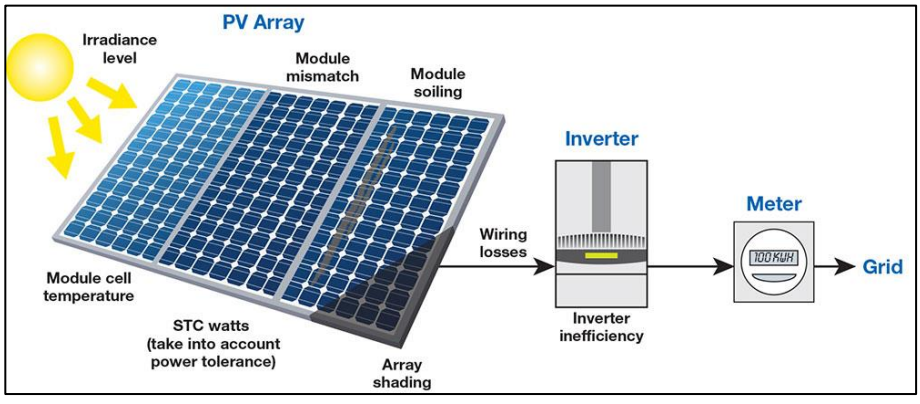

Figure 3.3. Diagram of a PV system showing sources of losses as well as energy flowing

[29]

PV systems have variable output power because they depend on the level of solar irradiation. PV systems generate electricity during daylight, and produce zero real power during night. Additionally, the panels are effected by weather conditions. For example, on a cloudy day the output voltage of the panels will drop. As a result, the rated power of the system cannot be drawn all the time. Even the angle of the sun will affect the output power. For example, in places which the sun angle varies between winter and summer, the panels' position should be changed to face the sun in each season, and the panel rotated over the course of a day to maximize output.

PV systems can be considered predictable sources on broader time scales. As an example, a four year study which took place in Germany showed evidence for how PV systems are predictable. The study was conducted from 2005 to 2008, and with the goal of measuring and calculating the monthly average output power for each year (Figure 3.4). In the study, the average output power over the course of a month did not change much over the four years. This can be useful advantage from the point of view of managing microgrid systems, as it allows for estimating the output power from the PV systems and performing feasibility studies for microgrids. However, the PV systems are not as predictable on short time scales in some types of weather conditions. As a result, effective short time solar forecasting is needed. Reference [30] discusses many solar forecasting techniques (such as sky imagers, satellite imaging, numerical weather prediction, and ensemble forecasting).

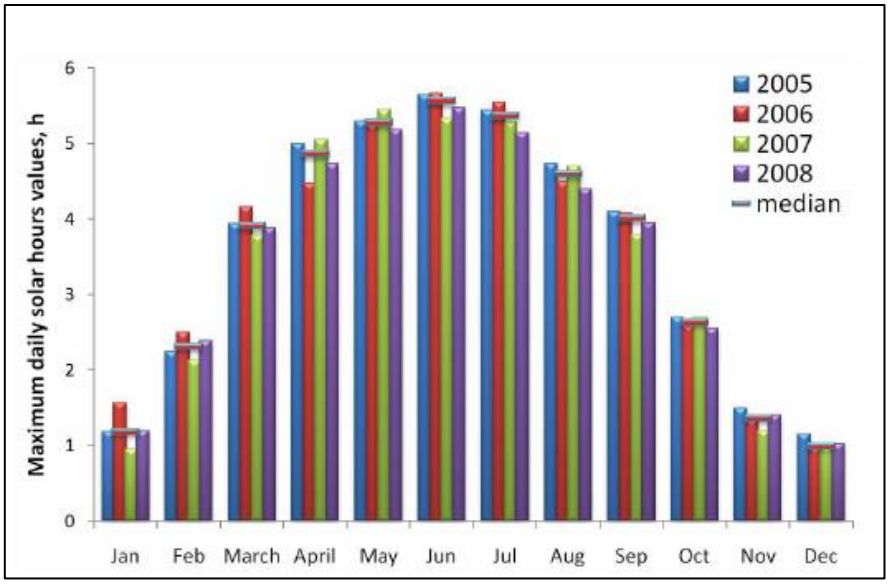

Figure 3.4. Result from a four year study about PV systems prediction [28]

3.2.2. Voltage Source Converter

Two level VSCs are the most commonly used power-electronic converters for all but highest power rated applications. For PV systems, the average power flows from the DC to the AC side, and the converter that does this conversion is called inverter. A three phase two level inverter consists of six fully controllable and unidirectional switches. The switches are semiconductor devices such as insulated-gate bipolar transistors (IGBT) or integrated gate-commutated thyristors (IGCT) [3]. The PV system is connected to the DC system, and the power grid or microgrid is connected to the AC system as labelled in Figure 3.5. Smaller PV units use single phase inverters.

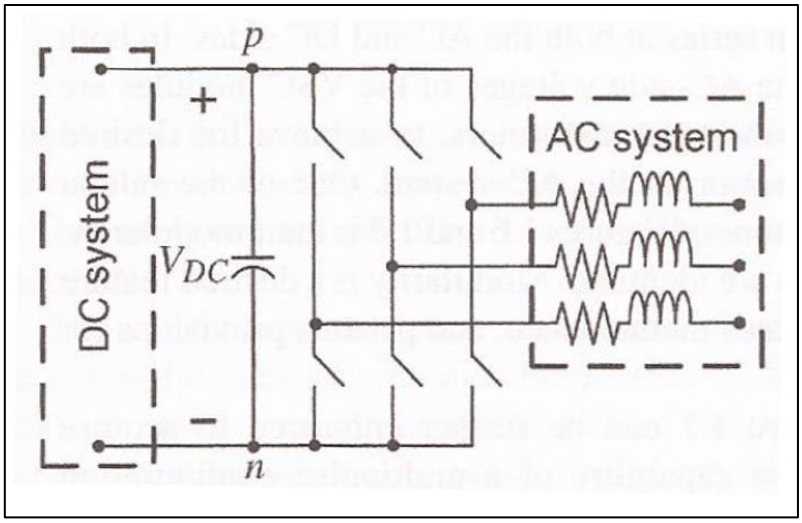

Figure 3.5. A three phase two level VSC with idealized switching devices [3]

For modeling purposes, VSCs can be represented as an averaged model as discussed in Chapter 2. The model can precisely represent the steady state and dynamic behavior of VSCs. The model neglects the high frequency behavior from the switching since it is not an important consideration in many power systems cases. As reference [3] states “for dynamic analysis and control design purposes, knowledge about the high-frequency details of variables is often not necessary.” Chapter 5 explains the three phase VSC averaged model in detail for the system at hand, along with a typical control system.

Chapter 4: Power Grid in a Pacific Northwest City and Data Analysis

This chapter provides information and data about the existing power grid in a medium-sized city in a Pacific Northwest state that is the object of study for a microgrid project. The chapter discusses the generation resources, along with the transmission lines, distribution systems, and critical loads that will be included in the microgrid. Information and field data for different components of the system will be analyzed and shown.

4.1. Power Grid Description:

The PANW city part of a vast power grid which contains different levels of voltages and types of transmission lines. The local area has different generation resources such as hydroelectric and PV, and the city is connected to the Western Electricity Coordinating Council (WECC) transmission network. The city utility generates, transmits, and distributes electricity to residential, commercial, and industrial customers. In this thesis, only the parts of the power grid relevant to the proposed microgrid are described and modeled.

The city has a variety critical loads with different levels of priority. According to the project sponsor, one of the high priority critical loads in the city is the jail and courthouse. Additionally, there are several hospitals which are considered medium priority critical loads since they have their own backup generators. The sponsor has also suggested including part of one commercial district and part of the downtown in the microgrid. Most of the city's critical loads have their peaks during summer, and by analyzing a daily profile, the loads tend to have their peaks around noon. Moreover, each load has its own load profile and maximum demand which, in the end, is what the generation in the microgrid should supply.

Lower priority loads will be shed during microgrid operation to ensure the highest priority loads are supplied.

The city has two hydroelectric generators located such that they can supply the microgrid. The two hydroelectric generators available output varies according to the flow in the downtown river. For example, the river has a high level of water discharge in spring; however the water discharge is very low during the late summer. In addition, there are some small PV systems distributed within the city area. The PV systems provide peak daily production in the summer, whereas in the winter they have their lowest production. Based on these observations there are different generation and load profiles, with different behaviors at different times of the year. These different profiles can affect power losses and voltage profiles at buses and transmission lines.

The city has 115 kV transmission lines, along with 13.2 kV, 4.16 kV, and 0.48 kV distribution systems in the area considered for the microgrid. For study and modeling purposes, and in order to form a microgrid, 18 transformers, 3 transmission lines, and 16 buses are included in the model. This configuration matches that of the existing system. The two hydroelectric generators are connected to the 115 kV bus through a step up transformer. There is some distance between the hydroelectric generators and the critical loads which the city utility would like to supply. The transmission lines and distribution systems will be discussed in more detail in Chapter 5. The following sections discuss generation resources over the course of the year based on historical data along with critical load profiles. Data analysis will be performed to create actionable information.

4.2. Generation Resources

4.2.1 Hydro Generation

The two hydroelectric generators are located on the downtown river as shown in Figure 4.1. The river is controlled with six dams. Most of the dams operate in a "run-of-the-river" mode. Two of the dams, Dam 1 and Dam 2 are located at the city downtown, and these are used to form the PANW city microgrid. Dam 1 is associated with hydroelectric generator 1 (HYD 1), and downstream Dam 2 is associated with hydroelectric generator 2 (HYD 2). The rating of HYD 1 is 10 MVA, and the rating of HYD 2 is 15 MVA. Dam 3 is located farther upstream, and it is associated with hydroelectric generator 3 (HYD 3). The rating of HYD 3 is 17.7 MVA. HYD 3 can be treated as a backup generator or as a sub-microgrid for the PANW city's main microgrid in some situations. However the transmission path to reach it from the microgrid is more complex. For this reason it is considered an extra dam in the analysis. Each hydroelectric generator has its own annual generation profile; however since all of them are located on the same river, they tend to have similar profiles.

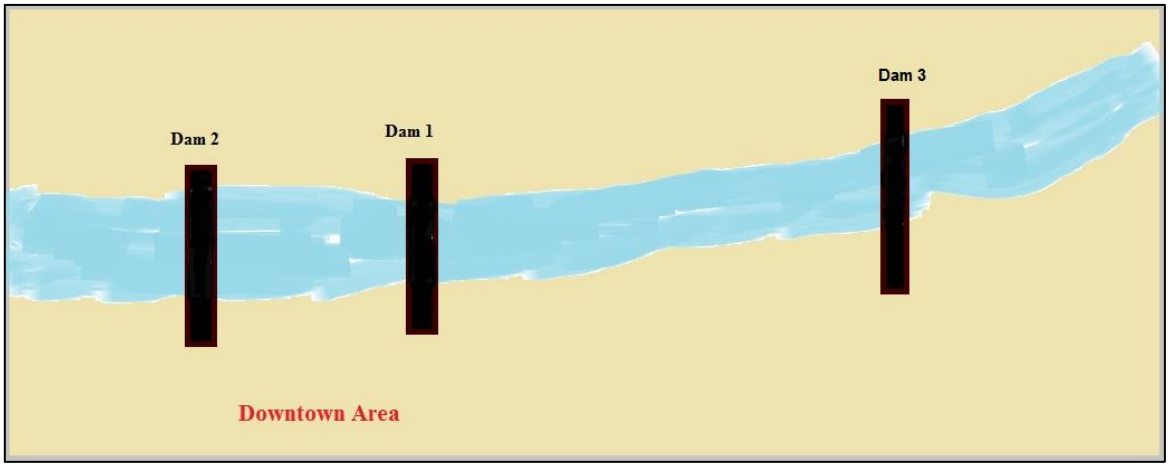

Figure 4.1. Relative locations of Dam 1, Dam 2, and Dam 3

The United States Geological Survey (USGS) has been recording the discharge of the river for 123 years. This data gives a clear image of the river behavior and the amount of power that can be generated. The data has been obtained from the USGS website and analyzed using MATLAB [31]. Figure 4.2 shows the monthly mean discharge in cubic feet per second. The mean is calculated from 1892 to 2015. The diagram clearly shows that the river has a mean average flow of more than 1.5 cubic feet per second from March until May, which can be considered as the peak of the river discharge. Moreover, July, August, September, and October are where the lowest discharge appears.

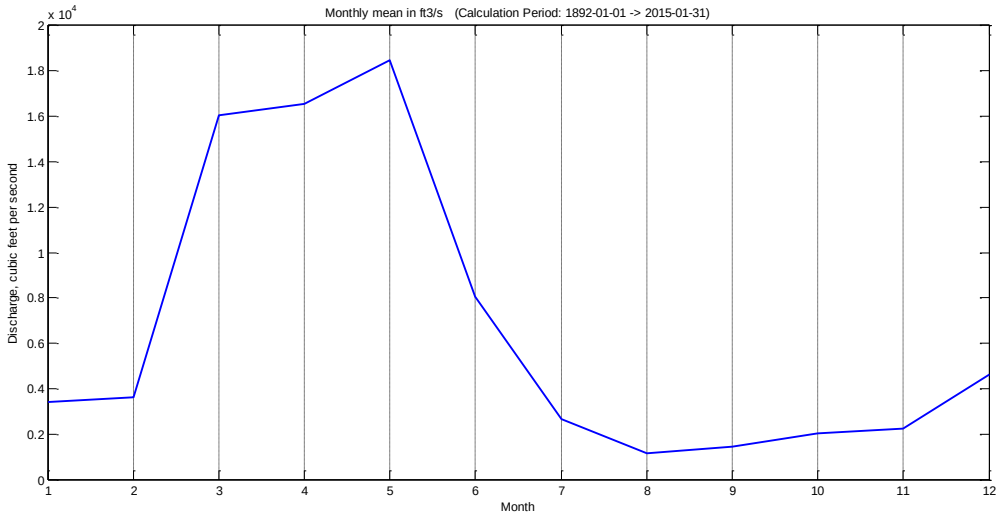

Figure 4.2. The monthly mean discharge of the river in ft^3/sec averaged over 123 years

In order to give an accurate image, the mean of each month of each year for the last 33 years has been analyzed and is shown in Figure 4.3. The flows in winter and spring vary significantly, but summer flows are more consistent. This variation in spring and winter can affect the seasonal prediction. Spring and winter can have the highest water discharge, but this is not necessarily the case for every year. As a result, this variation has to be considered

in the microgrid energy management scheme (as will be discussed later). In addition, USGS provides daily mean data for more accurate information. Figure 4.4 shows the daily mean averaged over the last 33 years. As mentioned above, generally spring has the highest discharge, whereas summer has the lowest. Since the two hydroelectric generators are located on the same river, their output power will vary according to the river discharge with respect to the generator max and min ratings among other ways.

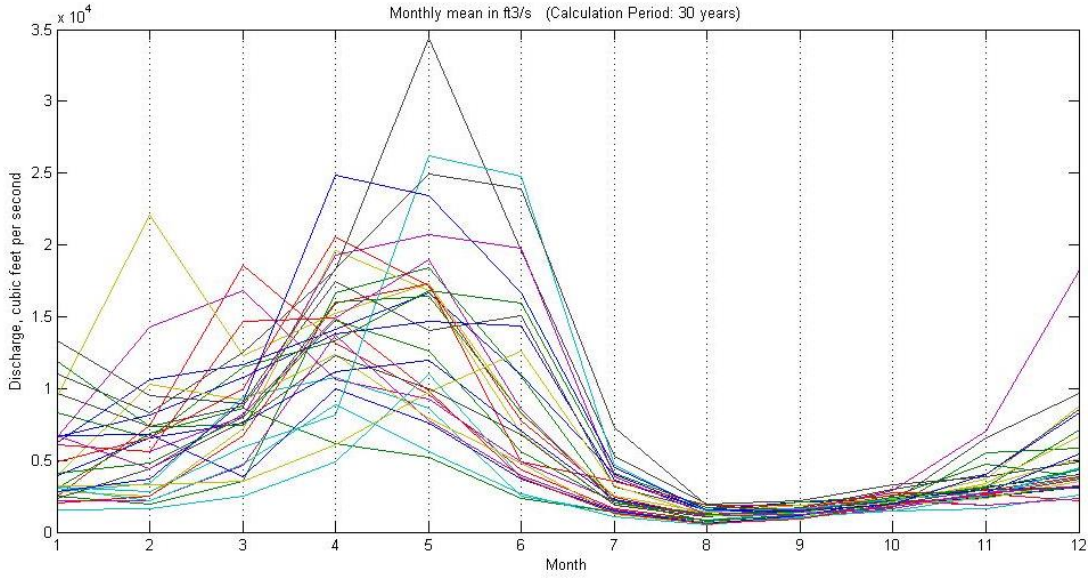

Figure 4.3. The monthly mean discharge of the river in ft^3/sec for 33 years

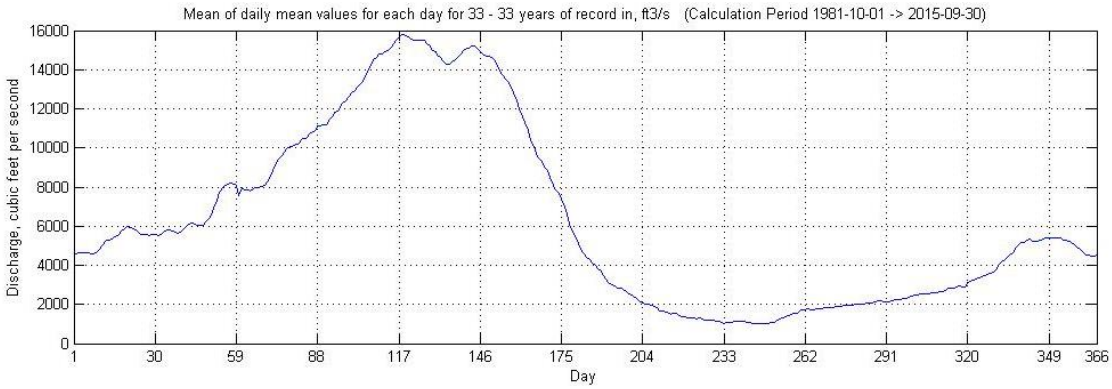

Figure 4.4. The daily mean discharge of the river in ft^3/sec averaged over 33 years

4.2.2 Solar Generation

The PANW city has a number of existing PV panels that are distributed around the area. In order to have detailed information about the PV production, solar irradiation data has been collected and analyzed. This solar irradiation data has been obtained from the National Renewable Energy Laboratory (NREL) website [32].

According to the NREL data, the city is considered one of the cities with the highest solar insolation in that state. The city is exposed to an estimated monthly average daily total solar irradiation between 4.5 – 5.0 kWh/m^2/day, averaged from hourly estimates over 8 years. The data was created using the SUNY Satellite Solar Radiation Model (Perez, et.al., 2002). Check reference [32] for more information about how NREL measures the solar irradiation. NREL uses three main types of measurements to estimate the kilowatt hour per square meter per day:

- Average Direct Normal Irradiance (DNI): "The insolation values represent the resource available to concentrating systems that track the sun throughout the day" [32]
- Average Global Horizontal Irradiance (GHI): "The insolation values represent the global horizontal resource - the geometric sum of direct normal and diffuse irradiance components, representing total energy available on a planar surface" [32]
- Average Tilt at Latitude (LATILT): "The insolation values represent the resource available to fixed flat plate system tilted towards the equator at an angle equal to the latitude" [32]

Figure 4.5 shows the monthly average and annual average daily total solar in kWh/ m^2/day for the three types of measurements (average over a 12 year period). As can be seen, the three types of measurements are similar to each other. The differences among the three measurement types are not important to the issues at hand. GHI is assumed. Additionally, the solar irradiation at the PANW city is above the annual average for six months starting from April due to clearer skies. The peak is approximately 7 – 8 kWh/ m^2/day July. During winter time the solar irradiation is at the lowest point of 1 – 2 kWh/ m^2/day. This variation on the solar irradiation will significantly affect the generation output of the PV system.

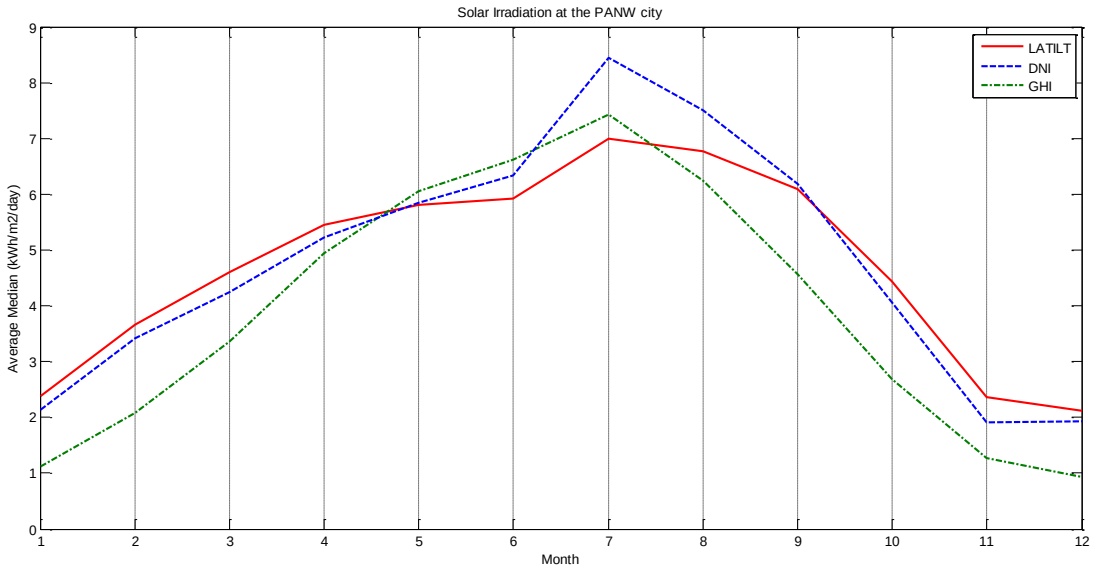

Figure 4.5. The monthly average and annual average daily total solar in kWh/ m^2/day

For purpose of this study, hourly data regarding solar irradiation were obtained and analyzed. NREL recorded the solar irradiation every 30 min for every day of each year. The data shown in Figure 4.6 was collected in 2014 based on the GHI method. The figure shows the daily variation over the year. The peak of each day represents the highest solar irradiation at that day; whereas, no solar irradiation occurs during the night time of each day.

Figure 4.7 describes an example of four days in four different months. The figure shows the first days of January, April, July, and October of 2014. As can be seen, each day has a different profile depending on the number of daylight hours and amount of solar irradiation. It is clear that the month of July has the highest peak and the largest number of daylight hours. In contrast, January has the lowest peak and the lowest number of daylight hours. The shapes of January and October are also probably showing clouds.

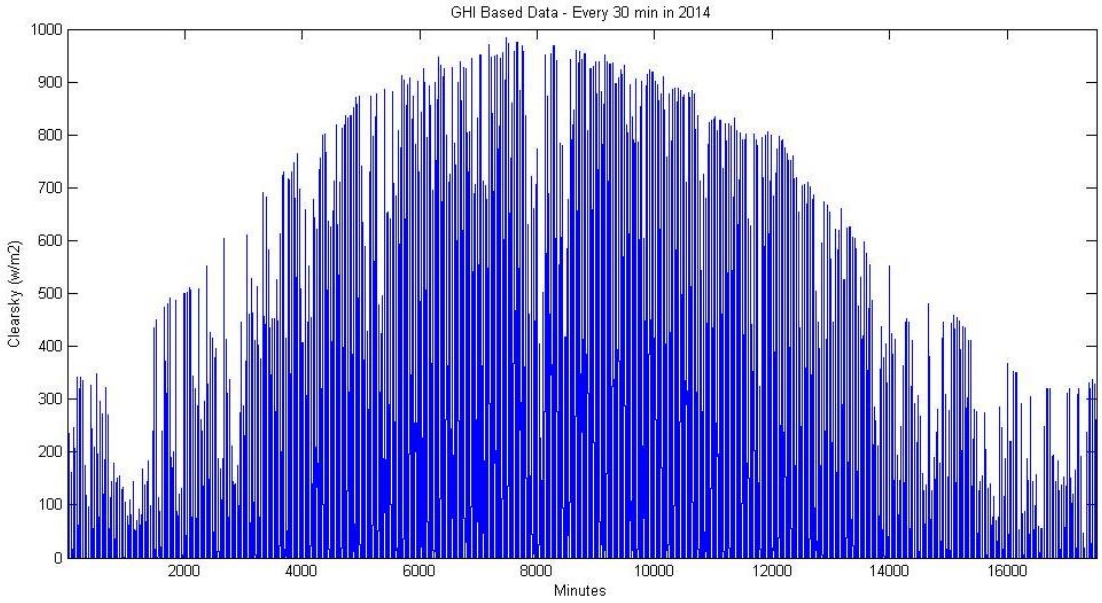

Figure 4.6. The solar irradiation every 30 min in 2014 based on GHI method

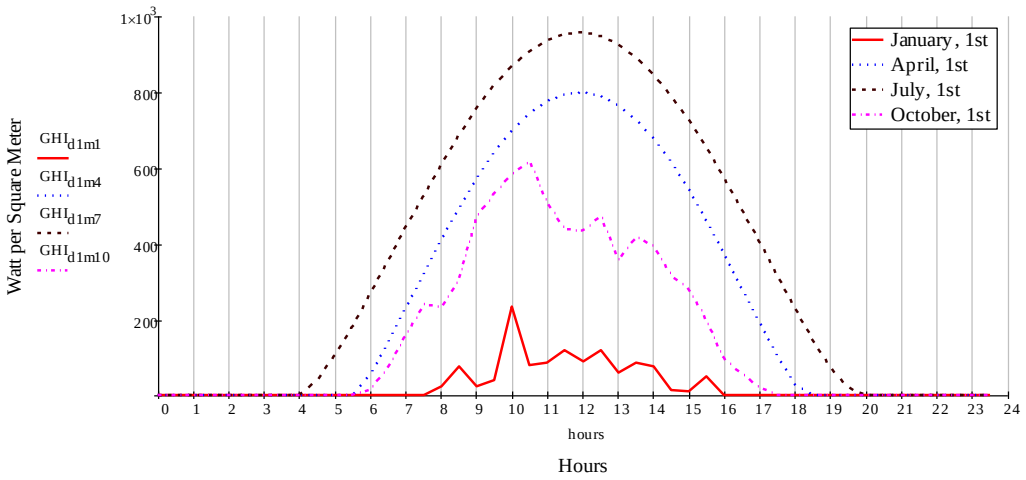

Figure 4.7. Solar irradiation in the first day of January, April, July, and October 2014

4.3 Daily Profile for the Critical Loads

Load profiles have different behavior when compared to the generation profiles. Load profiles can be divided into two general types based on analysis of the data: residential and commercial. Each type has its own unique characteristics that are variable through the seasons. The city aggregate loads tend to be proportional to the temperature of the weather. Seeking more accuracy, real load measurements have been obtained from the project sponsor from one of the aforementioned critical loads (Figure 4.8). The figure shows real power and reactive power from one of the medium priority critical loads (Hospital 1). The data has been recorded hourly for a year starting in January (8760 hours). The annual peak starts from the middle of June (approximately at 4,000 hours in Figure 4.11) and runs to the middle of October (approximately at 6,000 hours). The variation of reactive power is much smaller than that of real power. The load has a lagging power factor most the time, but sometimes it has a leading power factor in March and April.

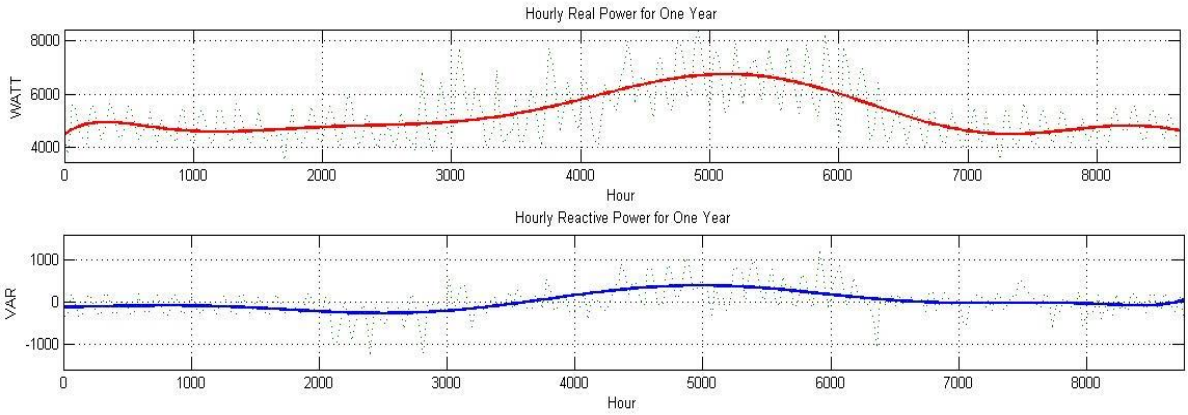

Figure 4.8. Hourly real and reactive load power for one year (Hospital 1)

In order to clearly visualize daily characteristics of the critical load on an hourly basis, three days in July have been chosen for further analysis. The daily peak of the real and reactive power is around the noon as shown in Figure 4.9. Both the real and the reactive power seem to have similar characteristics. Hourly characteristics are considered since the microgrid has limited generation and storage. In addition, it is important to consider the rate of rise and fall of the load. For these reasons, real data is used in this thesis.

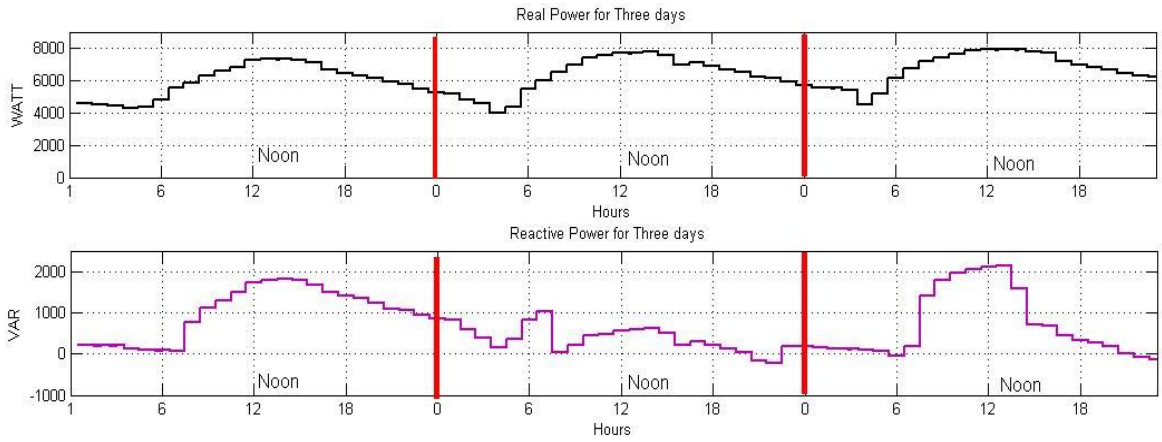

Figure 4.9. Real and reactive power for three days in July

4.4. Production vs. Consumption

In order to visualize the amount of energy production compared to energy consumption, generation and load profiles are put in the same figure. Figure 4.10 shows all of the data in a normalized perspective since they have different units. Each data set is divided by its respective peak; as a result, the peak of each normalized characteristic is 1 pu. As shown in the figure, the water discharge peak is around May, the solar irradiation peak is around July, and the critical load peak is around August. Figure 4.10 is simply for visualization purposes. However, the figure demonstrates the value in adding PV generation to the microgrid to offset the combination of the timing of annual peak load and minimum water flow. Figure 4.11 shows the same normalized data but with water and solar are combined. It can be observed that the PV system can help to balance the energy, but not offset the load peak completely unless a large amount is installed. Other DERs should be used to improve the microgrid system, such as storage systems. Chapter 5 describes how the data is used and modeled, with Chapter 6 discusses the results from using the models.

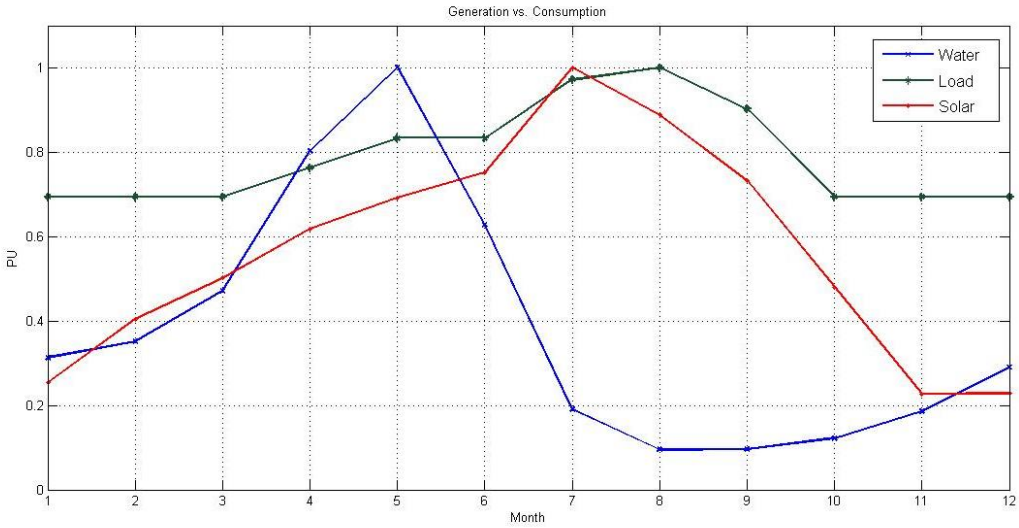

Figure 4.10. Energy production of water and solar compared to the amount of power consumption in pu

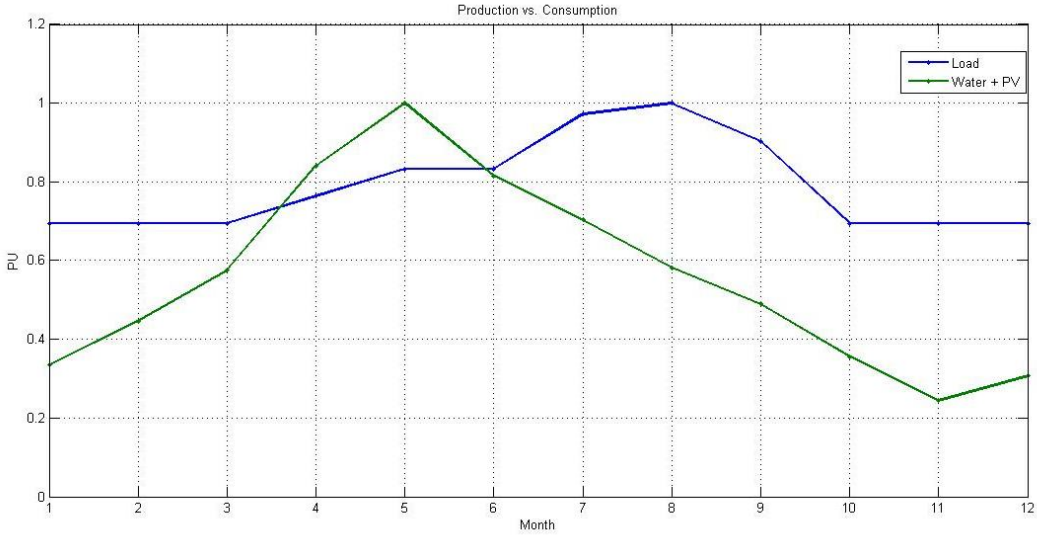

Figure 4.11. Energy production compared to the amount of power consumption in pu

Chapter 5: Modeling and Validation

This chapter discusses the PANW city microgrid model in detail along with the model objective. The ATP-EMTP program is used for modeling both the power and control systems. A Powerworld model and some analytical calculations are applied in order to validate the ATP-EMTP models. This chapter demonstrates the power system model, hydroelectric generators model, PV systems model, and variable loads model.

5.1. Model Description

The ATP-EMTP program has many features, such as the ability to change the input data in each time step. Even nonlinear inputs can be used in order to test the system and obtain nonlinear outputs. This feature allows dynamic field data to be included into the model to obtain more accurate results.

In order to build a reasonable model, field data is obtained and analyzed. Figure 5.1 summarizes the procedures used for analyzing the data and then modeling the PANW city microgrid. As a first step, hydro generation data is obtained from the existing hydroelectric units. Using real measurements, the approximate real and reactive power ranges are chosen. The same steps are made for the critical loads. For PV systems, the solar irradiation data for the PANW city area is obtained and converted to real AC power by using the PVWatts Calculator - an NREL online program that helps to estimate the energy production and cost of energy of grid-connected PV [33]. The calculator is using an hour-by-hour simulation over a period of one year in order to calculate the PV system real power output.

The next step is importing the data to the ATP-EMTP program. Transient Analysis of Control Systems (TACS) device 56, which is a nonlinear lookup table, inserts dynamic field data into to the program by distributing it over a specified number of time steps in the simulation. Every component, utilizing field data inputs will have an instance of device 56 connected to its control system. Then, the control systems are connected to the power system for regulation and monitoring. The power system parameters have been collected from the existing grid models in the sponsor's database, and are converted from per unit to the units Henries, Farads, and Ohms respectively.

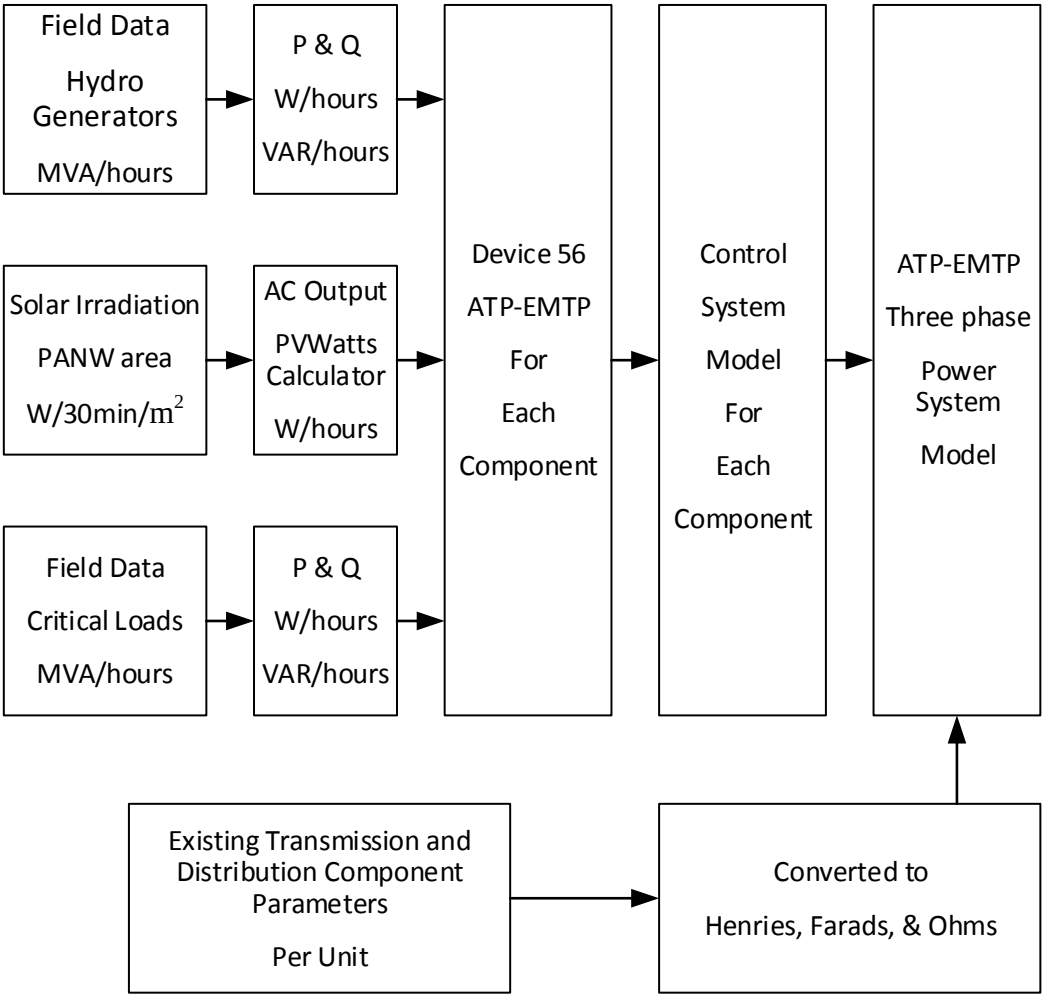

Figure 5.1. The procedures for using the data and modeling the PANW microgrid

5.2. Model Objective

The focus in this microgrid model is to represent the dynamics of the microgrid system in different seasons and different times over a month and day. The result can lead to benefits such as:

- A plan for each season and hour, and selection for appropriate forecasting schemes
- A plan for suitable load shedding schemes
- A tool for studying the potential of adding other generation to the microgrid
- Performing studies for sizing storage systems
- A study of the benefits of creating a second microgrid using HYD 3

Figure 5.2 illustrates the main components of the PANW microgrid. As was stated earlier, HYD 1, HYD 2, HYD 3, plus the transmission and distribution systems are part of the existing power system. The PV and storage systems are added as well. The charge and discharge of the storage system is monitored in order to obtain an energy shortage profile for the microgrid during islanded mode. The critical loads are connected to the distribution systems and then through the three transmission lines. The critical loads are divided into high priority, medium priority, and low priority. The high priority load includes the jail and courthouse, medium priority are three hospitals, and the low priority loads are the downtown 1 and university district 1 loads. The following sections explain each microgrid component in detail.

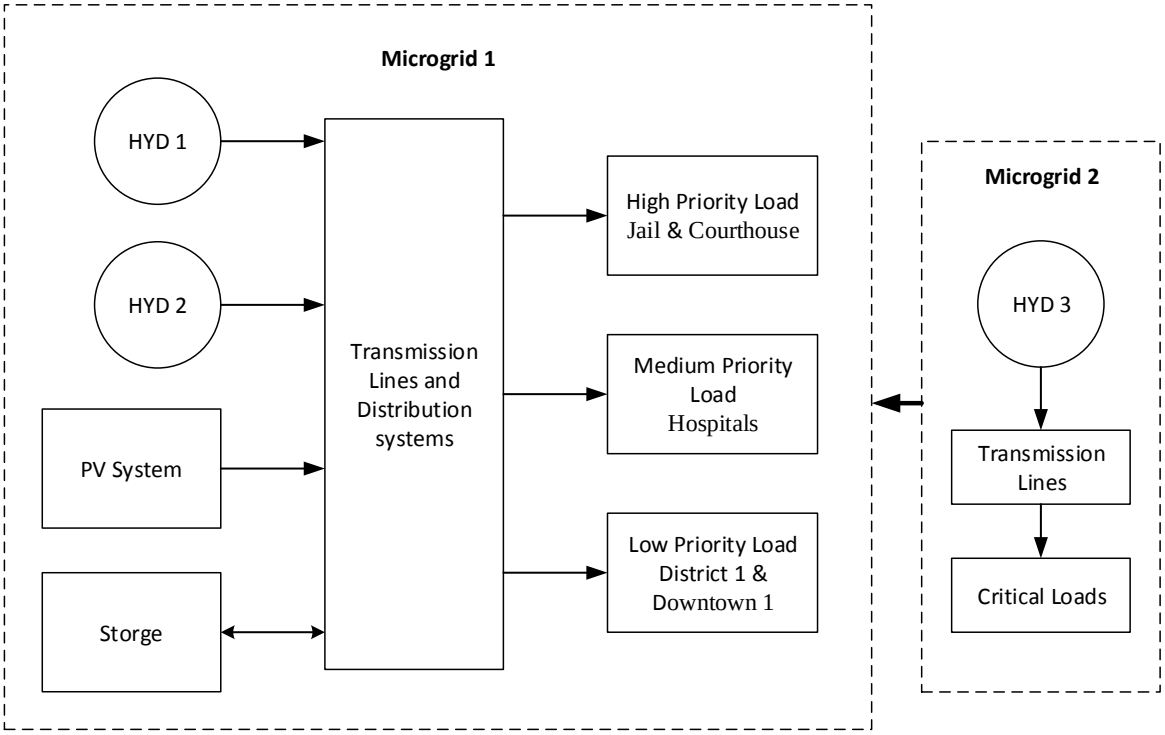

Figure 5.2. Main components of the PANW Microgrid 1 and Microgrid 2 Models

5.3. Power System Model

The model is divided into two microgrids. The PANW city microgrid 1 has three transmission lines, 17 transformers, and 16 main buses. Figure 5.3 shows a simplified one-line diagram of the PANW city microgrid 1 ATP-EMTP model and microgrid 2, while Appendix B includes the full microgrid model. Microgrid 2 will not be discussed further in this thesis.

The 115 kV transmission lines are modeled as three phase RLC coupled pi-equivalents. The distribution feeders are modeled as coupled RL three phase lines, and have three voltage levels: 0.48 kV, 4.16 kV, and 13.2 kV. The 4.16 kV is unique for the HYD 1

unit. HYD 2, PV, and the storage systems are connected at 13.2 kV. Also, the Downtown 1 critical load is connected at 13.2 kV since it is represented as a lumped load. The other loads are connected at 0.48 kV. Each power transformer is modeled as a three phase saturable transformer with two windings - each winding has series winding resistance and leakage reactance. Circuit breakers are represented as ideal switches. In addition, the system has several existing transmission level capacitor banks. Some additional capacitor banks will be proposed for addition later. The transmission level capacitor banks are disconnected since they raise the system voltage to undesired levels during islanded mode (total of the transmission level banks is 90 MVAR). The PV system and storage, hydroelectric generators, and critical loads models along with their control systems are discussed in the following sections.

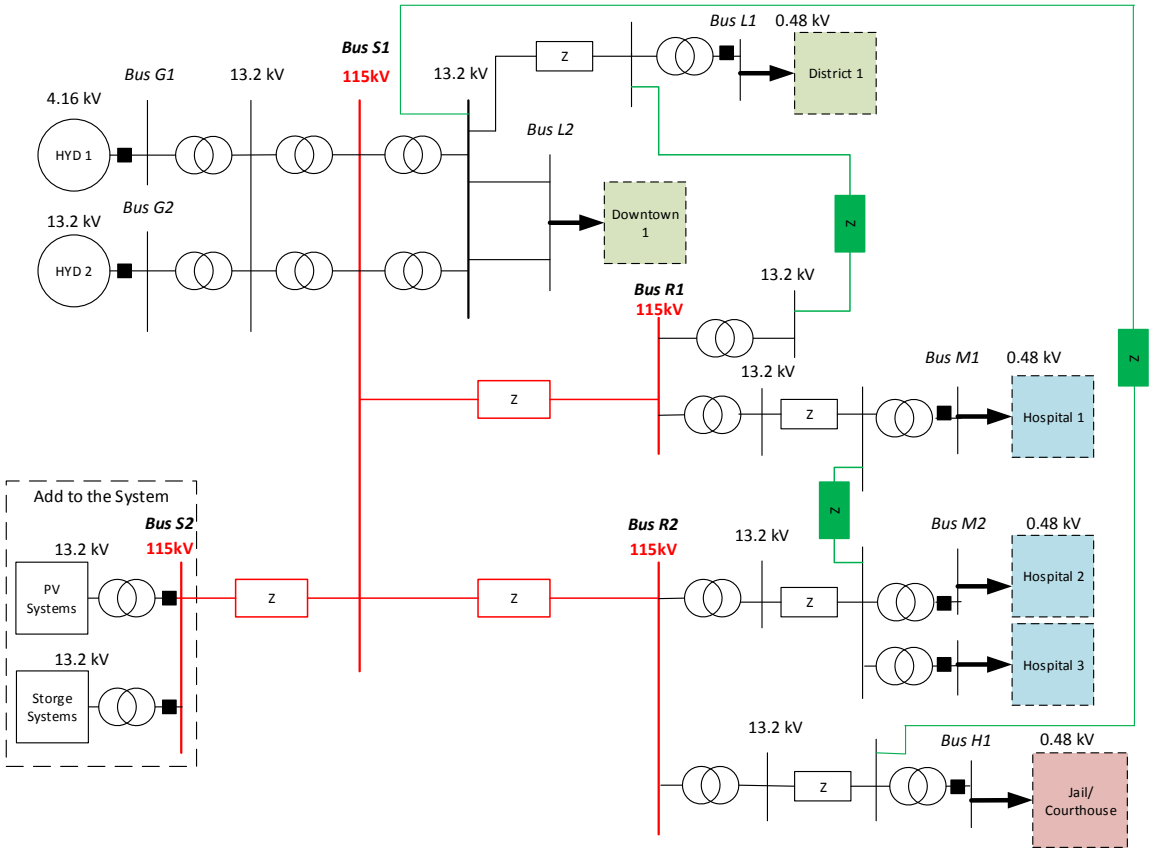

Figure 5.3. Simplified one-line diagram of PANW microgrid 1

5.4. Photovoltaic System Model

The PV system is connected to Bus S2 through a step up transformer (13.2 kV – 115 kV) as shown in Figure 5.3. Since the PV system has a DC output and interfaces with the three phase AC system, the ATP-EMTP model represents both the AC and DC sides. In addition, the control system and the DC-AC inverter is modelled. The model can be divided into four main parts:

- Clarke and Park's transformation for control purposes
- Phase locked loop (PLL)
- Controller
- Voltage source converter

The following sections will discusses each part in details.

5.4.1 Clarke and Park's Transformation

The controller uses current-regulated real and reactive power control loops in order to track the maximum PV power point and control the PV system output. The controller is based on a two-axes frame using a direct (d) axis and a quadrature (q) axis. The Clarke and Park's transformations have been used to develop controls in the two-dimensional frame. Figure 5.4 shows that the controller has six inputs and two outputs. The references for real and reactive power (P_{ref}, and Q_{ref}), and the d-axis and q-axis measured voltages (V_d, and V_q) are used in the outer control loops. The outputs of the outer control are the d-axis and q-axis reference currents (i_{dref} and i_{qref}). The inner control loops compare the d-axis and q-axis measured currents (i_d, and i_q) to the generated i_{dref} and i_{qref}. The controller then generates the

d-axis and q-axis modulation signals in order to control the VSC switching (the transformation from abc to dq is done in one step in the model; however, the figure shows two steps for more clarity).

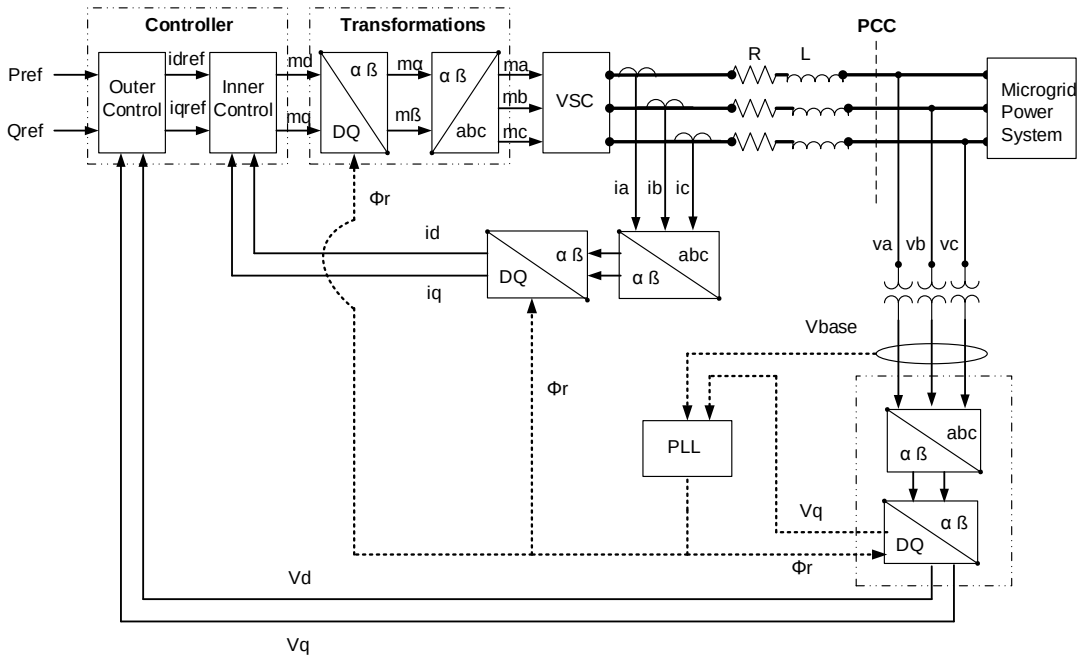

Figure 5.4. Schematic diagram of a current-controlled real and reactive power controller

The Clarke transformation is used to convert the abc to a two axis stationary reference frame (αβ). The transformation is used for voltages, currents and the inverse transformation for modulation signals. Equations (5.1) and (5.2) show the Clarke transformation equations used to convert the measured abc voltages to αβ voltages. Equation (5.3) calculates the zero sequence voltage. The currents use the same equation by substituting the line to ground voltages with the line currents.

$$V_{\alpha}(t) = \frac{2}{3}\cdot\left(V_a(t) - \frac{1}{2}\cdot V_b(t) - \frac{1}{2}\cdot V_c(t)\right) \quad (5.1)$$

$$V_{\beta}(t) = \frac{1}{\sqrt{3}}\cdot\left(V_b(t) - V_c(t)\right) \quad (5.2)$$

$$V_0(t) = \frac{1}{3}\left(V_a(t) + V_b(t) + V_c(t)\right) \quad (5.3)$$

V_a (t): Phase A line to ground voltage as a function of time

V_b (t): Phase B line to ground voltage as a function of time

V_c (t): Phase C line to ground voltage as a function of time

V_{α} (t): The real axis projection of the phase voltages

V_{β} (t): The imaginary axis projection of the phase voltages

V_0 (t): The zero sequence voltage

For the modulation signals, the inverse Clarke transformation is from αβ to abc. Equations (5.4), (5.5), and (5.6) are used.

$$m_a(t) = m_{\alpha}(t) \quad (5.4)$$

$$m_b(t) = \frac{1}{2}\cdot\left(\sqrt{3}\cdot m_{\beta}(t) - m_{\alpha}(t)\right) \quad (5.5)$$

$$m_c(t) = -\frac{1}{2}\cdot\left(\sqrt{3}\cdot m_\beta(t) + m_\alpha(t)\right) \tag{5.6}$$

m_a (t): Phase A modulation signal as a function of time

m_b (t): Phase B modulation signal as a function of time

m_c (t): Phase C modulation signal as a function of time

m_α (t): The real axis projection of the modulation signal

m_β (t): The imaginary axis projection of the modulation signal

Park's transformation is applied to convert αβ stationary frame quantities to the dq rotating reference frame quantities. However, the abc frame can be transformed to the dq rotating frame directly. The transformation is used for voltages, currents, and modulation signals. Equations (5.7) and (5.8) show the Park's transformation equations used to convert the measured αβ voltages to dq voltages. The same approach can be used for the currents by replacing the voltages with the line currents.

$$V_d(t) = V_\beta(t)\cdot\sin(\theta r(t)) + V_\alpha(t)\cdot\cos(\theta r(t)) \tag{5.7}$$

$$V_q(t) = V_\beta(t)\cdot\cos(\theta r(t)) - V_\alpha(t)\cdot\sin(\theta r(t)) \tag{5.8}$$

V_d (t): The direct axis measured voltage as a function of time

V_q (t): The quadrature axis measured voltage as a function of time

Θ_r (t): The phase angle from the PLL model

For the modulation signals, the transformation is from dq to αβ. Equations (5.9), and (5.10) are used.

$$m_\alpha(t) = m_d(t)\cdot\sin(\theta r(t)) + m_q(t)\cdot\cos(\theta r(t)) \tag{5.9}$$

$$m_\beta(t) = m_d(t)\cdot\cos(\theta r(t)) - m_q(t)\cdot\sin(\theta r(t)) \tag{5.10}$$

m_d (t): The direct axis modulation signal from the controller

m_q (t): The quadrature axis modulation signal from the controller

The dq quantities can be used to calculate the real and reactive power from measured voltages and currents. These calculations can be used in order to check the outputs from the PV model in comparison with the inputs. Equation (5.11) is for calculating real power, and equation (5.12) calculates the reactive power.

$$P_{0dq}(t) = \frac{3}{2}\cdot\left(V_0(t)\cdot i_0(t) + V_d(t)\cdot i_d(t) + V_q(t)\cdot i_q(t)\right) \tag{5.11}$$

$$Q_{0dq}(t) = \frac{3}{2}\cdot\left(V_q(t)\cdot i_d(t) - V_d(t)\cdot i_q(t)\right) \tag{5.12}$$

i_d (t): The direct axis measured current as a function of time

i_q (t): The quadrature axis measured current as a function of time

P_{0dq} (t): Real power calculated in the dq frame

Q_{0dq} (t): Reactive power calculated in the dq frame

5.4.2 Phase Locked Loop Scheme

Since the PV control uses a synchronous dq reference frame, a synchronization mechanism is required, and is implemented using a PLL. The PLL is important for tracking the AC system frequency, and synchronizing the converter output with the AC system. Figure 5.5 shows the PLL block diagram. The PLL model generates Φ_r by tracking the voltage at the PCC during all conditions, includes transients and oscillations. V_q is used to feed the PLL, and Φ_r is connected to the dq transformation block to close the loop. See Figure 5.4. ω_{ref} for the AC system is $2\pi \cdot 60$ Hz. As a result, the limiter has ω_{max} equal to 377 radians per second, with the ω_{min} equal to zero.

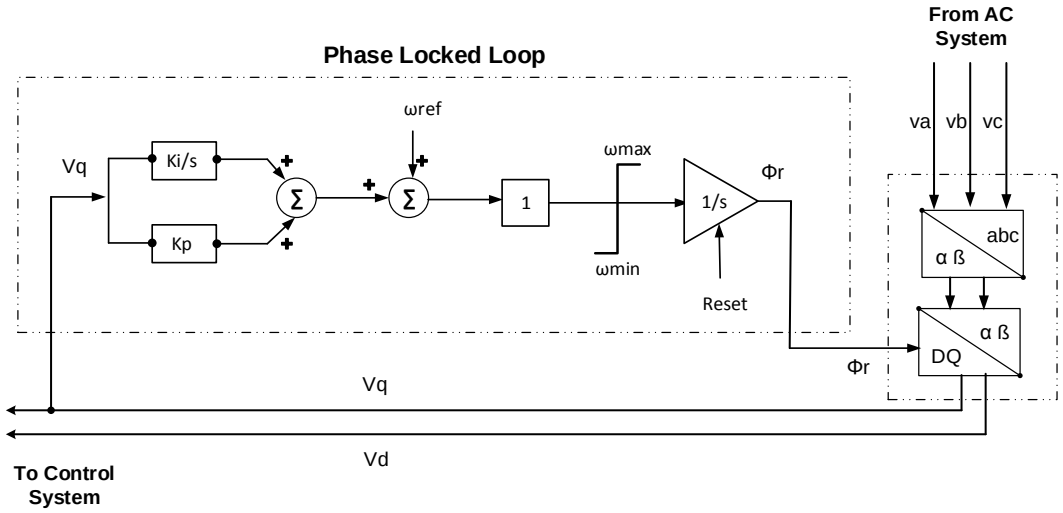

Figure 5.5. PLL block diagram

5.4.3 Controller Scheme

Commercial PV system controllers track the maximum PV power point in order to extract the maximum power from the unit. As a result, PV systems are considered a nondispatchable DG [17]. The output power of the PV system varies according to the solar irradiation conditions. The power flow control strategy is called maximum point of power tracking (MPPT). In addition, PV systems have DC link voltage controls [17].

In this particular PV model, an AC controller is used to control the AC side of the PV system model. There is no DC link controller because the DC side of the VSC is represented as an ideal DC source. Instead of using the MPPT control strategy, the controller is designed to have a variable real power reference based on the insolation data presented earlier and zero reactive power. In Figure 5.6, device 56 has a lookup table to represent the non-linear variable output power of the PV system, and it is connected to the controller. The

real power reference is actually the maximum power that can be extract from the PV system correcting for conversion efficiency. As a result, the real power reference for each time step is set according to the maximum solar irradiation. The PVWatts calculator is used to convert the solar irradiation to real power [33]. As a result, the PV system real power output varies according to the solar irradiation conditions.

Figure 5.6 shows both the inner and outer controls. The outer controllers generate the i_{dref} and i_{qref} according to the real and reactive power reference respectively (i_{qref} = 0 in the PV system model). Then, the inner controller generates the md (t) and mq (t) according to the i_{dref} and i_{qref} respectively. In addition, the controller is modeled to have voltage feed-forward and current decoupling compensations in order to avoid an undesirable response to transients, and to decouple the VSC from the AC system dynamics.

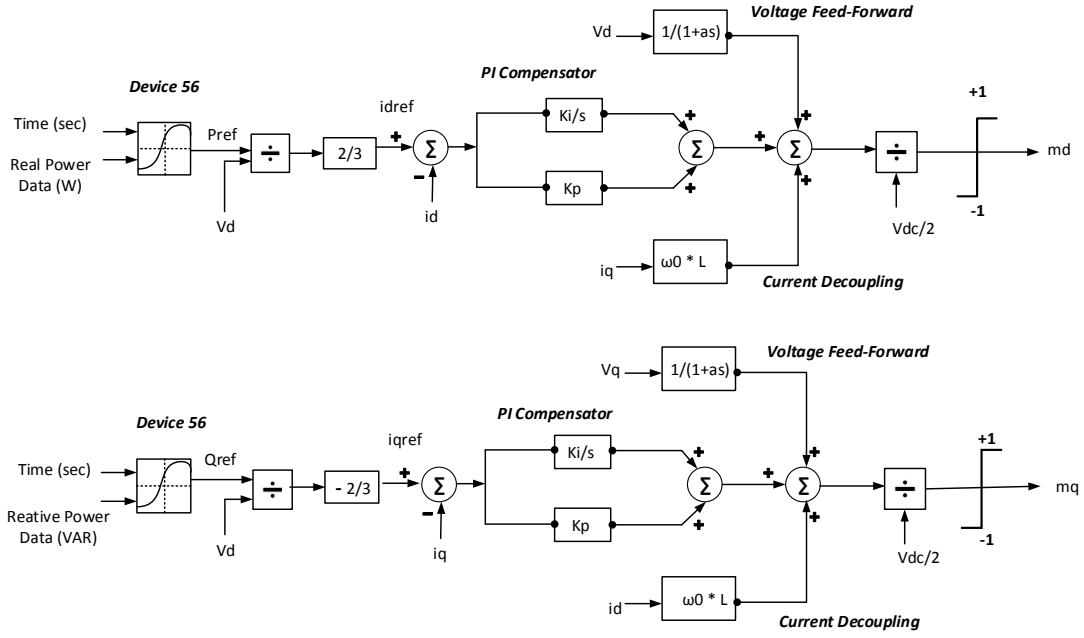

Figure 5.6. Controller block diagram

5.4.4 Voltage Source Converter

The three phase VSC switched model consists of fully controllable bidirectional switches with unilateral voltage blocking, and includes both power system dynamic and high frequency behavior. The VSC averaged model represents the steady state and slow dynamic behavior. However, the high frequency behavior is ignored. The VSC model in this work is based on a two level averaged converter model. Reference [3] provides tests and results that validate these types of VSC models.

The averaged VSC model can be represented using dependent voltage sources on the AC side and current sources on the DC side of the converter (Figure 5.7). The dependent current sources are connected to the DC side through small resistors for numerical reasons in this specific model. The DC side of the VSC is represented as an ideal source since the detailed behavior is outside the scope of this thesis. The VSC losses are ignored in the model because an approximate loss has been used to calculate the converter input data using the PVWatts calculator. The system losses of 14% are assumed according to several factors such as shading, wiring, and nameplate rating [33]. The positive dependent current source (i_p) and the negative dependent current source (i_n) are controlled by the abc modulation signals. Equations (5.11) and (5.12) the show mathematical relations between the dependent current sources and the modulation signals.

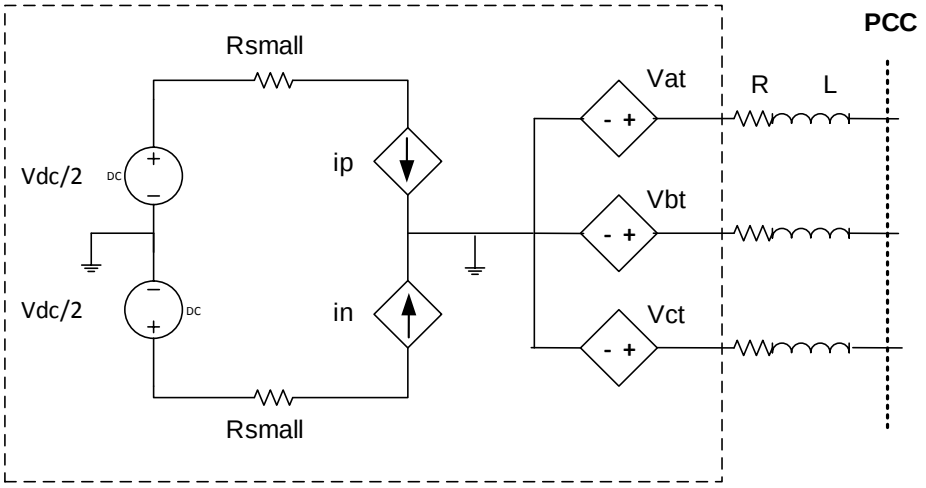

Figure 5.7. Schematic diagram of the averaged VSC model

$$i_p(t) = -i_a(t)\cdot\left(\frac{1+m_a(t)}{2}\right) - i_b(t)\cdot\left(\frac{1+m_b(t)}{2}\right) - i_c(t)\cdot\left(\frac{1+m_c(t)}{2}\right) \tag{5.11}$$

$$i_n(t) = -i_a(t)\cdot\left(\frac{1-m_a(t)}{2}\right) - i_b(t)\cdot\left(\frac{1-m_b(t)}{2}\right) - i_c(t)\cdot\left(\frac{1-m_c(t)}{2}\right) \tag{5.12}$$

i_p (t): Positive pole dependent DC current source

i_n (t): Negative pole dependent DC current source

The dependent voltage sources are facing the AC system and are also controlled based on the modulation signals. Equations (5.13), (5.14), and (5.15) express the mathematical relation between the dependent voltage sources and the modulation signals.

$$V_{at}(t) = m_a(t) \cdot \left(\frac{V_{dc}(t)}{2} \right) \tag{5.13}$$

$$V_{bt}(t) = m_b(t) \cdot \left(\frac{V_{dc}(t)}{2} \right) \tag{5.14}$$

$$V_{ct}(t) = m_c(t) \cdot \left(\frac{V_{dc}(t)}{2} \right) \tag{5.15}$$

V_{dc} (t): The ideal DC voltage source as a function of time

V_{at} (t): Phase A dependent AC voltage source as a function of time

V_{bt} (t): Phase B dependent AC voltage source as a function of time

V_{ct} (t): Phase C dependent AC voltage source as a function of time

For more explanation about this model approach, see reference [3]. Additionally, Appendix B includes more detailed block diagrams for the PV model.

5.5. Hydroelectric Generator Model

The objective of this model is to represent the dynamics of the hydroelectric generators in the PANW microgrid. The goal is to study the hourly and monthly variation of the output of the generation units and the real and reactive power drawn by the critical loads.

For the purpose of this study, the hydroelectric generators are represented as controlled voltage sources connected to the power system (see Figure 5.8). A detailed dynamic machine model is out of the scope of this thesis. HYD 1 and HYD 2 are each controlled with three phase dependent voltage sources similar to the VSC model above, so equations (5.13), (5.14), and (5.15) are applied. The control system is similar to the controller discussed earlier in Figures 5.4, 5.5, and 5.6, but with slower dynamics. This approach is adequate since the simulations are of steady state operating points.

By using this model, the field data from HYD 1 and HYD 2, which depend on the flow of the downtown river, can be used in order to represent the generators' variation. Power flow tests using Powerworld have been used in order to validate this model. Section 5.7 discuses some of the validation procedure.

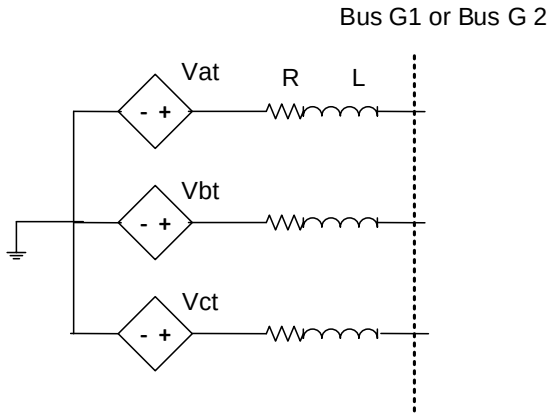

Figure 5.8. Schematic diagram of the controlled voltage source

5.6. Variable Load Model

The three phase variable load can be defined as a current injection to the AC system that varies based on a reference apparent power and measured voltage, and maintains a constant power factor (pf). The injected current can be represented as a dependent current source as seen in Figure 5.9.

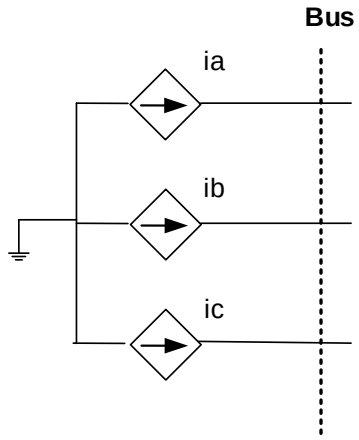

Figure 5.9. Schematic diagram of the controlled current source

Equations (5.16), (5.17), and (5.18) express the mathematical approach to calculate currents by using first order transfer functions [34]. C_1 and C_2 can be calculated by using (5.19), and (5.20). Figure (5.10) shows the controller block diagram for the variable load, along with the TACS device 56 for the real power input data.

$$ia(t) = Va(t) \cdot C_1(t) \cdot \left(\frac{1}{C_2(t) + s} \right) \tag{5.16}$$

$$ib(t) = Vb(t) \cdot C_1(t) \cdot \left(\frac{1}{C_2(t) + s} \right) \tag{5.17}$$

$$ic(t) = Vc(t) \cdot C_1(t) \cdot \left(\frac{1}{C_2(t) + s} \right) \tag{5.18}$$

i_a: Phase A dependent AC current source

i_b: Phase B dependent AC current source

i_c: Phase C dependent AC current source

s: Laplace variable

$$C_1(t) = \frac{\omega_{ref} \cdot \left(P_{ref}(t) \right)}{\left(\left| V_{rms}(t) \right| \right)^2} \cdot \left(\frac{P_{ref}(t)}{Q_{ref}(t)} + \frac{Q_{ref}(t)}{P_{ref}(t)} \right) \tag{5.19}$$

$$C_2(t) = \omega_{ref} \cdot \left(\frac{P_{ref}(t)}{Q_{ref}(t)} \right) \tag{5.20}$$

C_1 (t): Represents the “power” level

C_2 (t): Represents the “power factor”

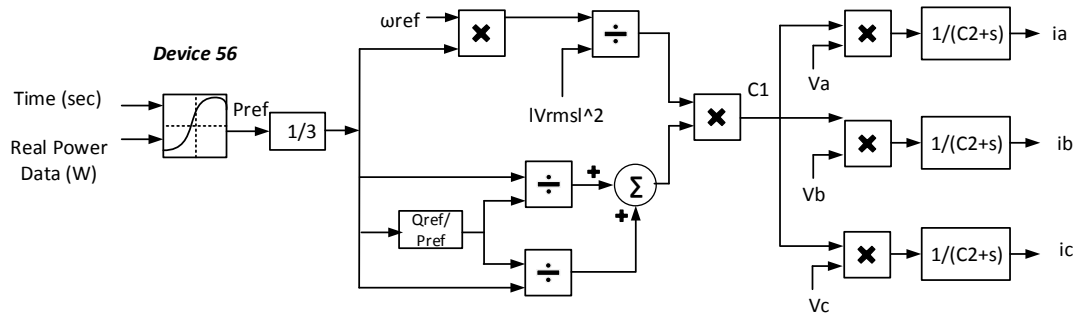

Figure 5.10. Variable load controller block diagram

5.7. Model Validation

Different validation approaches have been used for different components. For the transformers and transmission lines, short circuit tests at each ATP-EMTP node are applied and compared with analytical calculations. In the short circuit tests, the two hydroelectric generators are represented as voltage sources behind their impedances. Table 5.1 shows the short circuit currents when short circuit tests are applied at Bus S2, Bus R1 and Bus R2. The errors are small

Additionally, equations (5.16), (5.17), (5.18), (5.19), and (5.20) are used for analytical calculations. The results are compared with the output currents from the ATP-EMTP load model. The PV model is validated by checking the real and reactive power at the PCC with P_{ref} and Q_{ref}. Additionally, some analytical calculations have been used in order to check the output currents from the model.

Power flow analysis has been used for validating HYD 1, HYD 2, and the variable loads. In order to simplify the validation process, only the three transmission lines, seven transformers, the two hydroelectric generator models, an ideal storage device, and the five

variable load models have been chosen to be active in the ATP-EMTP model during this process. A Powerworld model has been designed having the same components. The two hydroelectric generators are represented as synchronous machines with internal impedances, and the variable load is represented as constant real and reactive power. Table 5.2 shows the percentage errors when the real and reactive total power, and the output real and reactive power from the ideal storage are compared. Table 5.3 compares between currents on some of the buses and shows the percentage errors.

Table 5.1 Short circuit current magnitude errors at each transmission line

	ATP-EMTP (Amp.)	Calculated (Amp.)	Error %
Bus S2	660.5	660.464	0.00547
Bus R1	654.7	654.61	0.0137
Bus R2	660.4	660.464	0.011

Table 5.2 Real and reactive power errors

	ATP-EMTP	Powerworld	Error %
P storage	4.911 MW	4.903 MW	0.163
Q storage	9.723 MVAR	9.907 MVAR	1.857
P total	23.874 MW	23.841 MW	0.138
Q total	10.762 MVAR	10.907 MVAR	1.329

Table 5.3 Current magnitude errors at Bus 1-5

	ATP-EMTP (Amp.)	Power World (Amp.)	Error %
Bus 1	494.8	499.61	0.963
Bus 2	486.4	491.15	0.967
Bus 3	44.58	45.86	2.791
Bus 4	9.48	9.73	2.6
Bus 5	64.52	66.49	2.963

In summary, Table 5.1 shows that short circuit current magnitude errors at the ends of each transmission line are less than one percent. The total generation and the total storage real and reactive power errors are less than two percent as shown in Table 5.2. The current magnitude errors at each bus are less than three percent as shown in Table 5.3. The errors are acceptable since the two models are in two different domains. Moreover, the hydroelectric generators model is not represented as synchronous machines in the ATP-EMTP model. In addition, the representation of the load in the Powerworld is different than the ATP-EMTP variable load model. However, these errors will not have significant effects on the results. For that reason, the ATP-EMTP model is considered to be valid for this study.

Chapter 6: Study Cases and Results

A set of study cases are described, followed by a presentation and discussion of results from the cases. All cases are tested during islanded mode (Figure 6.1 shows microgrid 1 power system). Generator models include HYD 1, HYD2, PV, and storage system (STR). Variable load models include a Jail and Courthouse (JC), Hospital 1 (H1), Hospital 2 (H2), Hospital 3 (H3), District (DT), and Downtown (DN).

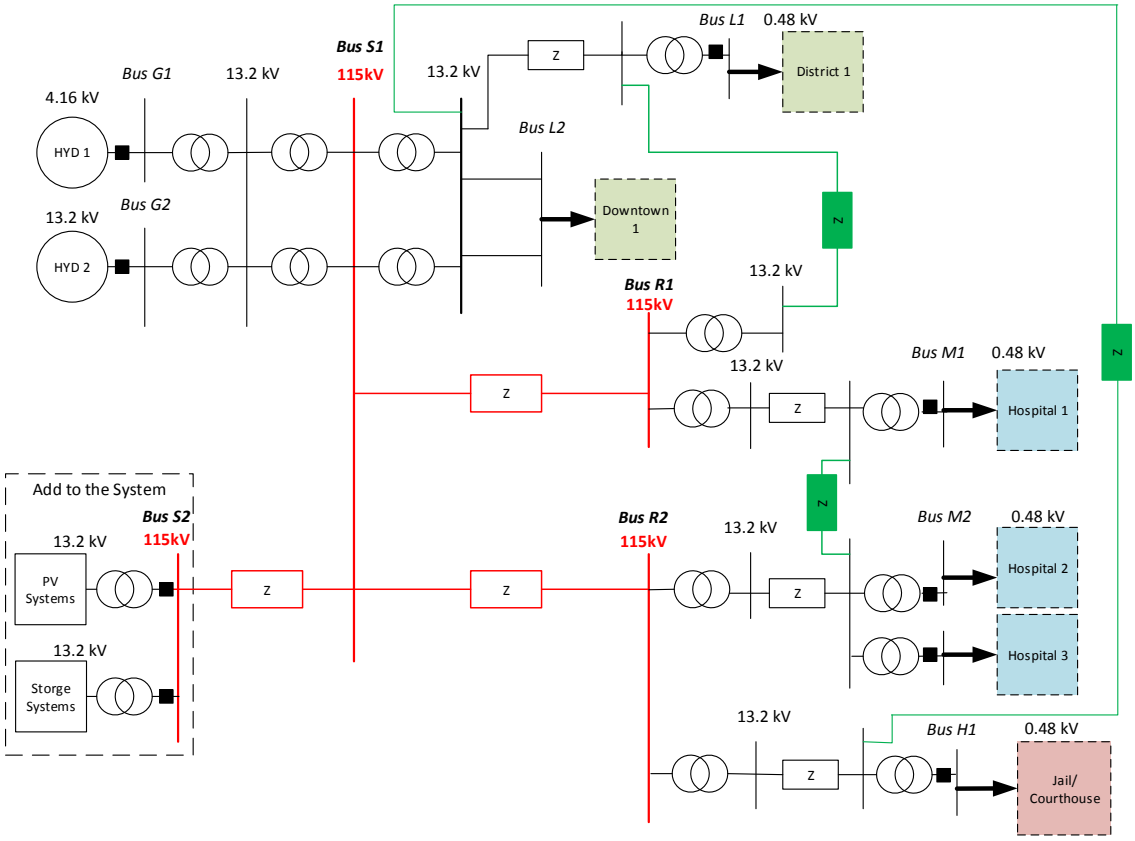

Figure 6.1. Simplified one-line diagram of PANW city microgrid 1

6.1. Case 1: Load, Hydroelectric Generator, and Storage System

Case one tests the microgrid system with HYD 1, HYD 2, and STR along with all variable load models. These loads and hydroelectric generators are existing components of the grid, with the STR added as a theoretical component. The PV system model is not connected in this case.

The data used for the loads, and hydroelectric output are averaged values for a high average for each season (winter, spring, summer, and fall) provided by the project sponsor. The data is averaged in order to simplify the dynamic generation-load profiles and to begin with simple steps (whereas some of the following sections study the hourly variation). Each season is represented in the ATP-EMTP program in 0.3 sec. steps starting from 0.1 sec. (Figure 6.2). The first 0.1 sec. is ignored since it includes model startup behavior. Each 0.3 sec. represents three months which is one season. For example, the winter season represents three months. Winter starts from 0.1 sec. and ends at 0.4 sec.

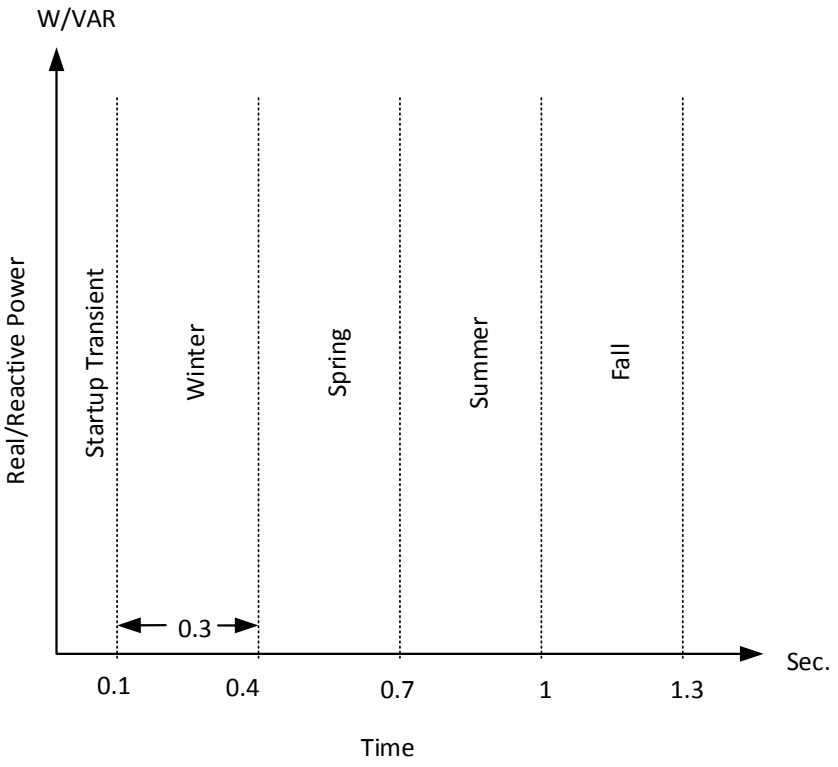

Figure 6.2. Representation of seasons in ATP-EMTP, where 0.3 sec. equals three months

6.1.1. Variable Load

Figure 6.3 shows the total real and reactive power drawn by the critical loads over the course of a year with a representative day in each season. Figures 6.4 and 6.5 show real and reactive power for each critical load for the same period. Table 6.1 summarizes load consumption of real and reactive power each season. During summer the loads have the highest peaks. The reactive power for each load is based on maintaining fixed power factors. The worst power factor for each load is calculated and considered in the variable load model from the load data provided by the project sponsor.

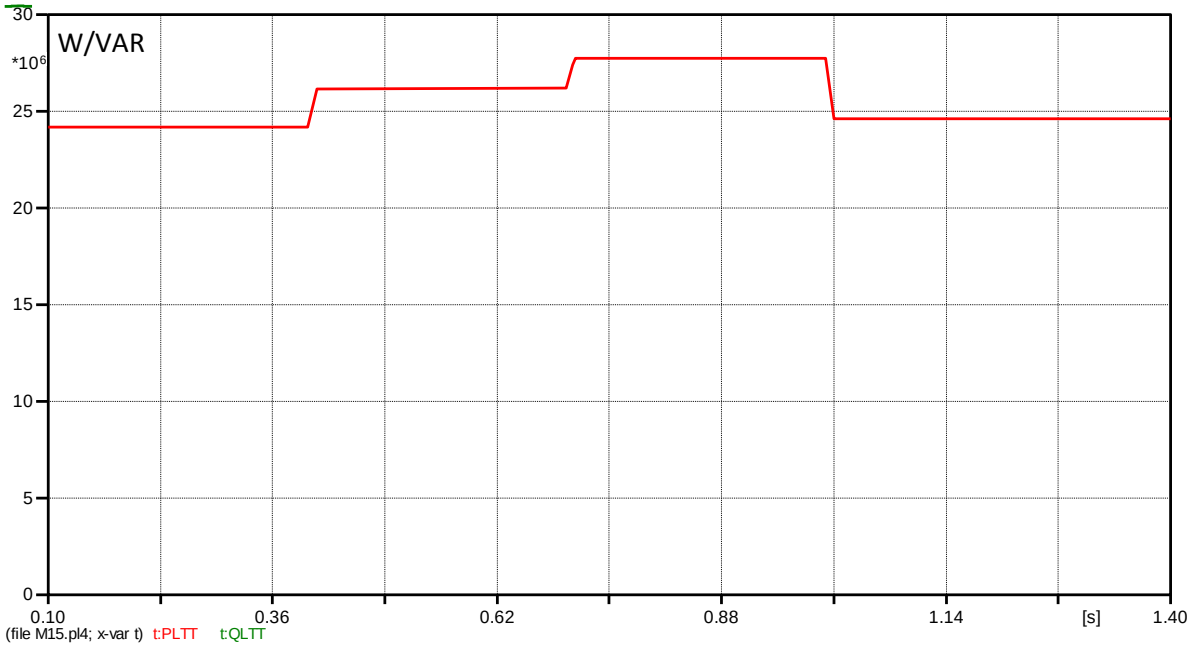

Figure 6.3. Total load real and reactive power consumption per season (red for P and green for Q)

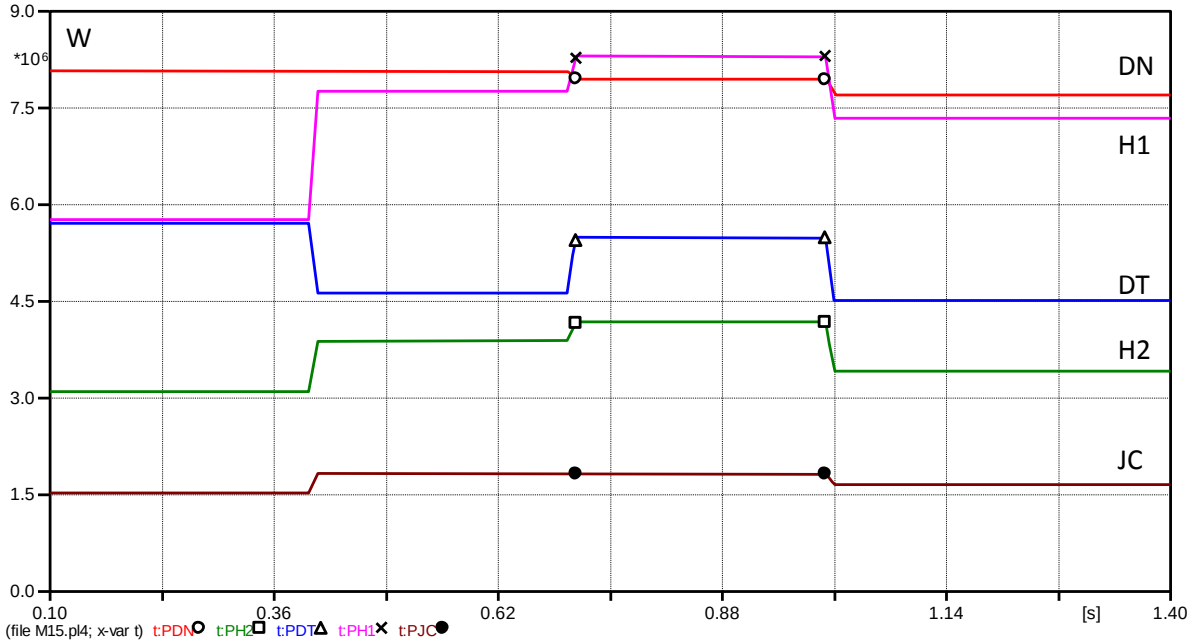

Figure 6.4. JC, H1, H2, DT, and DN real power consumption per season

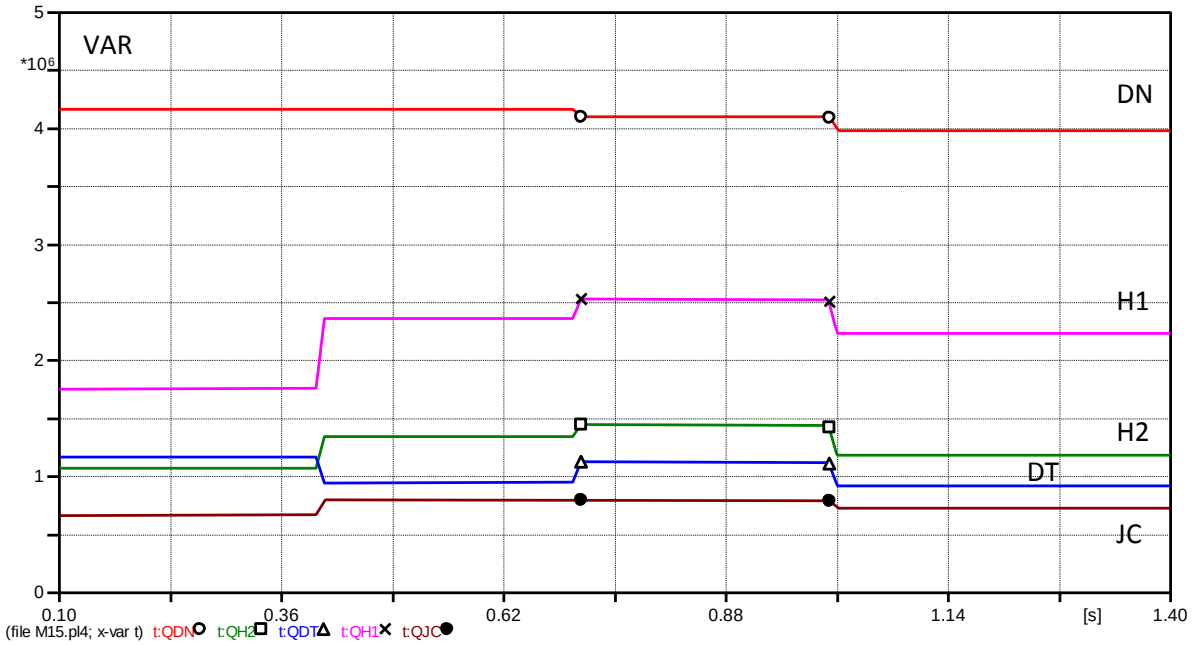

Figure 6.5. JC, H1, H2, DT, and DN reactive power consumption per season

Table 6.1. High average peak seasonal load consumption of real and reactive power

	Real Power (MW)				Reactive Power (MVAR)			
	Winter	Spring	Summer	Fall	Winter	Spring	Summer	Fall
JC	1.52	1.8	1.83	1.66	0.67	0.8	0.8	0.73
H1	5.77	7.75	8.3	7.34	1.75	2.36	2.53	2.23
H2 and H3	3.1	3.88	4.18	3.41	1.07	1.34	1.45	1.18
DN	8.07	8	7.95	7.7	4.17	4.17	4.1	3.98
DT	5.7	4.63	5.5	4.51	1.17	0.95	1.13	0.925
Total Load	24.17	26.16	27.75	24.4	8.83	9.62	10	9.05

6.1.2. Variable Hydroelectric Generators Output

The hydroelectric generator model power outputs are based on averaged data for the power output from HYD 1 and HYD 2 from historical data (Figure 6.6). Both HYD 1 and HYD 2 operate at 0.99 leading power factor. The reactive power is fixed in this model. Each hydroelectric unit generates a fixed 0.5 MVAR (Figure 6.7). The overshoot transients in Figure 6.7 can be ignored since they are from the sudden change in set point at the start of each season. Again the first 0.1 sec is a startup transient. Table 6.2 summarizes the output real and reactive power from HYD1 and HYD 2. As it can be gathered, summer has the lowest generation from both hydroelectric generators due to reduced river flows.

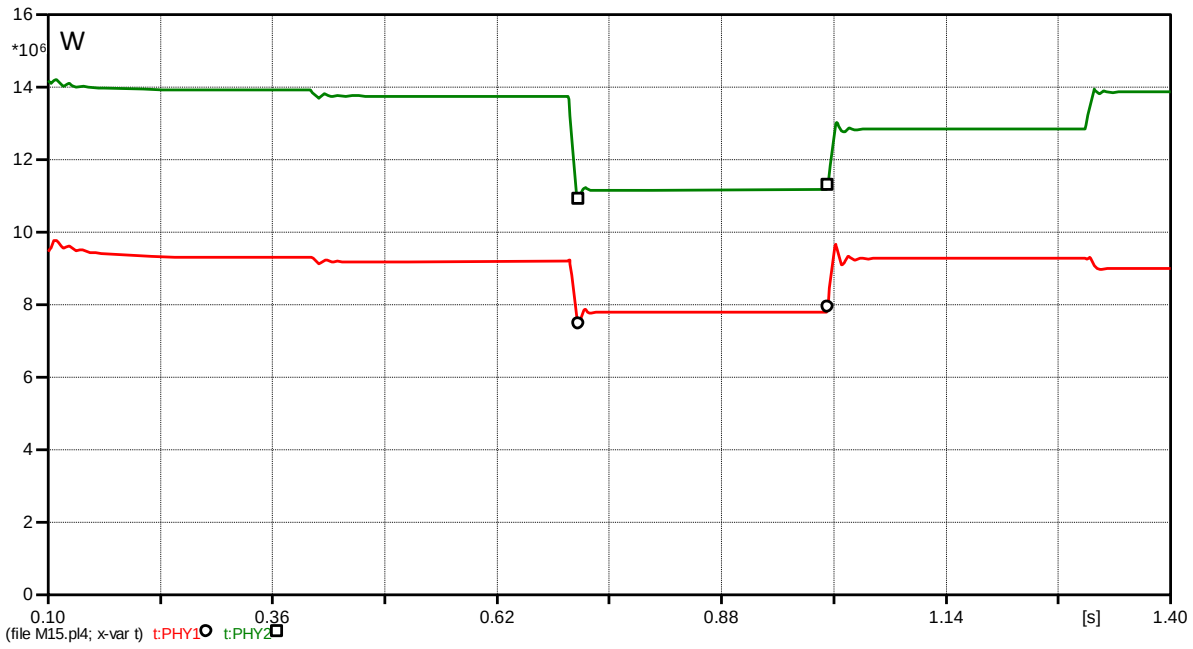

Figure 6.6. HYD 1 and HYD 2 real power production per season (red for HYD 1 and green for HYD 2)

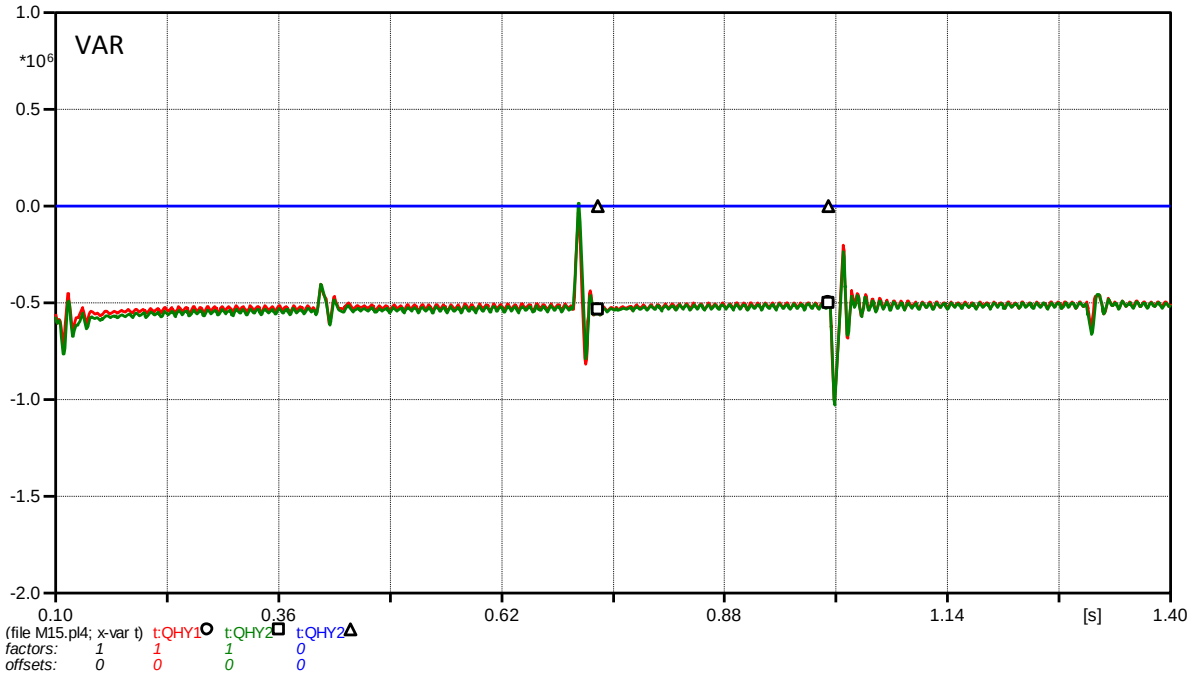

Figure 6.7. HYD 1 and HYD 2 reactive power supplied assuming production per season (red for HYD 1, green for HYD 2 and blue is the 0 reference)

Table 6.2. HYD 1 and HYD 2 variable generation

	Real Power (MW)				Reactive Power (MVAR)			
	Winter	Spring	Summer	Fall	Winter	Spring	Summer	Fall
HYD 1	9.82	9.74	7.78	9.79	- 0.5			
HYD 2	14.25	14.18	11.15	12.83	- 0.5			
Total Power Production	24.07	23.92	18.93	22.62	- 1			

6.1.3. System Total Losses

The real power losses in each season have been recorded (Figure 6.8). The variation shows peak seasonal losses with losses around 1 MW during the summer peak. The transients at each season transitions are ignored since they are artifacts from the model behavior. The real power losses is calculated in the ATP-EMTP model by subtracting the total load consumption from the total generation production.

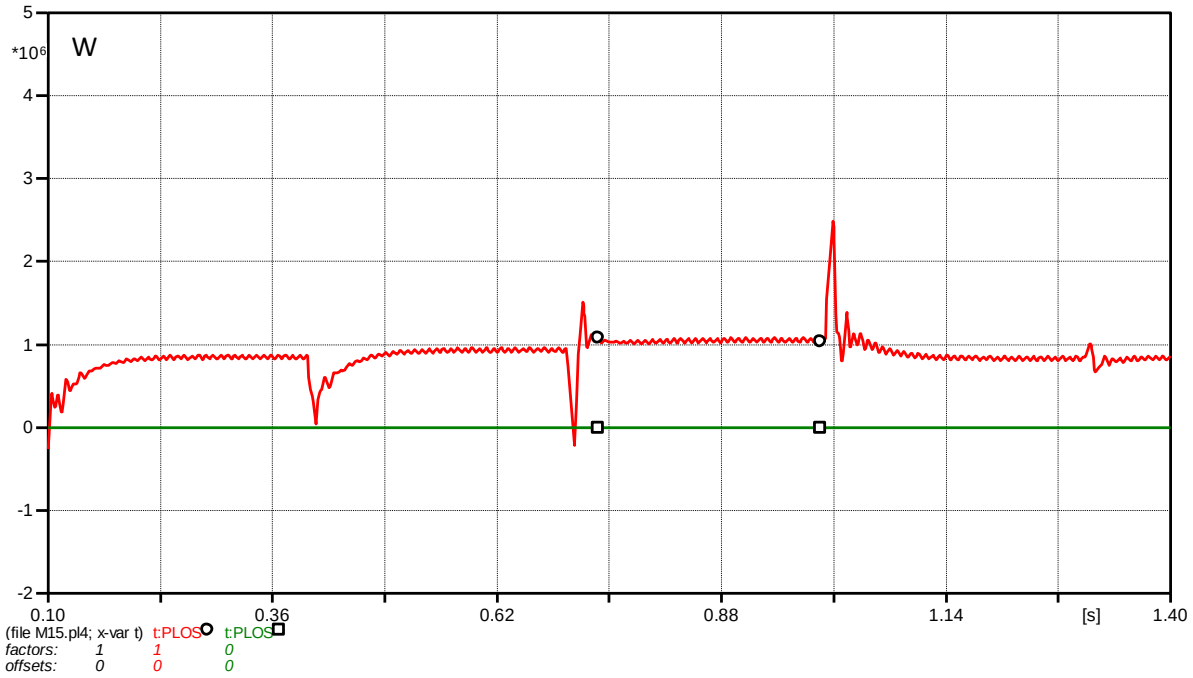

Figure 6.8. Real power losses variation per season (red for losses, green is the 0 reference)

6.1.4. Energy Storage System

The STR is modeled as an ideal storage device that can charge or discharge real power as needed. Also, reactive power has been supplied from an ideal source in order to stabilize and regulate the voltage in the system. The reason for choosing ideal sources is to

find real and reactive power shortage in microgrid 1. The idea is to have a clear image of the size of storage system peak MW plus MVAR capability needed during each season. Figure 6.9 shows a plot of the real and reactive power requirements from the STR system. Table 6.3 summarizes the output from the STR system. As can be realized, the peak of the STR system is during summer because the loads peaks are in the summer, and HYD 1 and HYD 2 have their lowest production during that season. PANW city microgrid 1 is difficult to form during summer unless additional generation units are considered or many of critical loads are shed. The reactive power part in the table is only to show the MVAR shortage in microgrid 1. It is not a practical solution to supply this much reactive power from a storage system. Instead, the hydroelectric generators can supply and regulate the reactive power in the microgrid system along with capacitor banks. Distribution capacitor banks will be considered in the following study case.

Microgrid 1 system peak generation has roughly a 10 MW shortage during summer peak, whereas the second highest shortage is about 4 MW during spring. This difference cannot be overcome practically with only one storage system. Load shedding should also be applied to the critical loads, which will reduce the benefits of forming a microgrid.

Another suggestion is to consider additional generation resources along with a storage system. In case 3, a PV system is considered along with the STR in order to explore a potential option for solving this issue. In addition, distribution capacitor banks are added to the microgrid system in case 2 in order to supply the reactive power needed.

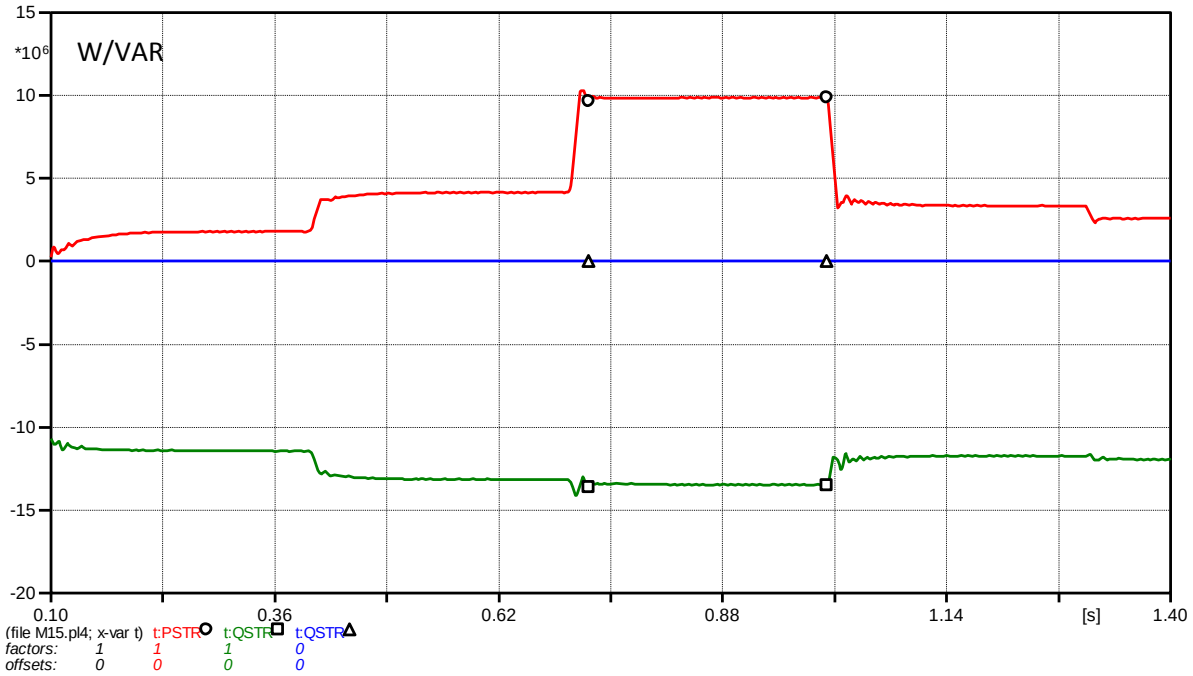

Figure 6.9. STR peak real and reactive power charge and discharge per season (red for P and green for Q, blue is the 0 reference)

Table 6.3. Storage system peak variable charge and discharge by seasons

	Real Power (MW)				Reactive Power (MVAR)			
	Winter	Spring	Summer	Fall	Winter	Spring	Summer	Fall
STR	1.82	4.18	9.84	3.36	-11.37	-13.14	-13.47	-11.76

6.1.5. Voltage Profiles

Since the power system has no capacitor banks (and as mentioned earlier, the transmission level capacitor is not appropriate for islanded mode), relatively low voltage profiles are expected. Figure 6.10 shows the voltage profile over the representative year at

each load bus and at Bus S1. The acceptable range of voltages, as the IEEE Recommended Practice for Monitoring Electric Power Quality recommends is plus or minus 5% (0.95-1.05) [35]. The figure shows the voltages in per unit beside the 5% range. As can be seen, almost all voltage profiles fall below 0.95. Some voltages are very low which can cause the undervoltage protection to operate. The voltage profile during the summer shown in the figure was verified with a Powerworld model which has been designed by another team who is working on the same project. Case 2 discusses adding distribution capacitor banks to PANW city microgrid 1.

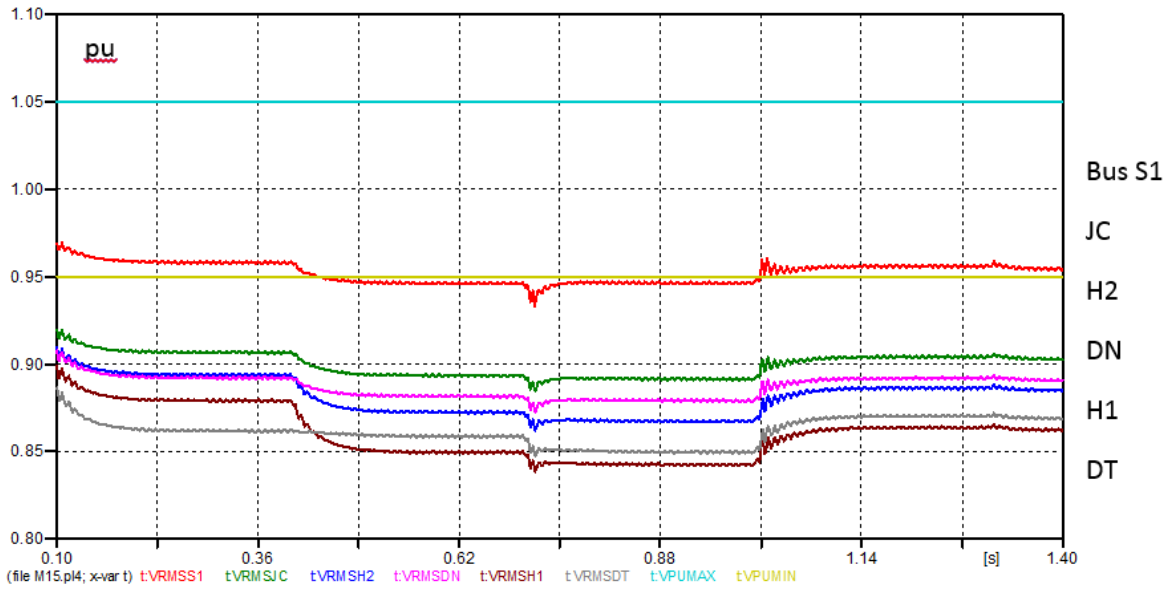

Figure 6.10. Per unit voltages at each load bus and Bus S1 (Bus S1 where is both HYD 1 and HYD 2 are connected) – Bus S1, JC, H2, DN, H1, DT

6.2. Case 2: Capacitor Banks

In this case, distribution capacitors are added to the microgrid system. The PANW city microgrid 1 system is tested with HYD 1, HYD 2, and STR along with all the variable load models.

Capacitor banks are required in order to supply reactive power and improve the low voltages at the buses. One simple approach for finding approximate capacitor bank ratings is to calculate the reactive power absorbed at each bus. Then the next step is to calculate how much capacitance is needed to support the voltage. The sponsor of this project suggested using a 300 kVAR three phase capacitor bank as a standard for the distribution level. As a result, each bus has to have one or more 300 kVAR banks. Table 6.4 summarizes the number of capacitor banks at each load bus, and the total amount of reactive power which the set of banks' produce.

The distribution capacitor bank model is delta connected, and each bank is shunt-connected at each load bus (Figure 6.11 shows the DN capacitor banks model). Then, the banks are connected in parallel to produce the desired reactive power. The voltage profiles at each load bus and at Bus S1 are displayed in Figure 6.12. Almost all voltages are within the IEEE recommended range [35]. Since the same number of capacitors are connected during the four seasons, the voltage profiles vary at each season.

Table 6.4. Capacitor banks information

	Number of Capacitor Banks	MVAR of Capacitor Banks
JC	3	0.9
H1	10	3
H2 and H3	6	1.8
DN	16	4.8
DT	4	1.2
Total	39	11.7

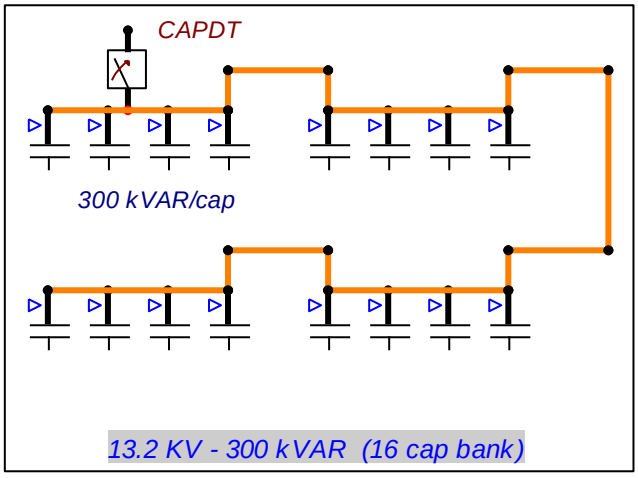

Figure 6.11. ATP-EMTP DN load bus capacitor banks model

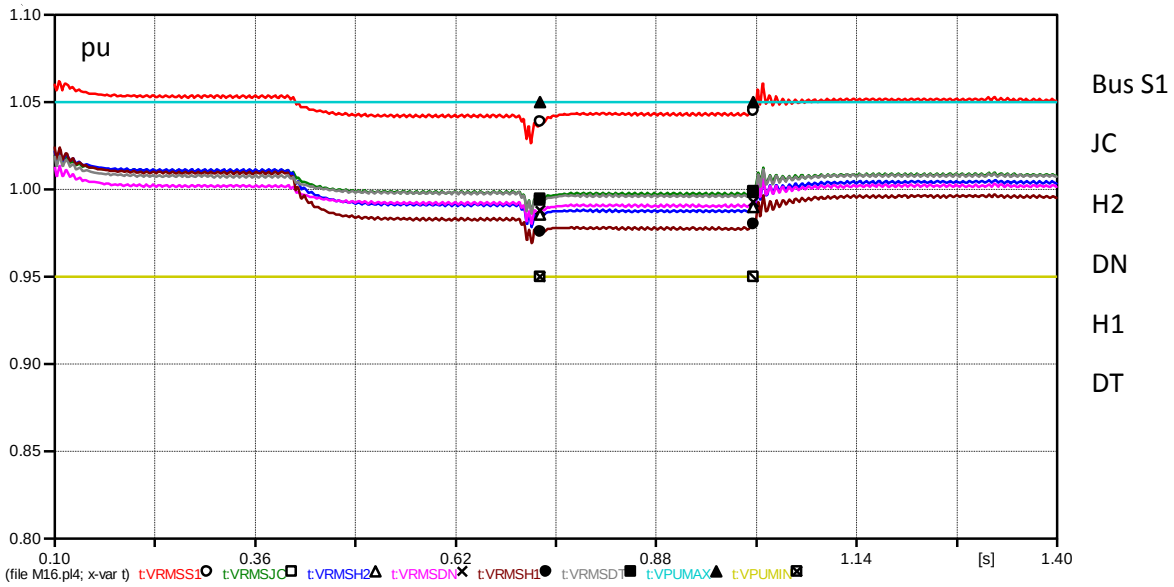

Figure 6.12. Per unit voltage profile with adding extra capacitor banks

6.3. Case 3: Photovoltaic System

A centralized PV system is then added to the system, and operated at unity power factor. The PV system is connected at Bus S2 (13.2 kV) as shown in Figure 6.1. In reality many smaller PV systems would be distributed around the microgrid. The microgrid 1 system is tested with HYD 1, HYD 2, PV, and STR along with all variable load models and distribution capacitor banks.

The total rating power of the PV arrays is assumed 8 MW at the DC side. The PVWatts calculator (beside the PV system model) calculates the three phase AC real output power based on historical data from solar irradiation provided by NREL [32] [33]. As explained in Sections 5.4.3 and 5.4.4, the PV model produces the maximum real power according to the solar irradiation. Figure 6.13 shows the average real and reactive power

generated from the PV system. The average PV power for each season appears low compared to the PV rating because the PV system has zero real power during night and real power varies over course of daylight hours. Table 6.5 summarizes the real power output per season from the PV system. It is notable that PV system generates a decent amount of real power during summer. The PV system has to be studied hourly in order to consider the day and night behavior.

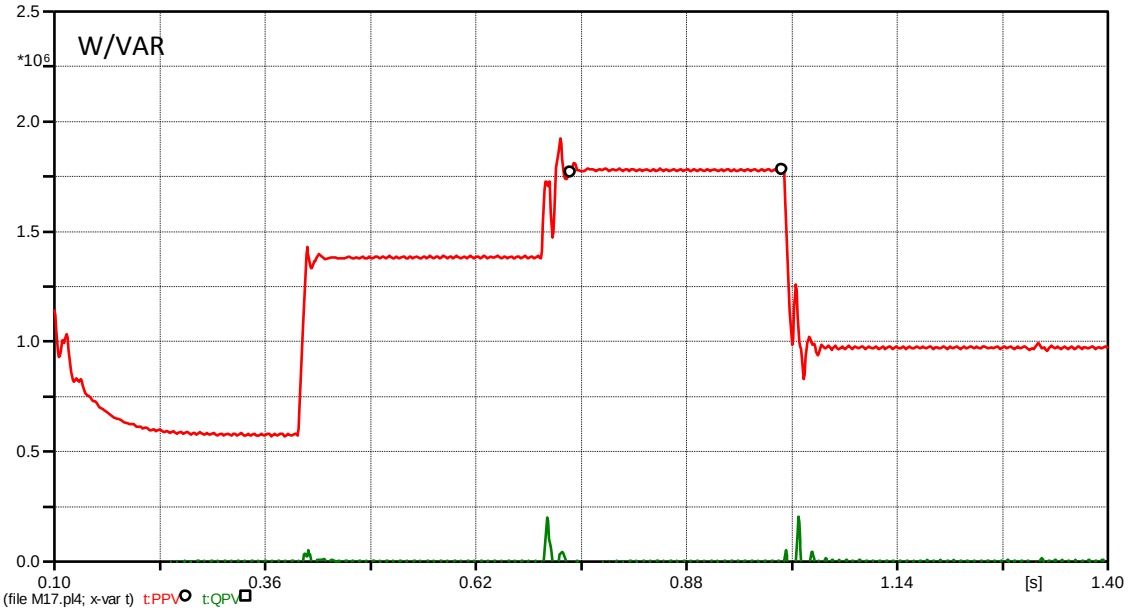

Figure 6.13. Averaged real and reactive power generated from the PV system (red for real power and green for reactive power)

Table 6.5. PV system variable generation per season

	Real Power (MW)				Reactive Power (MVAR)			
	Winter	Spring	Summer	Fall	Winter	Spring	Summer	Fall
PV system	0.6	1.4	1.8	1	0			

6.3.1. Storage System with Photovoltaic and Capacitors

Obviously, the storage system is affected by the presence of the PV system (Figure 4.16). Table 6.4 summarizes the STR output. An ideal STR is used to consume or supply reactive power in this case to regulate the terminal voltage. Note that HYD 1 and HYD 2 are suppling fixed reactive power; however, the generators should first regulate their terminal voltage to higher values, before scheduling the connection and disconnection of capacitor banks.

The total real power drawn by the critical loads is reduced during winter. During winter hydroelectric generation along with the PV generation almost matches the loads. As a result, load shedding is only used for a cloudy day or maybe at night. On the other hand, the generation shortage is at its peak in the summer. Table 6.6 shows the difference between case 2 (the system with the PV system and capacitor banks) and case 1. A planned load shedding is required for each season in order to form PANW city microgrid 1 even with energy storage.

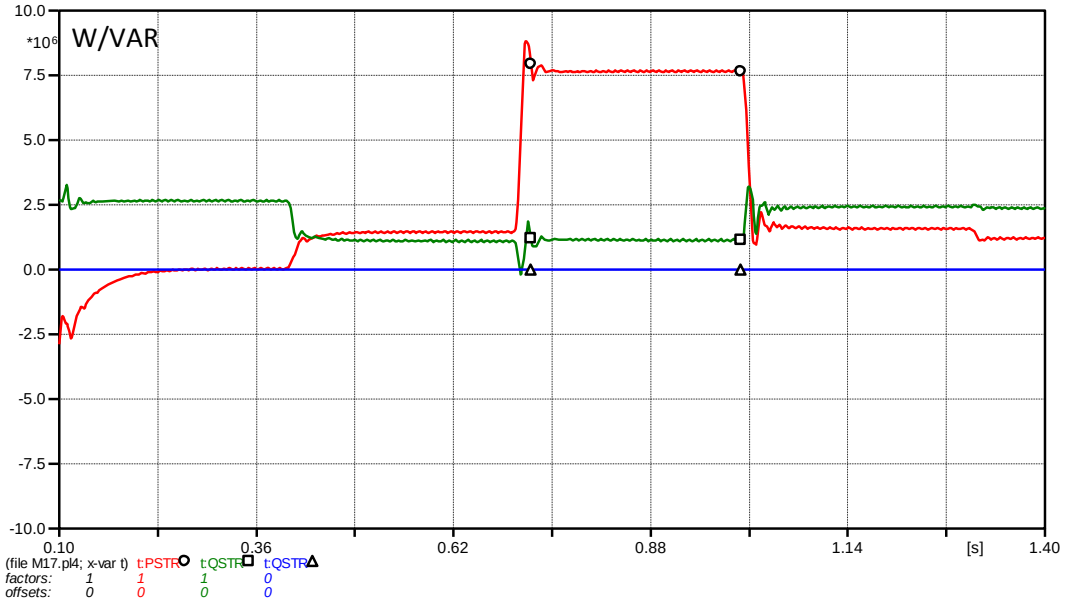

Figure 6.14. STR real and reactive power charge and discharge with PV system (red for P and green for Q, blue is the 0 reference)

Table 6.6. STR variable charge and discharge with PV system

	Real Power (MW)				Reactive Power (MVAR)			
	Winter	Spring	Summer	Fall	Winter	Spring	Summer	Fall
STR with PV and capacitors	0	1.45	7.65	1.55	2.65	1.1	1.16	2.4
STR	1.82	4.18	9.84	3.36	-11.37	-13.14	-13.47	-11.76
Difference	1.82	2.73	2.19	1.81	-8.72	-12.04	-12.31	-9.36

6.3.2. Load Shedding

Planning load shedding for each season is necessary for PANW microgrid 1. The microgrid should be managed according to the seasons, and night cycles. Even with the addition of the PV system, it is not possible to form the microgrid during summer without load shedding. The load demands are high compared to the generation units' production. It is costly to overcome this shortage in energy by using a storage system. The rating of storage is a tradeoff between STR cost and load shedding.

Some of the lower priority critical loads (DT and DN) would need to be shed during summer for example. Figure 6.15 shows the STR output when DN load is disconnected from the microgrid during summer. Similarly, part of DN or DT can be disconnected from the microgrid during spring and fall. The overshoot transients in the figure can be ignored since they are from the sudden disconnecting of the load model, the response is not needed for this discussion.

The strategy for shedding loads depends on many factors such as: energy storage capability, load and generation forecasting, and seasons. Additionally, the shedding scheme should be used over the course of day night variation. Case 4 shows the hourly variation of loads and generation units.

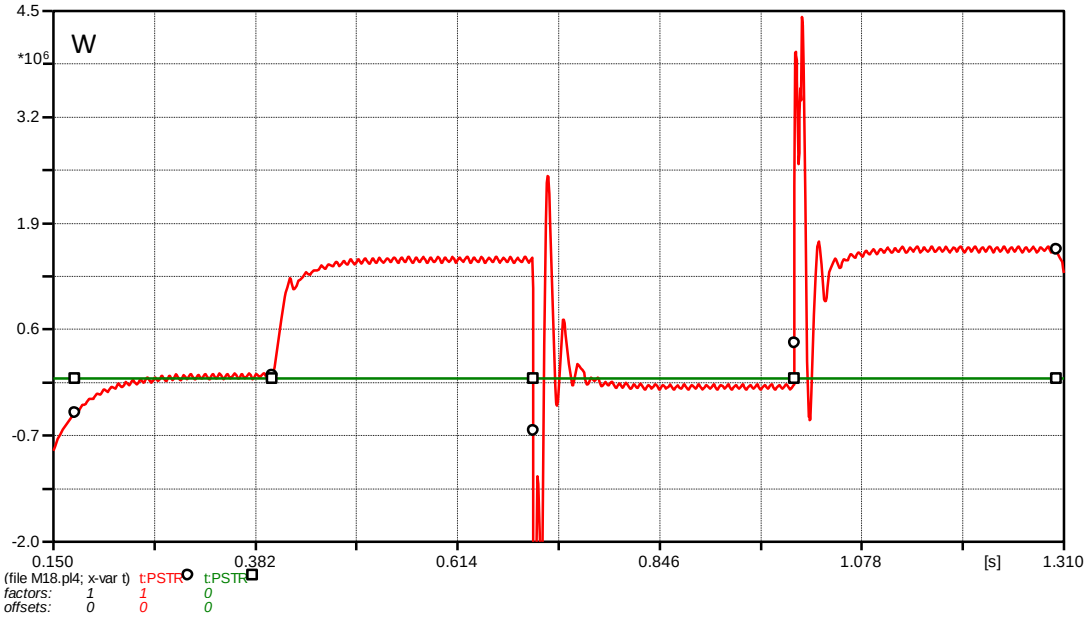

Figure 6.15. STR real power charge and discharge with PV system and shed DN load (red for P and green is the 0 reference)

6.4. Case 4: Hourly Variation

In this case, a period of 32 days is analyzed starting from the 10th of July to the 10th of August, inclusive. The hourly data (historical data from 2014) of each load and generation unit from the sponsor and the PVWatts calculation [33] are imported to the model. The model includes all the loads, generation units, capacitor banks, and PV system. In order to represent each day and hour in ATP-EMTP, the time steps are specified. As shown in Figure 6.16, every 0.01 second represents an hour. As a result, a day is represented as a 0.24 sec. and the 32 days is represented as 7.68 sec. The reasons for choosing this specific 32 days period of time are:

- HYD 1 and HYD 2 generate minimum power

- PV system produces maximum power
- Critical loads hit their peaks during those days

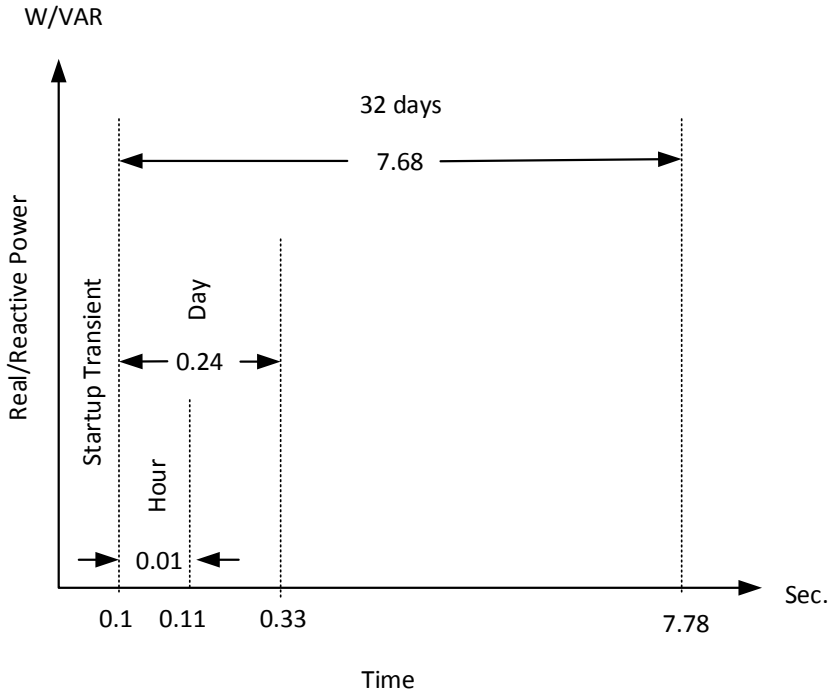

Figure 6.16. Representation of 32 days data in ATP-EMTP

6.4.1. Variable Load

The critical loads do not only vary seasonally; loads vary during day and night. This variation must also be considered. Figure 6.17 shows the total load demand for the specified 32 days. As it can be noticed, each day has a peak time. Figure 6.18 is a zoom in of two days: the first and second of August. The figure starts from the midnight of day 1 and ends at 11 pm of the second day (from 5.38 sec. to 5.85 sec.). The peak consumption appears to be around 1 pm to 4 pm for the two days, whereas the lowest load consumption appears to

be around 1 am to 6 am. The difference between the two peaks and the lowest consumptions is about 8 MW. As a result, the day-night variations have to be considered for load shedding planning and rating energy storage. For example, after checking generation forecasting at noon time, low priority loads can be disconnected before forming a microgrid.

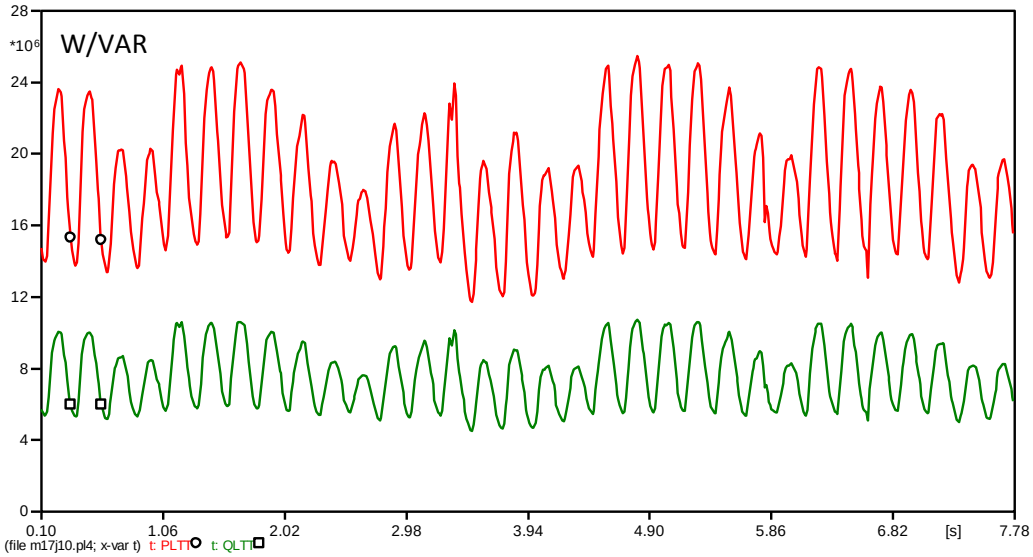

Figure 6.17. Total load's active and reactive power variation for 32 days (red for P and green for Q)

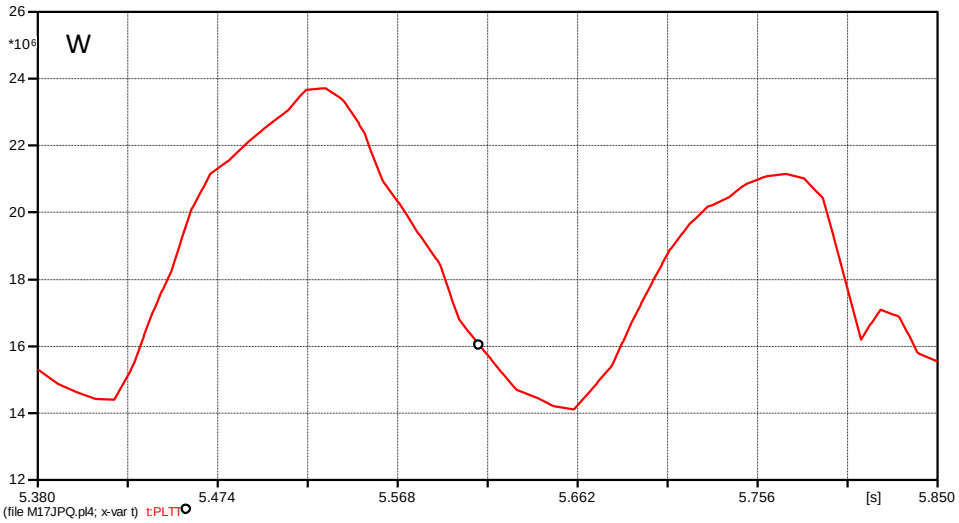

Figure 6.18. Zoomed in plot of the total load's active power at the 1st and 2nd day of August

The same thing can be done for capacitor banks. Figure 6.19 shows the reactive power of the total loads on the same two days. Similar to the real power, a reactive power peak appears around 1 pm to 4 pm. The difference between the two peaks and the lowest consumption is about 4 MVAR. The capacitors should be scheduled according to the voltage profile of the system which depends on the load demand during islanded mode.

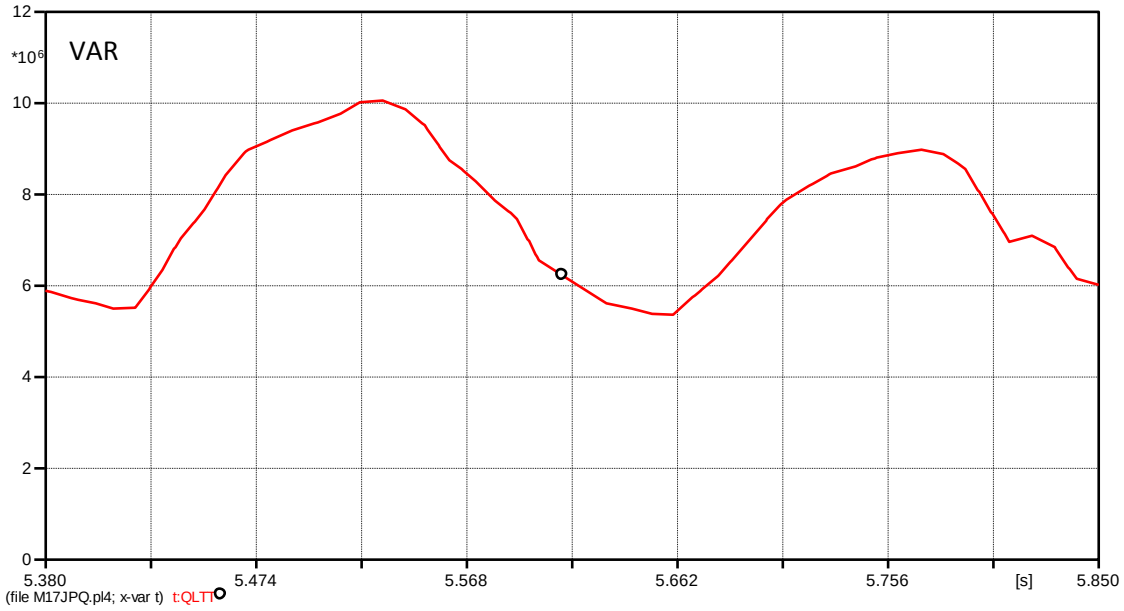

Figure 6.19. Zoomed in plot of the total load's reactive active power at the 1st and 2nd day of August

6.4.2. Variable Hydroelectric Generators

As mentioned earlier, the two hydroelectric generators are dependent on the downtown river and are controlled in a run-of-the-river mode. One of the hydroelectric generators, or both in some cases, might need to be shut down some days of the summer because of the very low water level. Figure 6.20 shows HYD 1 and HYD 2 real power

output during the 32 days. As it can be seen, HYD 1 is shut down for almost three days (July 29, 30 and 31 – 4.74 sec.-5.28 sec.). The project sponsor stated that this shutdown was due to scheduled maintenance during low flow. During islanded mode the maintenance would be need to be postponed. Even HYD 2 falls under 6 MW on some days and can be shut down in other cases.

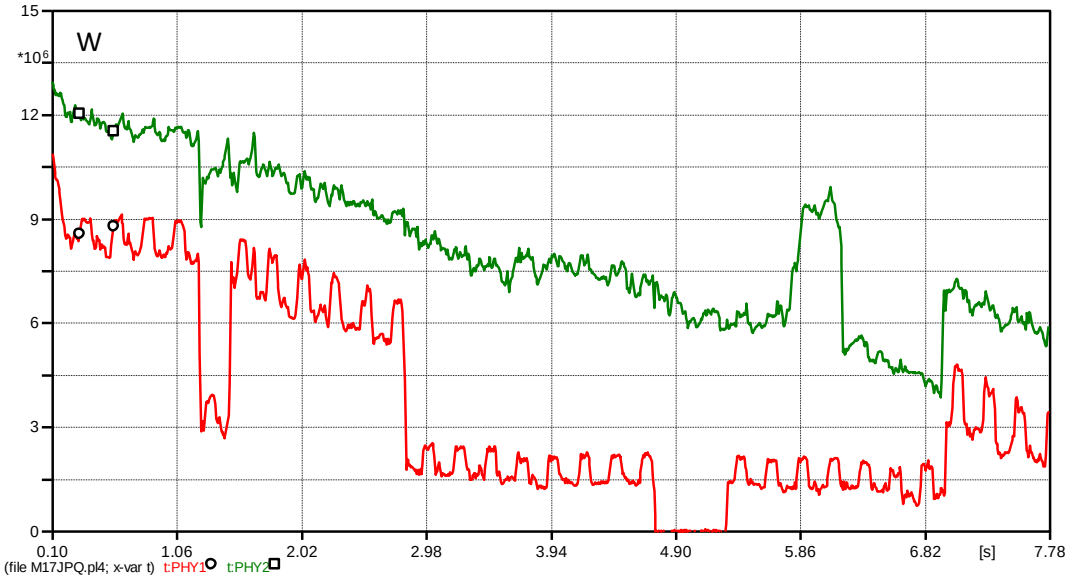

Figure 6.20. HYD 1 and HYD 2 active power for 32 days (red for HYD 1 and green for HYD 2)

Figure 6.21 shows the output from HYD 1 and HYD 2 for the first and second day of August for comparison. The variation in this case does not depend on the load since the goal is to get the maximum power from the hydroelectric generators. It can be noticed that the day-night cycle does not affect the hydroelectric generators. However, the PV system output characteristics are absolutely is based on a day-night variation.

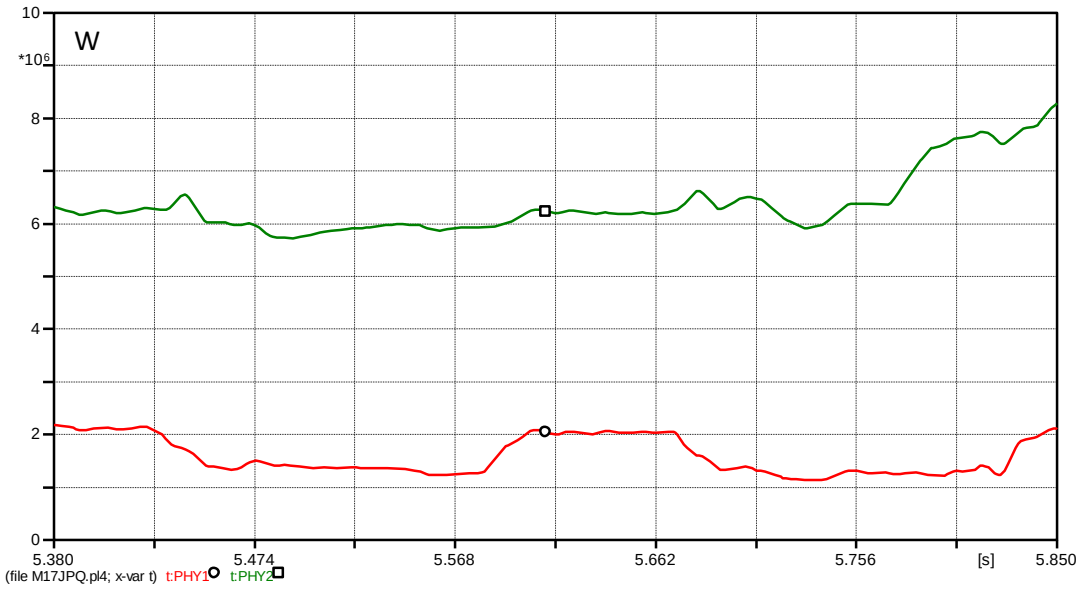

Figure 6.21. Zoomed in plot of the HYD 1 and HYD 2 active power at the 1st and 2nd day of August (red for HYD 1 and green for HYD 2)

6.4.3. Photovoltaic System

The PV system variation is significant because it produces zero real power during night time. The PV system controller allows the system to produce the maximum real power during daylight and zero reactive power. Figure 6.22 shows the real and reactive power generated by the PV system for the 32 days. The peaks every day for the installed system is between 5 MW to 6 MW during the time period.

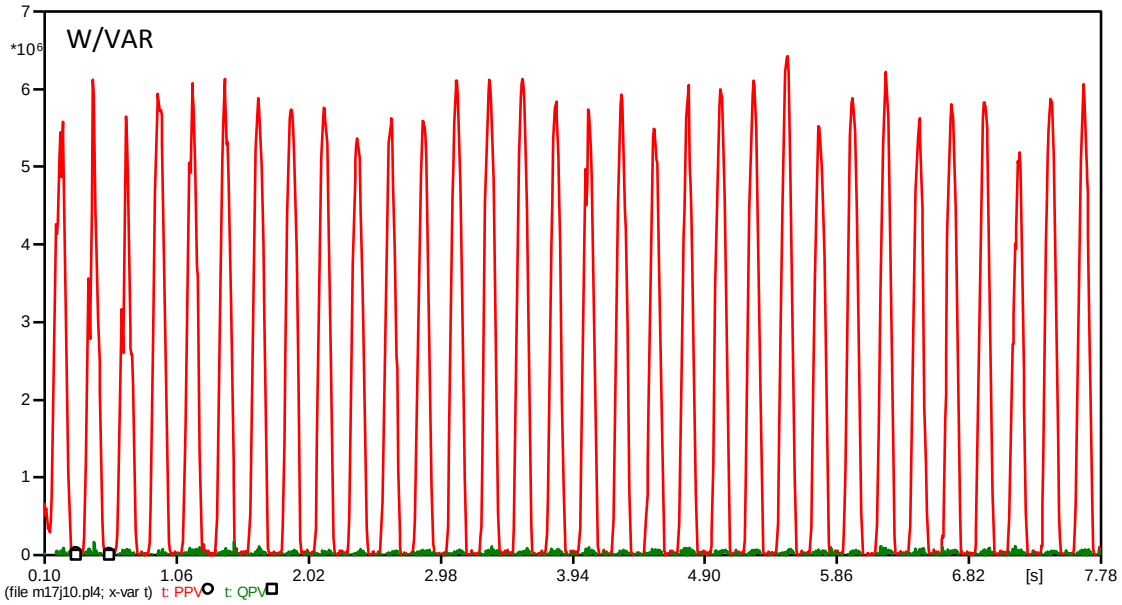

Figure 6.22. Total PV active and reactive power for 32 days (red for P and green for Q)

Figure 6.23 shows a zoomed in view of the PV system production of real power for the first and second day of August. The PV system generates real power for approximately 13 hours during summer (in clear sky). The production starts around 4 am, and stops around 6 pm. As can be seen in the figure, the peak of the real power appears from 9 am to 1 pm every day. When PV peak is compared to the load peak, there is a shift of around a three hours between the two. Figure 6.24 shows the total load consumption and the PV system production in per unit base for two days. This shift can be overcome by sizing the storage system to supply during the shortage. This can increase the benefits of having a PV system in the PANW microgrid 1.

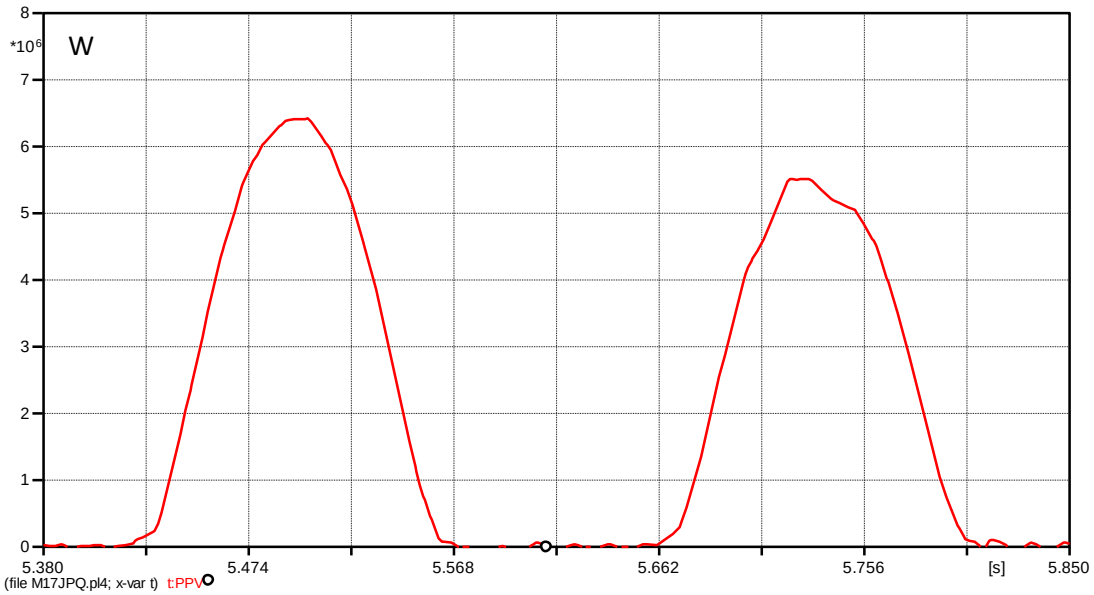

Figure 6.23. Zoomed in plot of the PV system active power at the 1st and 2nd day of August

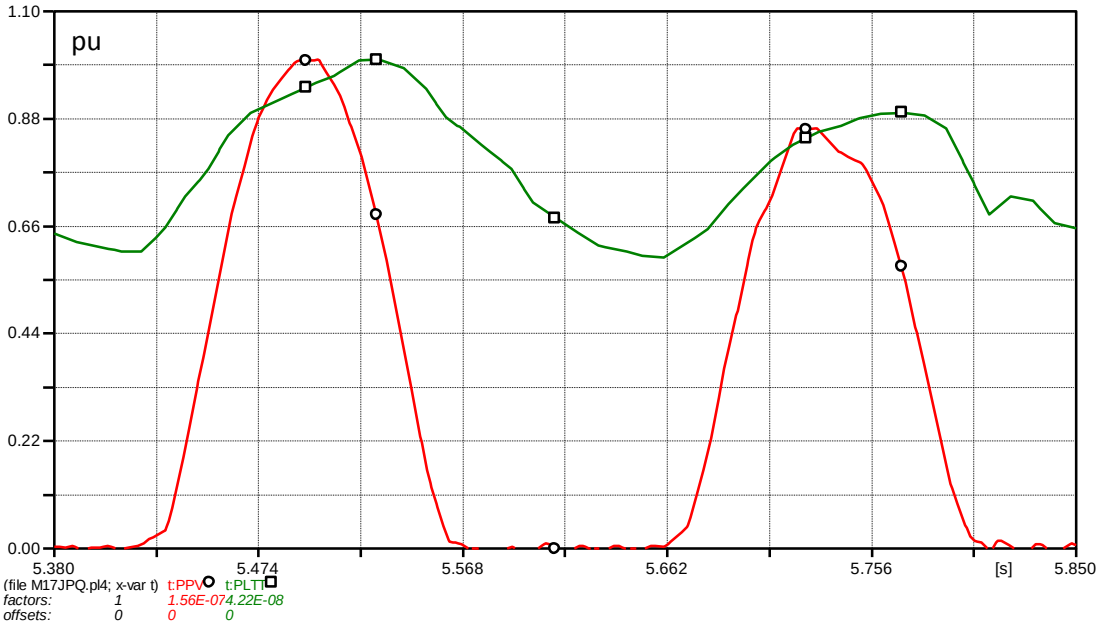

Figure 6.24. Comparing power between load and PV in a per unit base at the 1st and 2nd day of August (red for PV and green for load)

6.4.4. Storage System

The ideal STR model responds to the variation of the load mismatch over a 24 hour period. Figure 6.25 shows the STR real power charge and discharge for the 32 days. It can be seen that in some days the STR is not charging. It is costly to size a storage system which can supply this amount of energy. Instead, a planned load shedding for each season can be used to reduce rating. The storage system can be sized to balance the PV system peak with the load peak. Moreover, taking the overall day-night variation into account for sizing the storage system can be a solution for to load generation matching.

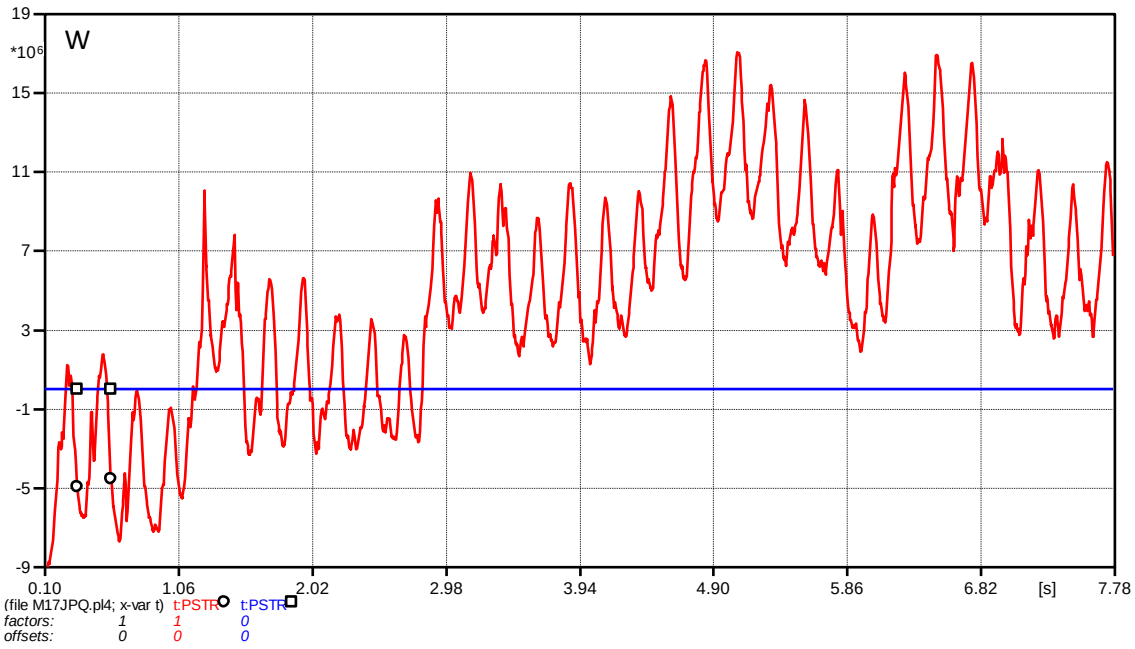

Figure 6.25. STR active power charge and discharge for 32 days (red for STR and blue is the 0 reference)

In Figure 6.26, the discharge of the STR system on the first and second day of August is shown. The difference between the highest discharge and the lowest discharge is

around 6 MW. In some days, the storage system cannot continuously supply this amount of power since it is always discharging and is never able to charge. As a result, a load shedding scheme has to be applied. The peak should be about 3 MW and the bottom should be around – 3 MW. This amount can be approximated for sizing the real power of storage system based on summer with PV system and a load shedding scheme. Figure 6.27 shows STR, PV and load power in normalized base. The point is to compare between the three. As it can be seen, the STR peak is shifted in order to fulfill the reduction on the PV system generation.

However, the amount of energy has to be calculated based on how many hours the storage supplies energy.

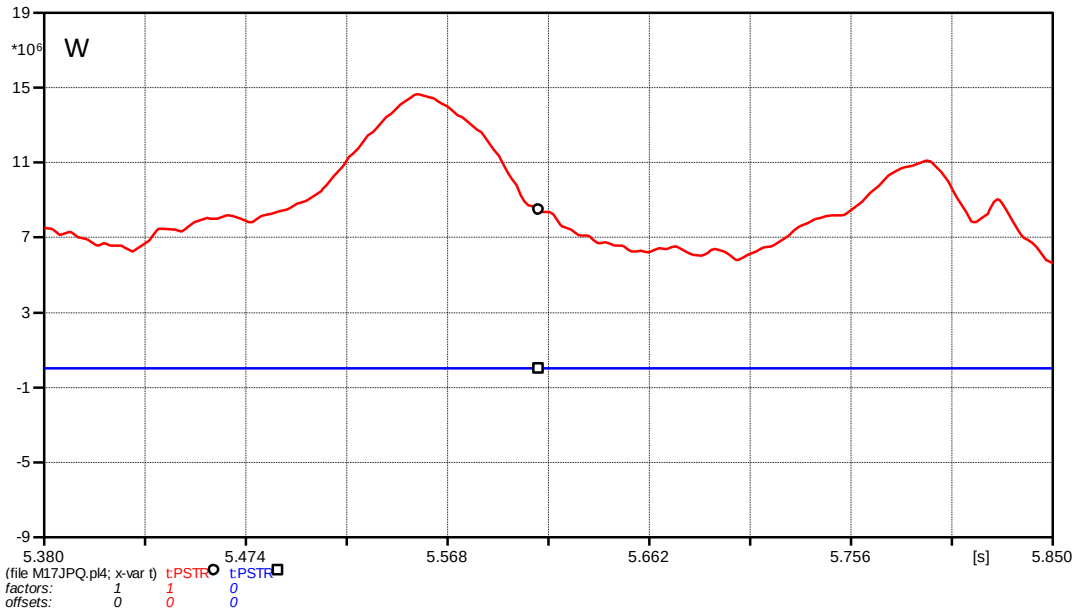

Figure 6.26. Zoomed in plot of the STR system active power at the 1st and 2nd day of August

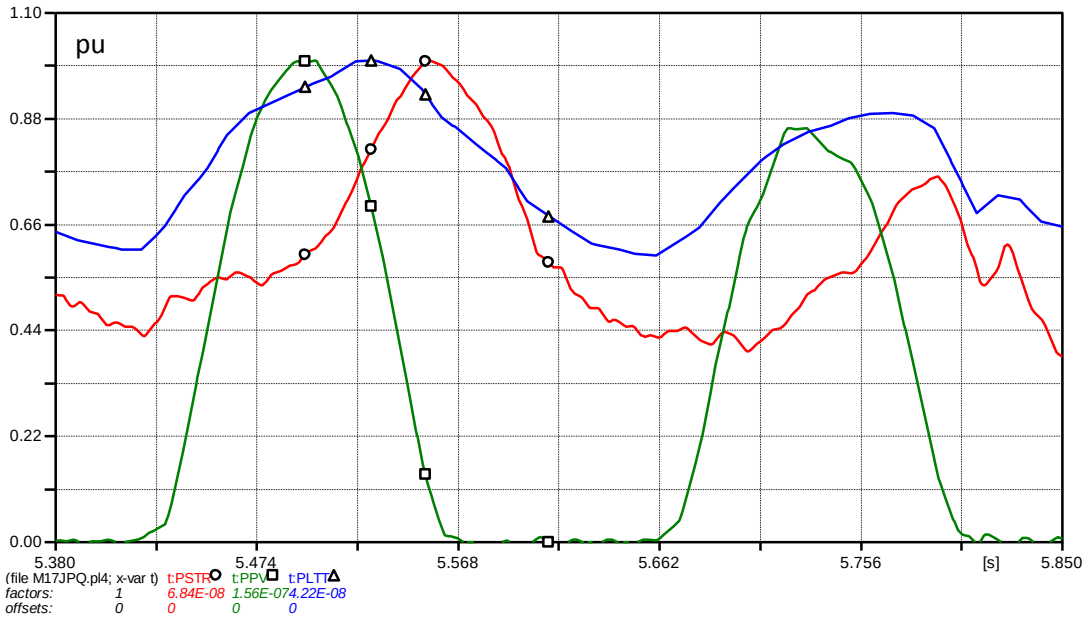

Figure 6.27. Comparing power between load, PV and STR in a per unit base at the 1st and 2nd day of August (red for STR, green for PV and blue for load)

For demonstration, the days from the 16th to the 20th of July are chosen in order to approximate the energy needed each day. The reason for choosing these specific five days is the balance between the charged and discharged energy during night and daylight over a course of each day respectively (see Figure 6.28 – the five days is from 1.54 sec. to 2.74). However, each day has similar profile and similar energy variation, again a load shedding scheme has to be used. Figure 6.29 shows the charge in stored energy in MWh at the STR for the five days, and Figure 6.30 shows the energy in MJ. Each peak represents the total charge stored energy. The sum of the peaks in each day should be near to zero when the amount of the energy is balanced during a one day period. Table 6.7 summarizes the total stored energy in each day of the five days.

Table 6.7. STR charged and discharged energy for five days (16^{th} – 20^{th} of July)

	Energy in MWh		Energy in MJ	
	Charge	Discharge	Charge	Discharge
16^{th} of July energy	-2.26	3.85	-8140	13850
17^{th} of July energy	-1.84	3.56	-6600	12800
18^{th} of July energy	-2.2	2.4	-7950	8680
19^{th} of July energy	-3.26	1.86	-11750	6700
20^{th} of July energy	-2.69	1.3	-9680	4720
Five days averaged energy	-2.45	2.59	-8824	9350

The size of the storage system should be based on daily variation since the power system varies over the course of the day. The idea is to charge the storage system during night (low demand) and discharge the storage during the day (high demand). An average of the three days of the energy needs is calculated. A suggested size of the storage system is 2.5 MWh. However, as noted earlier, a load shedding scheme is needed in order to efficiently operate microgrid 1.

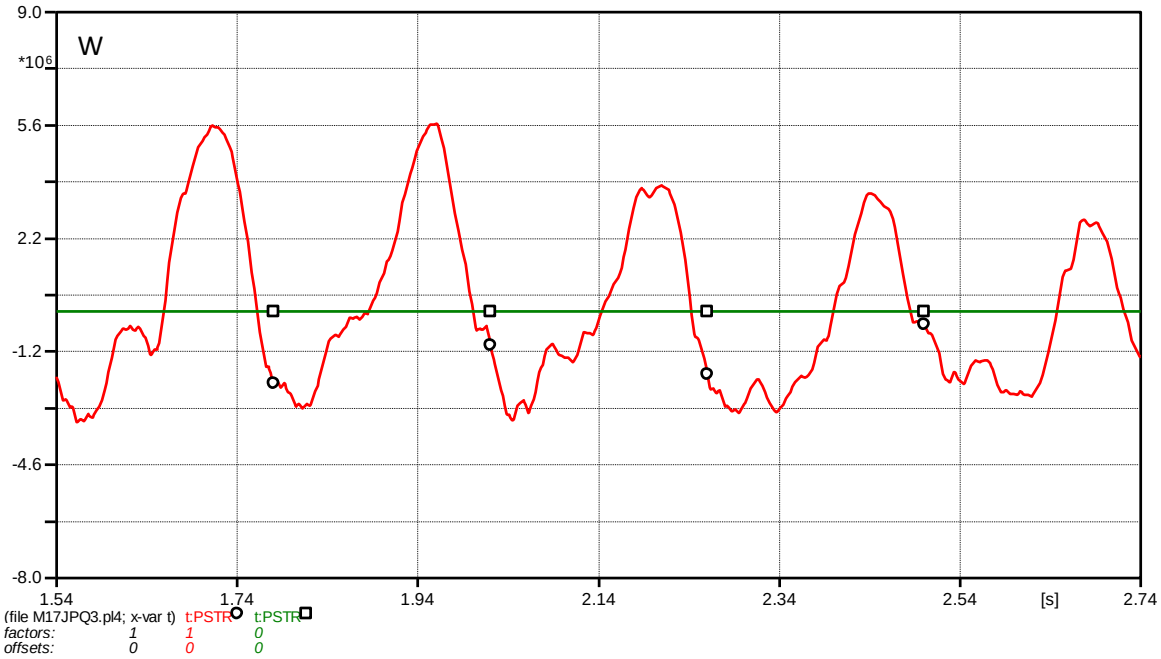

Figure 6.28. Zoomed in plot of the STR system active power in MW from the 16st to the 20th day of July (red for STR MW, green is the 0 reference)

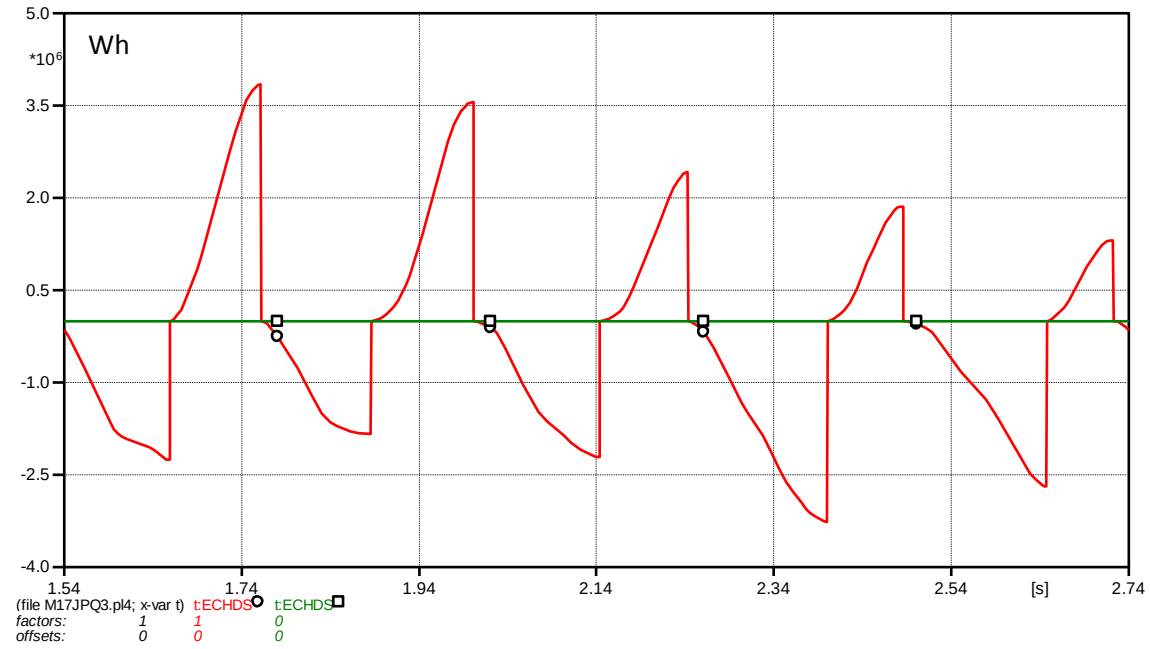

Figure 6.29. STR energy charge and discharge in MWh for 5 days from the 16st to the 20th day of July (red for MWh, green is the 0 reference)

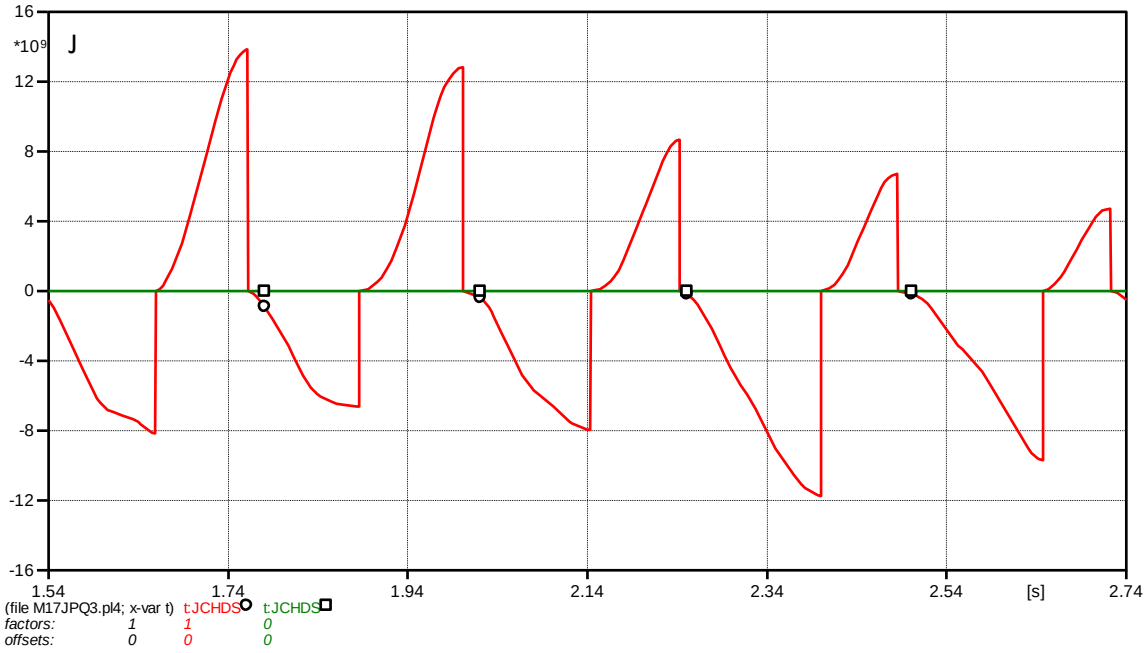

Figure 6.30. STR energy charge and discharge in MJ for 5 days from the 16st to the 20th day of July (red for MJ, green is the 0 reference)

Figure 6.31 shows the 18th of July hourly energy in MWh in order to visualize the peak stored energy. As expected, the high discharge from the STR occurs from 4 pm to 9 pm. The discharge peak is about 3.7 MWh which occurred in the hour starting at 6 pm.

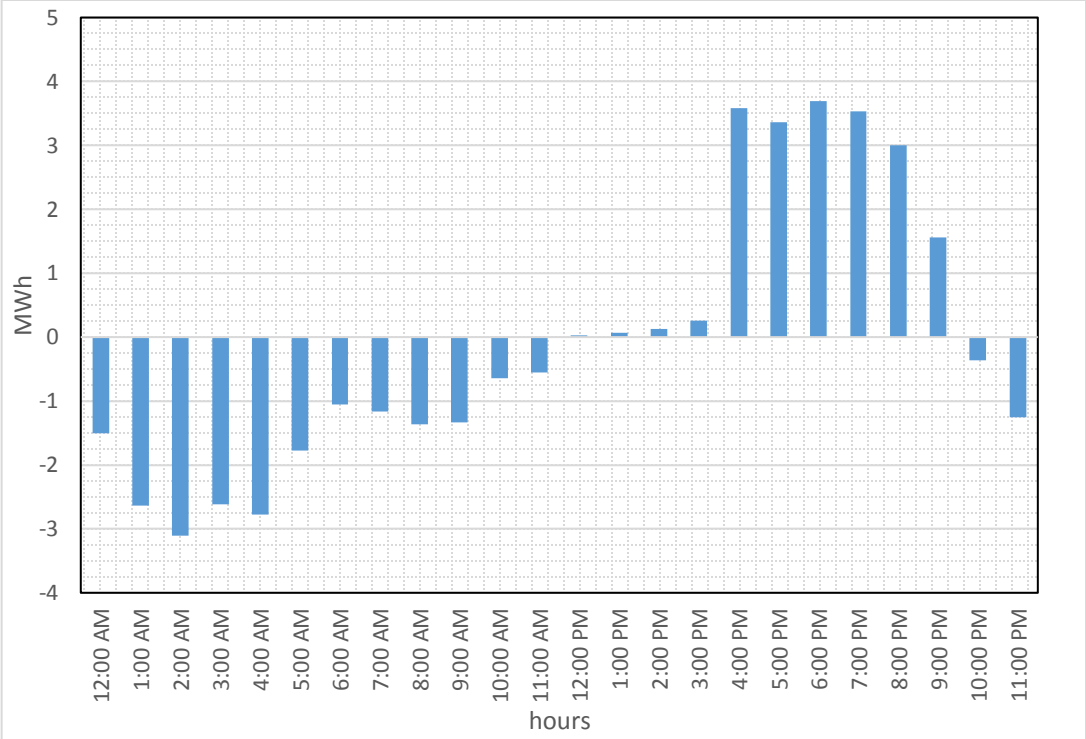

Figure 6.31. STR hourly energy in MWh charge and discharge at the 18st of July

The rating of the storage system is a tradeoff between the storage system cost and load shedding. To make a more reliable microgrid system, the storage system should be sized to cover the worst case scenarios. For example, the storage system can be sized to supply high load demands during periods of very low production from both the PV system and the hydroelectric generators. The size of the storage depends on how much of the critical loads have to be supplied in each case. However, load will also need to be lower if it is cloudy and PV production is reduced.

In this study, the size of the storage is not based on the worst case. It is based on the five days on summer season used as an example. The summer season has low total hydroelectric production, high total PV system generation, and high total load demand. This

approximation can be effective most the time. However, it may not be as effective during abnormal conditions such as cloudy days, hydroelectric generator shutdown, and very high load demand. Moreover, hydroelectric generators may produce low power during spring and winter during dry years (as discussed in Chapter 4 - Figure 4.3 shows the variation of the river discharge). It can be challenging to supply all the critical loads since the PV system is not generating its maximum power. As a result, the PMS/EMS schemes can manage the microgrid by shedding more load.

6.5 Summary

This study contributes to achieve part of the project goal, which is to verify whether it is feasible to form a microgrid in part of the PANW city. The study focuses on developing an energy management scheme in order to enhance the PANW microgrid system. In this study, the ATP-EMTP program is used to study the system in the time domain. One of the benefits of using the time domain is to represent the generation/load variation over time.

The study supports part of the project and the work of other groups who are working on the same project. One of the groups is using Powerworld program in order to model the PANW microgrid system. The Powerworld model is used to represent the system in the phasor domain. As a result, it is not easy to represent the generation/load variation over time. Also, the full PV system model cannot be represented in Powerworld. The contribution of this study is to provide seasonally and hourly variation studies of microgrid 1, and enhance the system by adding a PV system and sizing a storage system based on these variations.

Chapter 7: Planning Considerations for Future Work and Analysis

In this chapter, some of the planning considerations related to this study are discussed. PANW city microgrid is to be formed on an existing grid, and as a result the existing grid components, generator variation, and load profiles need to be considered. Reliability, quality, and resilience of the system, are discussed. Additionally, some considerations from IEEE Standard 1547.4 are included [22].

7.1. Existing Power Grid and Control System

As a first step, the microgrid configuration for the existing power grid has been chosen based on the generators and loads physical locations (Figure 7.1). The PCCs are identified based on the main feeders and buses. The microgrid boundary during islanded mode is defined, along with which parts of the grid should be connected and disconnected. Finding exactly how many/what types of transformers, transmission lines, circuit breakers, etc. is important. The physical location of each component is useful for configuring the microgrid geographical borders inside the power system grid.

The next step involves collecting the power system parameters for modeling purposes. The length, power limit, type (overhead or underground) of transmission line and distribution feeder is collected. Also, the resistance, inductance, and capacitance parameters are gathered. For the power transformers, the configuration, rating, voltage level, saturation data, and impedance parameters are collected. Additionally, the location of each capacitor bank complete with their ratings are obtained. Generators parameters, data, and ratings are

collected and used in the model as well. In addition, cold load pickup and warm load pickup, which were not studied in this thesis, need to be addressed. The issues to consider include:

- Transmission energizing currents
- Transformer magnetizing inrush currents
- Motor starting inrush currents

Figure 7.1 shows a flow chart of the planning steps.

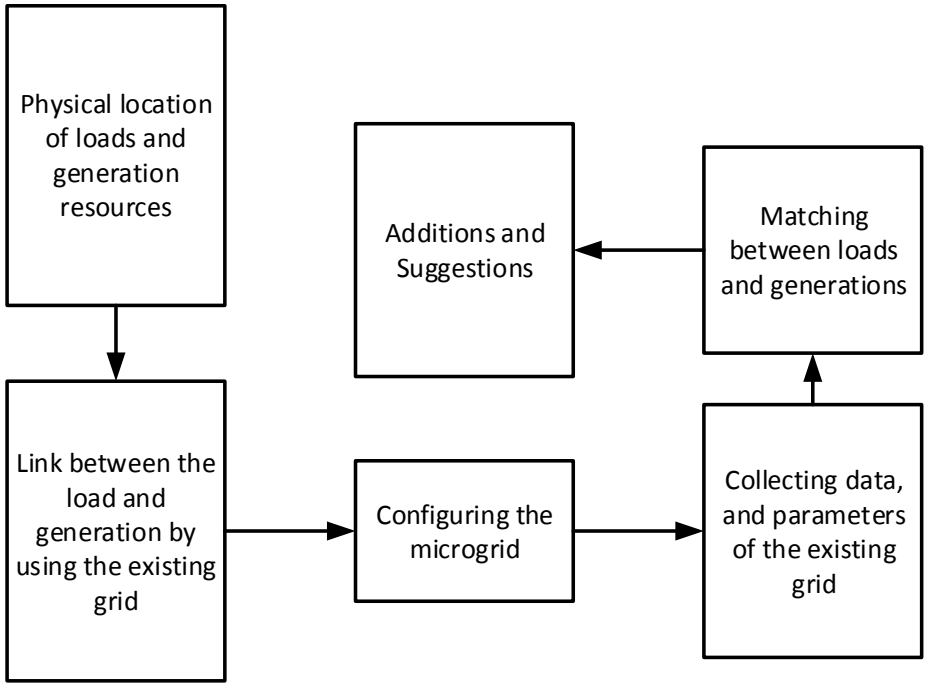

Figure 7.1. Summary of the planning steps

An inventory of the available controls for the generation and loads through the distribution management system (DMS) that can be ported for controlling the microgrid is needed. Moreover, monitoring the system and obtaining data are also key points. For example, the microgrid can use an existing Supervisory Control and Data Acquisition

(SCADA) system for monitoring and controlling the microgrid. But, this needs to be reconfigurable.

However, the control should be adjusted in order to control the microgrid separately from the rest of the power grid during islanded mode. Also, since microgrid systems need to have extra monitoring and control, the existing SCADA system might need to be expanded inside the microgrid. Additionally, remotely control of PCC circuit breakers is needed for isolating the microgrid, and for load shedding schemes.

7.2 Load Considerations

The main purpose of forming microgrid is to efficiently and continuously supply the most important loads. Since the microgrid has limited and variable generation sources, load profiles are equally as important as the generation profiles. The power consumption data is obtained for each load in order to study the hourly/monthly behavior. Each type of load tends to have a different demand profile. Depending on the month or time of the day, the total demand must be maintained during islanded mode. Moreover, loads are divided into three types depending on the priorities: high, medium, and low priority. Additionally, reference [22] states many considerations related to loads such as:

- Large spot loads such as motors
- Realistic profile of the instantaneous loads (P and Q)
- Load imbalance
- Current imbalance
- Ripple

- Cold load pickup
- Steady-state reactive power demands
- Dynamic reactive power demands such as motor starting

7.3 Generation Resources

The existing generation was studied in detail earlier to obtain profiles that can be used to check the load and generation matching. It is important to plan for intentional and unintentional islanding events; generators should be able to supply real and reactive power for both cases. After studying the existing generation profiles, the potential of adding new distribution resources should be studied. For example, PV systems are considered in this thesis after collecting information and data about the geographical area. The control system for each source is checked and adjusted to work during islanding modes. Reference [22] has some considerations related to distributed resources such as:

- Reactive power capabilities
- Non-participating generation resources; such as PV systems
- Plan for generation outage by planned load or load shedding scheme
- Undervoltage and underfrequency conditions

7.4 Human in the Loop

In the PANW city microgrid, some of the loads, fuses, and circuit breakers have to be switched manually; the operation crew should have a plan for switching them on and off.

The time needed for these processes has to be measured. For example, during a planned islanding, the total time of the switching procedures has to be considered. This time period, along with time needed for activating microgrid's controls and settings for islanding mode should be determined. The result period is called the transition time. The transition can be called a planned transition when the timing of the transition and the duration of the mode operation is known. On the other hand, unplanned transitions can be due to abnormal conditions such as long duration faults. The planned transition between non-islanding and islanding is a key point for the operating system. In addition, a planned transition between islanding and non-islanding can have a different period of time, so it must be considered.

As was described earlier, the microgrid most likely needs to have control systems that are activated during the islanded modes. The operators have to be aware of this transition, and should be trained to move from the traditional control to islanded mode control. Not only do the operators in the control rooms need to have this knowledge, field operators and maintenance crews should be in the loop of this transition. The maintenance schedules of some of the components inside the microgrid should also be considered. For example, some maintenance might need to be postponed during islanded mode. Rescheduling switching some shunt-connected capacitor banks and shunt reactors are one of the important consideration for operators. Moreover, attention to general public and operators' safety is substantial.

7.5 Reliability, Quality, and Resilience

Even though microgrids are considered a great solution for supplying loads during blackouts and power outages, microgrid systems might be less reliable than a normal system. As reference [22] states, "operating distributed generators may reduce reliability due to increased system complexity." This is true since the power system has more than one mode. Control, protection, and power systems have different settings for each mode. In addition, some extra equipment should be added to the microgrid system. Some of this equipment should be active only during islanded or non-islanded mode (for example, capacitor banks).

As the reliability maybe reduced, there is a good chance that power quality could be reduced as well. Reference [22] indicates that possible reduction in power quality is expected. An islanded microgrid system is often weaker than is the case in grid connected operation. During non-islanded mode, the system is connected to the main power system which includes thousands of generation resources connected to transmission lines and which tends to be a stiff system. This reduces concern when experiencing a change in the load, or faults. On the other hand, these minor events can raise issues during islanded mode. When the microgrid is disconnected from the rest of the power system, the energy is limited to only generation resources and storage systems that are contained inside the microgrid. For example, if for any reason there is a shortage in real or reactive power, the frequency, voltage magnitude or both can be effected. As a result, customers may experience power quality issues such as voltage drop (sag), fluctuation, or interruptions. In the worst case, the system may face a blackout.

In order to truly get the benefits of utilizing a microgrid system, some resilience must be added to the system. Resilient plans for outages, generation shortages, unexpected load demands, severe weather or even cloudy days are critical. Studying these type of events before they occur, and finding more than one solution, can make the system more reliable and resilient. In addition, resilient systems are more flexible for accepting new resources that will be added to the distribution system.

Chapter 8: Summary, Conclusions and Future Work

The chapter summarizes, and provides conclusions for the second topic of the thesis. In addition, limitations and future work for this topic are discussed. Note that Section 2.6 provided conclusions and future work for the study of impacts of STATCOMs on distance protection.

8.1 Summary

The second topic of the thesis develops a microgrid energy management scheme for a PANW City during islanded mode. The study includes background information about microgrid concepts and management, and analyzes generation resource availabilities and the critical load profiles for the system at hand. Moreover, an ATP-EMTP model is developed and used to represent the power grid and the control system. The program is used to model the hydroelectric generator, PV system, and variable loads. The models include control systems, although only steady state operating points are needed.

The simulation results for each study case are presented. The first study case shows the microgrid seasonal peak load and generation variation per season built from averages of several peak years. Each critical load and generation resource is represented in a model that varies seasonally. The case studies looked at the system with added distribution capacitor banks, and then a PV system, and the load shedding. The fourth case presents the microgrid variation per hour. Part of the summer is chosen for demonstration. Generation units, and loads are compared with the storage system in order to characterize the shortage during

islanded mode. Suggested solutions and planning considerations are discussed for managing the power and energy inside the PANW City microgrid.

8.2 Conclusions

The objective of the second topic is to develop an energy management scheme for the PANW City, and as part of a study of the feasibility of forming the PANW microgrid by adding a PV system and energy storage, load shedding, and capacitor banks. By looking to the results from the study cases, it can be said that it is possible to form microgrid in the PANW city. However, the performance can be improved by adding other generation sources such as PV systems, using load shedding schemes, adding a storage system sized based on the day/night and seasonal variation, and adding distribution capacitor banks. These additions can be beneficial to the PANW microgrid. The combination of the existing power system components and the additional components enhances the microgrid.

A PV system has been chosen as an additional generation resource due to its effectiveness in this particular city. The PV system can produce its maximum power during summer when the hydroelectric generators produce their minimum power. The PV system generates its power during daylight when the total load demand is at its peak. As a result, the PV system can support the shortage in energy inside the microgrid during low hydroelectric production, and during high load consumption. Moreover, adding a storage system is an important addition in order to have a reliable microgrid system. The storage system can fulfill the gap between the peak of the load consumption and the PV system production

instead of shedding loads. The storage system also can be used to ride-through the dynamic variations of the PV system.

Additionally, the energy inside the microgrid can be managed by using appropriate load shedding schemes based on the variation of the energy and power. Low priority loads should be shed during high load demand and low power generation. Also, disconnecting the transmission level capacitor banks and adding distribution capacitor banks results in acceptable voltage profile by supplying reactive power to the microgrid system.

8.3 Limitations

In this thesis, part of the existing power grid is evaluated and modeled. However, not all of the power grid is modeled in detail; steady state models are used for hydroelectric generators and transformers. The hydroelectric generators are represented as controlled voltage and current sources instead of full synchronous machines. The model is limited to this type of study which represents hourly and seasonally variation. For example, it cannot be used for fault studies, or to represent machine dynamic response. Moreover, the model does not to control the reactive power output from hydroelectric generators. Instead, the reactive power is held constant.

The thesis also provides a study and model for a specific microgrid during islanded mode. The model assumes that microgrid (PANW City) is successfully switched to islanded mode. The transition from grid connected mode to islanded mode is not investigated; the processes can be challenging and is beyond the scope of this thesis. For example, at the distribution level, non-critical loads are disconnected from the microgrid without

considering their circuit breakers and fuses. Some of these circuit breakers have to be disconnected manually which increase the time to form the microgrid. It might be necessary to consider replacing fuses and circuits with switches controlled over SCADA in order to remotely disconnect the loads. Moreover, PCCs and the synchronization between the main power grid and the microgrid are not examined here.

The storage system is represented as an ideal device that can supply real and reactive power. Accurate models of energy storage systems can improve the model by testing the microgrid within the availability of energy but with a cost trade off due to losses and response time. In addition, critical loads are currently modeled to consume reactive power based on their worst case power factor. Including variation in power factor can be beneficial for studying voltage profiles at each bus. Distribution capacitor banks can also be more accurately scheduled daily and seasonally, or better managed using an active volt/var scheme.

8.4 Future Work

The dynamics of the PANW City microgrid need to be studied in a small time scale in order to examine the dynamic response associated with each component. For example, the transmission lines have charging current, and transformers experience saturation and draw magnetizing inrush currents when they are first connected. Moreover, cold load or warm load pickup can be an issue if the microgrid is formed by shutting everything down and then restarting. Since capacitor banks are added to the microgrid, the transient associated with connecting and disconnecting the banks can affect the system.

Additionally, the stability of the microgrid system is one of the most important parts to study since the microgrid is considered a weak system with limited generation resources. Planned and unplanned transitions between non-islanded mode to islanded mode and back also is a substantial study. There will also be a dynamic response each time a load is picked up or dropped. All these cases are important need to be examined to evaluate system stability.

Using detailed models can improve the outcome from the simulations. For example, representing a storage system in detail with limited energy capacity and power rating is an important aspect. In addition, the hydroelectric generators should be modeled as synchronous machines along with governor and exciter control systems. The variation of the river can be correlated with the mechanical power in the governor control system in order to represent the hourly, and seasonally variation.

The results in this thesis examine some scenarios but not all. The case studies can be expanded to cover more situations such as cloudy days and partly cloudy days, a hydroelectric unit outage, and a sudden load pickup or rejection. Optimum PV system rating, storage system sizing, and load shedding schemes should also be taken into consideration (considering system constraints). Moreover, the locations for some components such as the storage system model, PV system, capacitor banks have to be examined.

For improving the overall study cases, real time model with accurate controllers should be added. Having hardware-in-the-loop testing will accurately demonstrate the behavior of the PANW city microgrid. Different scenarios can be tested with the real time model to evaluate the microgrid efficiency and reliability.

References

[1] H. Samkari, M. Allehyani and B. K. Johnson, "Modeling and simulation the impacts of STATCOMs on distance protection," *North American Power Symposium (NAPS), 2015*, Charlotte, NC, 2015, pp. 1-5.

[2] Varma, R.K., "Introduction to FACTS Controllers," *Power Systems Conference and Exposition, 2009. PSCE '09. IEEE/PES*, pp.1,6, 15-18 March 2009

[3] R. I. Amirnaser Yazdani, *Voltage-sourced Converters in Power Systems.* New Jersey: John Wiley & Sons, Inc., 2010

[4] Abande, G.B., Satarkar, M.F.A.R., Rawoot, M.H. and Thakre, M.; Kale, V.S., "Impact of STATCOM on distance relay," *Circuit, Power and Computing Technologies (ICCPCT), 2014 International Conference on*, pp.809,813, 20-21 March 2014

[5] Schweitzer, E.O and Altuve, H.J, *Modern Solutions for Protection, Control, and Monitoring of Electric Power System.* Pullman: Schweitzer Engineering Laboratories, Inc., 2010

[6] Blackburn, J.L and Domin, T.J, *Protective Relaying Principles and Application.* 4th Ed. NewYork: Taylor & Francis Group, LLC, 2014

[7] Albasri, F.A., Sidhu, T.S. and Varma, R.K., "Performance Comparison of Distance Protection Schemes for Shunt-FACTS Compensated Transmission Lines," *Power Delivery, IEEE Transactions on* , vol.22, no.4, pp.2116,2125, Oct. 2007

[8] Salemnia, A., Khederzadeh, M. and Ghorbani, A., "Impact of static synchronous compensator (STATCOM) on performance of distance relay," *PowerTech, 2009 IEEE Bucharest,* pp.1,8, June 28 2009-July 2 2009

[9] Karbalaye Zadeh, M., Akmal, A.A.S. and Ravaghi, H., "Analysis of impedance relaying procedure effected by STATCOM operation," *Power Electronics and Intelligent Transportation System (PEITS), 2009 2nd International Conference on* , vol.1, pp.256,261, 19-20 Dec. 2009

[10] Liu Qing, and Wang Zeng-ping; Zhang Yuan, "Study on a Novel Method of Distance Protection in Transmission Line with STATCOM," *Power and Energy Engineering Conference (APPEEC), 2010 Asia-Pacific* , pp.1,5, 28-31 March 2010

[11] Hemasundar, D., Thakre, M. and Kale, V.S., "Impact of STATCOM on distance relay - Modeling and simulation using PSCAD/EMTDC," *Electrical, Electronics and Computer Science (SCEECS), 2014 IEEE Students' Conference on* , pp.1,6, 1-2 March 2014

[12] U.S. Department of Energy. 2016. *The Role of Microgrids in Helping to Advance the Nation's Energy System* [Online]. Available: http://energy.gov/oe/services/technology-development/smart-grid/role-microgridshelping-advance-nation-s-energy-system. (URL) date accessed: 2016, May 20.

[13] R. H. Lasseter, "MicroGrids," *Power Engineering Society Winter Meeting, 2002. IEEE*, 2002, pp. 305-308.

[14] B. Kroposki, R. Lasseter, T. Ise, S. Morozumi, S. Papathanassiou and N. Hatziargyriou, "Making microgrids work," *in IEEE Power and Energy Magazine*, vol. 6, no. 3, pp. 40-53, May-June 2008.

[15] D. E. Olivares et al., "Trends in Microgrid Control," *in IEEE Transactions on Smart Grid*, vol. 5, no. 4, pp. 1905-1919, July 2014.

[16] M. Barnes et al., "Real-World MicroGrids-An Overview," *2007 IEEE International Conference on System of Systems Engineering*, San Antonio, TX, 2007, pp. 1-8.

[17] F. Katiraei, R. Iravani, N. Hatziargyriou and A. Dimeas, "Microgrids management," *in IEEE Power and Energy Magazine*, vol. 6, no. 3, pp. 54-65, May-June 2008.

[18] *IEEE Standard for Interconnecting Distributed Resources with Electric Power Systems - Amendment 1*, IEEE Standard 1547a, 2014.

[19] *IEEE Standard Conformance Test Procedures for Equipment Interconnecting Distributed Resources with Electric Power Systems*, IEEE Standard 1547.1, 2005.

[20] *IEEE Application Guide for IEEE Std 1547(TM), IEEE Standard for Interconnecting Distributed Resources with Electric Power Systems,* IEEE Standard 1547.2, 2009.

[21] *IEEE Guide for Monitoring, Information Exchange, and Control of Distributed Resources Interconnected with Electric Power Systems,* IEEE Standard 1547.3, 2007.

[22] *IEEE Guide for Design, Operation, and Integration of Distributed Resource Island Systems with Electric Power Systems*, IEEE Standard 1547.4, 2011.

[23] *IEEE Recommended Practice for Interconnecting Distributed Resources with Electric Power Systems Distribution Secondary Networks*, IEEE Standard 1547.6, 2011.

[24] *IEEE Guide for Conducting Distribution Impact Studies for Distributed Resource Interconnection*, IEEE Standard 1547.7, 2014.

[25] *IEEE Guide for Smart Grid Interoperability of Energy Technology and Information Technology Operation with the Electric Power System (EPS), End-Use Applications, and Loads*, IEEE Standard 2030, 2011.

[26] *IEEE Standard Technical Specifications of a DC Quick Charger for Use with Electric Vehicles*, IEEE Standard 2030.1.1, 2016.

[27] *IEEE Guide for the Interoperability of Energy Storage Systems Integrated with the Electric Power Infrastructure*, IEEE Standard 2030.2, 2015.

[28] Karabanov, S., Kukhmistrov, Y., Miedzinski, B. and Okraszewski, Z., "Photovoltaic systems," *Modern Electric Power Systems (MEPS), 2010 Proceedings of the International Symposium* , pp.1,5, 20-22 Sept. 2010

[29] Home Power. 2016. Picture [Online]. Available: http://www.homepower.com/sites/default/files/articles/ajax/docs/10_Wilensky-block diagram.jpg. (URL) date accessed: 2016, May 14.

[30] A. Tuohy et al., "Solar Forecasting: Methods, Challenges, and Performance," *in IEEE Power and Energy Magazine*, vol. 13, no. 6, pp. 50-59, Nov.-Dec. 2015.

[31] United States Geological Survey (USGS). 2015. Data [Online]. Available: https://www.usgs.gov/. (URL) date accessed: 2015, Dec. 10.

[32] National Renewable Energy Laboratory (NREL). 2015. Data [Online]. Available: http://www.nrel.gov/. (URL) date accessed: 2015, Dec. 2.

[33] PVWatts Calculator. 2016. Data [Online]. Available: http://pvwatts.nrel.gov/. (URL) date accessed: 2016, May 4.

[34] R. H. Lasseter, et at., *Electromagnetic Transients Program (EMTP) Workbook IV*. EPRI Report EL-4651-V4, 1986-89

[35] *IEEE Recommended Practice for Monitoring Electric Power Quality*, IEEE Standard 1159, 2009.

Appendix A: Impacts of STATCOMs on Distance Protection

A.1. ATP-EMTP Power System Model

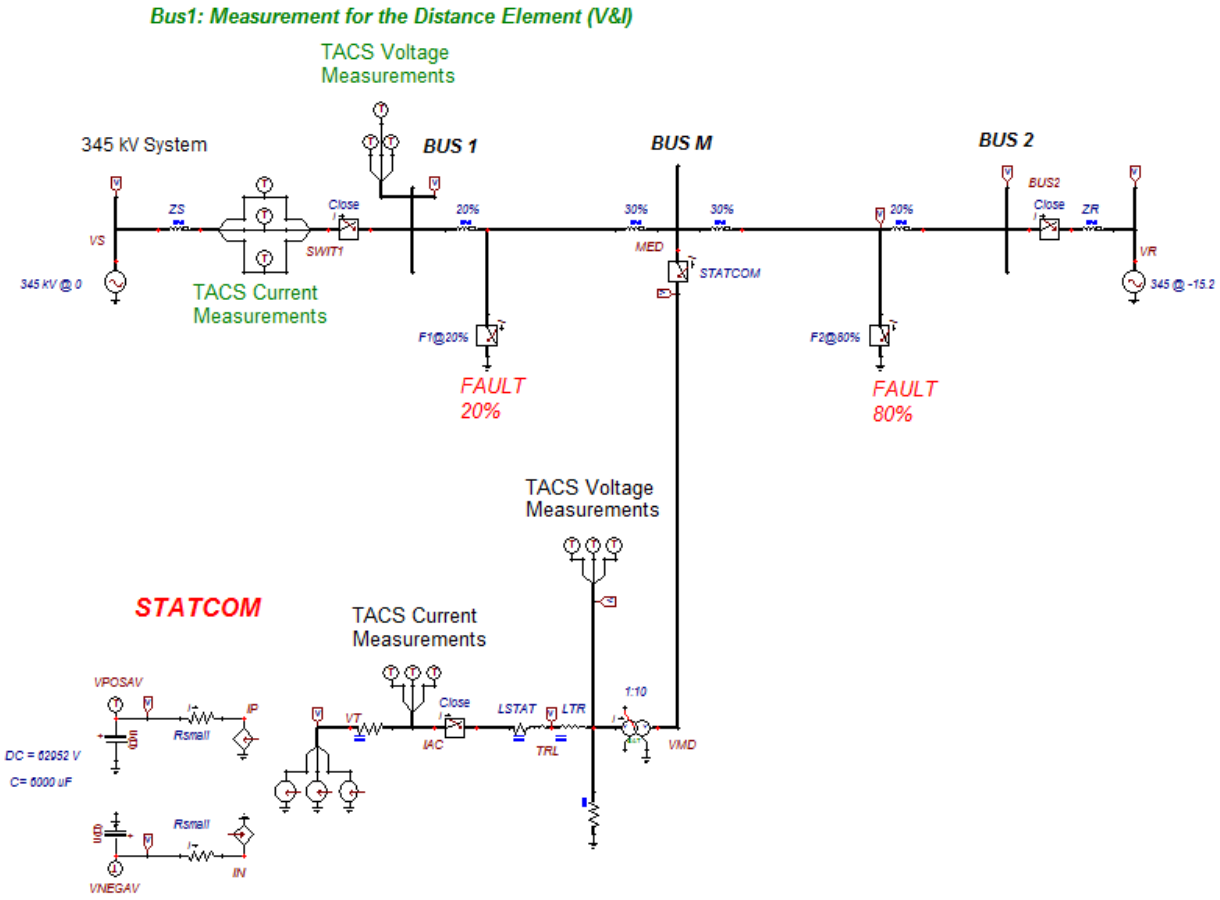

Figure A.1. ATP-EMTP power system model

- **Power System Parameters:**

Positive sequence sending end source impedance:

Z_{s1}= (0.238 + j 5.72) ohm

Zero sequence sending end source impedance:

Z_{s0}= (2.738 + j 10) ohm

Positive sequence receiving end source impedance:

Z_{r1}= (0.238 + j 6.19) ohm

Zero sequence receiving end source impedance:

Z_{r0}= (0.833 + j 5.12) ohm

Positive sequence line impedance (length = 100 km):

Z_{line1}= (0.028 + j 0.507) ohm/km

Zero sequence line impedance (length = 100 km):

Z_{line0}= (0.275 + j 1.404) ohm/km

STATCOM's external impedance:

Z_{stat_lead}= (0.00588 + j 0.26012) ohm

STATCOM's power transformer impedance:

Z_{xfmr}= j 0.15 pu S_{base}= 100 MVA

STATCOM's DC side capacitor:

C_{cap}= 6000 uF

A.2. ATP-EMTP Control System Model

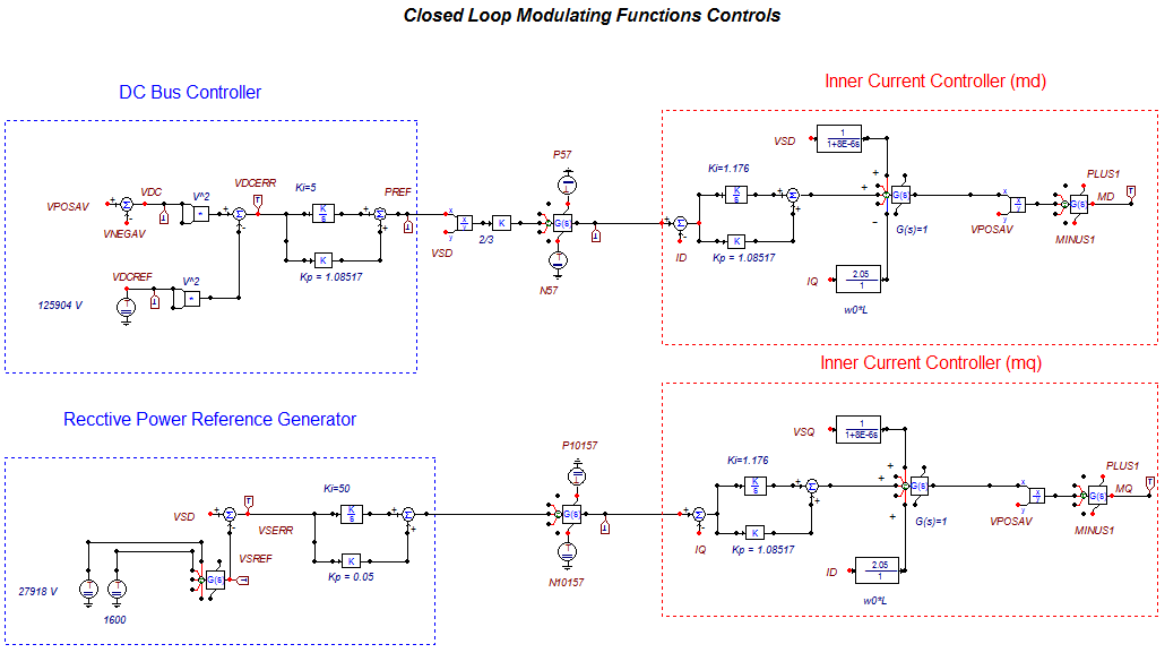

Figure A.2. ATP-EMTP control system model

- **Control System Parameters:**

Proportional gain constant for the inner current controller:

K_p= 1.085 ohm

Integral gain constant for the inner current controller:

K_i= 1.176 (1/F)

The feed forward constant for the inner current controller:

$K_{feed\_forward}$= 2.045 ohm

Proportional gain constant for the DC bus controller:

K_p= 1.085 ohm

Integral gain constant for the DC bus controller:

K_i= 5 (1/F)

A.3. Calculating the Effective Impedance (Mathcad Sheet)

An example of a SLG fault is chosen. The fault is applied at 80% of the line with the presence of the STATCOM. The example shows the digital filter and the distance relay model in the Mathcad sheet. The first step is calculating the effective impedance using phasor domain from the Powerworld model.

- **Digital Filter and Distance Mho Element:**

$$k_0 := 0.59691 - 0.13033i \qquad V_{base} := \frac{345kV}{\sqrt{3}}$$

- **Phasor Domain Calculations from Powerworld:**

$$V_A := V_{base} \cdot \left(0.90831 e^{-j \cdot 0.32 deg}\right)$$

$$I_A := 2636.24 \cdot e^{-j \cdot 74.5379 deg} A$$

$$I_0 := 867.12 \cdot e^{-j \cdot 93.64057 deg} A$$

$$ZAG := \frac{V_A}{I_A + k_0 \cdot 3 \cdot I_0 + 0.000000001A}$$

$$ZAG = (3.14 + 44.258i)\ \Omega$$

The second step is calculating the effective impedance using the ATP-EMTP model. The data from the ATP-EMTP model is imported to the Mathcad file. In the file, digital filtering is applied to the data.

Importing Plot Data from ATP:

- **Voltages, Currents, and I0 measurments at BUS1:**

data :=
...\slg80stat.ADF

Now we can apply digital filtering to the data....

RS := 16 — Set desired final sampling rate per cycle

R := rows(data) − 1 — Count rows of matrix "Data"

i := 0 .. rows(data) − 1 — Create an index, "i" as a row pointer

$t := data^{\langle 0 \rangle}$ $\Delta t := t_1 - t_0$ — Create time vector "t" from imported data and calculate the input data file time-step, Δt.

$LPW := floor\left(\frac{2}{60 \cdot \Delta t \cdot RS}\right)$ — Calculate the number of samples to create an averaging LP filter with at cutoff frequency at 1/2 the sampling frequency, RS.

In this case: LPW = 20

- Create a function for an Averaging Filter to smooth the input data prior to resampling it.

$$LP(C, a) := \left(1 + \frac{1}{RS}\right) \cdot \sum_{k=0}^{LPW-1} \frac{C_{a-LPW+k}}{LPW}$$

ii := LPW .. R — Create an index "ii" for the LP filtered quantities

- Calculate low pass filtered quantities using averaging filter function defined above

$$ia_{ii} := LP\left(data^{\langle 1 \rangle}, ii\right) \qquad va_{ii} := LP\left(data^{\langle 4 \rangle}, ii\right)$$

$$ib_{ii} := LP\left(data^{\langle 2 \rangle}, ii\right) \qquad vb_{ii} := LP\left(data^{\langle 5 \rangle}, ii\right)$$

$$ic_{ii} := LP\left(data^{\langle 3 \rangle}, ii\right) \qquad vc_{ii} := LP\left(data^{\langle 6 \rangle}, ii\right)$$

$$i0_{ii} := LP\left(data^{\langle 7 \rangle}, ii\right)$$

$S := floor\left(t_R \cdot 60 \cdot RS\right)$ Calculate the number of samples available in the data at the desired sampling rate per second -> 60*RS

$s := 0 .. S$ Create an index "s" as a row pointer

- Create vectors representing re-sampled current and voltages in the relay

$$Ia_s := linterp\left(t, ia, \frac{s}{RS \cdot 60}\right) \qquad Va_s := linterp\left(t, va, \frac{s}{RS \cdot 60}\right)$$

$$Ib_s := linterp\left(t, ib, \frac{s}{RS \cdot 60}\right) \qquad Vb_s := linterp\left(t, vb, \frac{s}{RS \cdot 60}\right)$$

$$Ic_s := linterp\left(t, ic, \frac{s}{RS \cdot 60}\right) \qquad Vc_s := linterp\left(t, vc, \frac{s}{RS \cdot 60}\right)$$

$$I\_0_s := linterp\left(t, i0, \frac{s}{RS \cdot 60}\right)$$

- Create a filter index, "if" (which includes RS samples of past history (so it starts at (RS - 1))

$if := (RS - 1) .. S$

- Create a filter index, "v" (which includes RS/4 samples of past history for delaying cosine filter output put a quarter cycle (so it starts at (RS/4 - 1))

$$v := \left(\frac{RS}{4}\right) .. S$$

- Define a function for a full cycle cosine filter, "CF" to current and voltage vectors

$$CF(A,q) := \frac{2}{RS}\cdot\sum_{k=0}^{RS-1}\left[\cos\left(k\cdot\frac{2\cdot\pi}{RS}\right)\cdot A_{[q-(RS-1)]+k}\right]$$

- Apply digital cosine filter to data:

$IA_{if} := CF(Ia,if)$ $\quad$ $VA_{if} := CF(Va,if)$

$IB_{if} := CF(Ib,if)$ $\quad$ $VB_{if} := CF(Vb,if)$

$IC_{if} := CF(Ic,if)$ $\quad$ $VC_{if} := CF(Vc,if)$

$I0_{if} := CF(I\_0,if)$

- Compare raw current to cosine filtered current

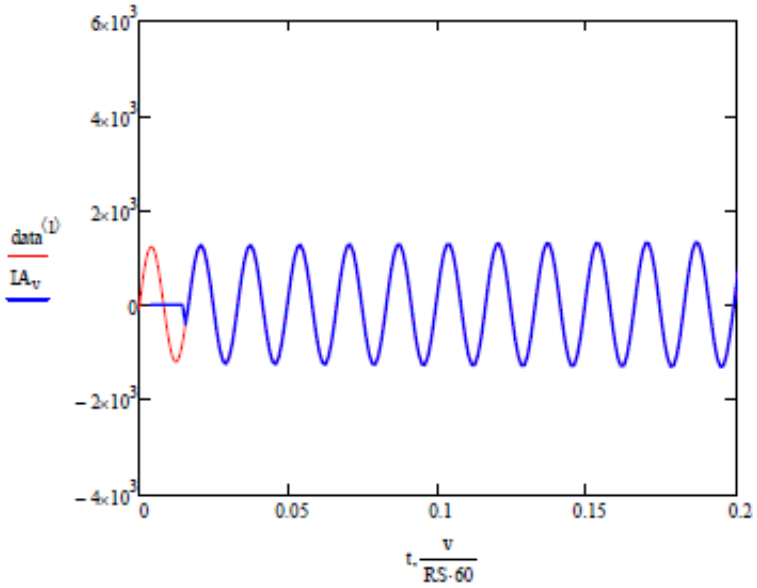

- Note removal of DC offset,
- And lack of filtered data for first cycle

In this step, phasor quantities for both voltage and current measurments are created.

- Create Phasors (replace Sine filter output with Cosine Filter Output delayed by 1/4 cycle.

$$IAcpx_v := \frac{1}{\sqrt{2}}\left(IA_v + j \cdot IA_{v-\frac{RS}{4}}\right) \qquad VAcpx_v := \frac{1}{\sqrt{2}}\left(VA_v + j \cdot VA_{v-\frac{RS}{4}}\right)$$

$$IBcpx_v := \frac{1}{\sqrt{2}}\left(IB_v + j \cdot IB_{v-\frac{RS}{4}}\right) \qquad VBcpx_v := \frac{1}{\sqrt{2}}\left(VB_v + j \cdot VB_{v-\frac{RS}{4}}\right)$$

$$ICcpx_v := \frac{1}{\sqrt{2}}\left(IC_v + j \cdot IC_{v-\frac{RS}{4}}\right) \qquad VCcpx_v := \frac{1}{\sqrt{2}}\left(VC_v + j \cdot VC_{v-\frac{RS}{4}}\right)$$

$$I0cpx_v := \frac{1}{\sqrt{2}}\left(I0_v + j \cdot I0_{v-\frac{RS}{4}}\right)$$

Phase A, B, C and zero sequence currents (in phasor domain) at Bus 1 when a SLG fault is applied at 80% of the line with the presence of the STATCOM.

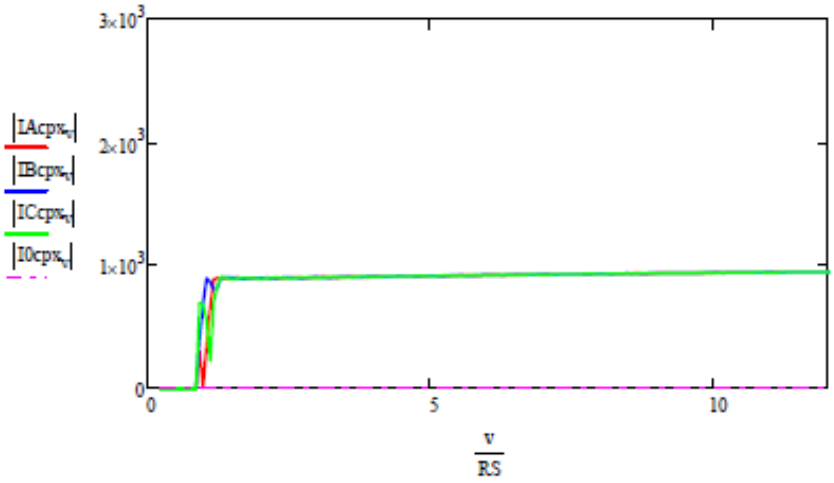

Phase A, B, C voltages (in phasor domain) at Bus 1 when a SLG fault is applied at 80% of the line with the presence of the STATCOM.

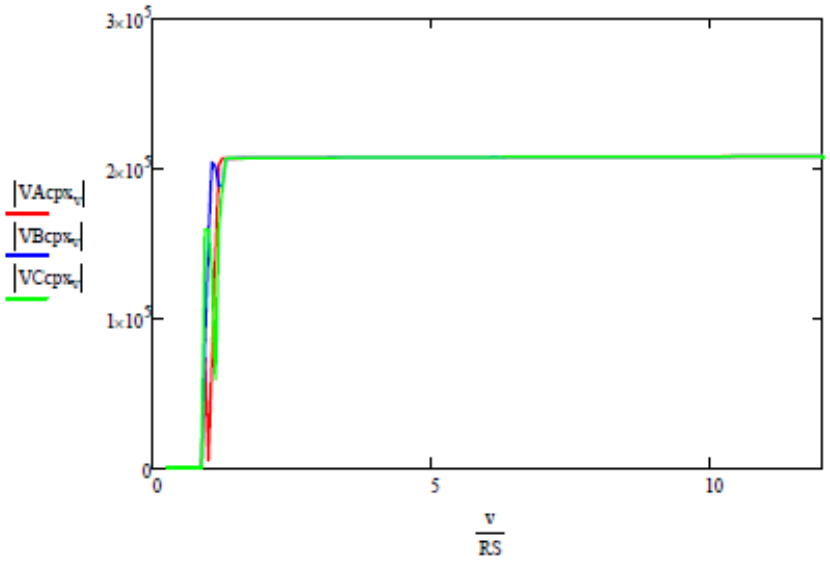

After applying the digital filter, the measurements is applied to the distance relay model.

- **ATP Effective Impedance Calculation:**

$$ZAG\_ATP := \frac{VAcpx}{IAcpx + k_0 \cdot 3 \cdot I0cpx + 0.000000001}$$

- AG Loop only

- **Mho Element Setup:**

$$Z_{line1} := (2.75 + 50.7053i)\ \Omega$$

$$m := 0, 1 .. 360 \qquad reach := \frac{0.85 \cdot |Z_{line1}|}{\Omega} \qquad reach = 43.163 \frac{1}{\Omega} \cdot \Omega$$

$$\theta_m := m \cdot \frac{\pi}{180} \qquad ang := 90deg$$

$$mho_m := \frac{reach}{2} \cdot \left(e^{j \cdot \theta_m} + e^{j \cdot ang}\right) \qquad sz := \begin{pmatrix} 0 \\ \frac{Z_{line1}}{\Omega} \end{pmatrix}$$

The next figures shows both effective impedances that is calculated from the ATP-EMTP model and the Powerworld mode. The ATP-EMTP model is the red dots, and the Powerworld model is the pink cross.

The effective impedance seen by the relay at Bus 1 when a SLG fault is applied at 80% of the line with the presence of the STATCOM.

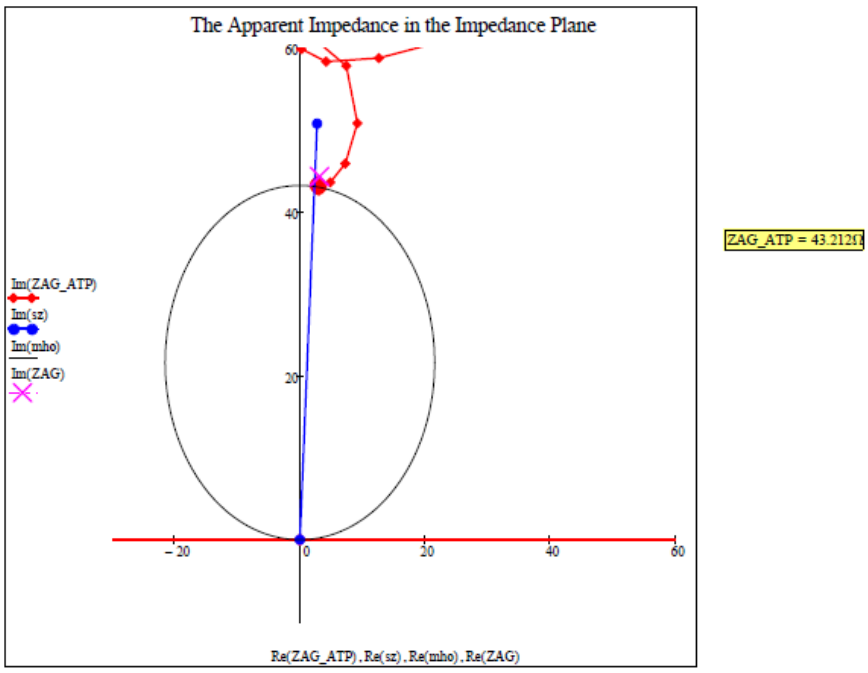

Zoomed in the effective impedance.

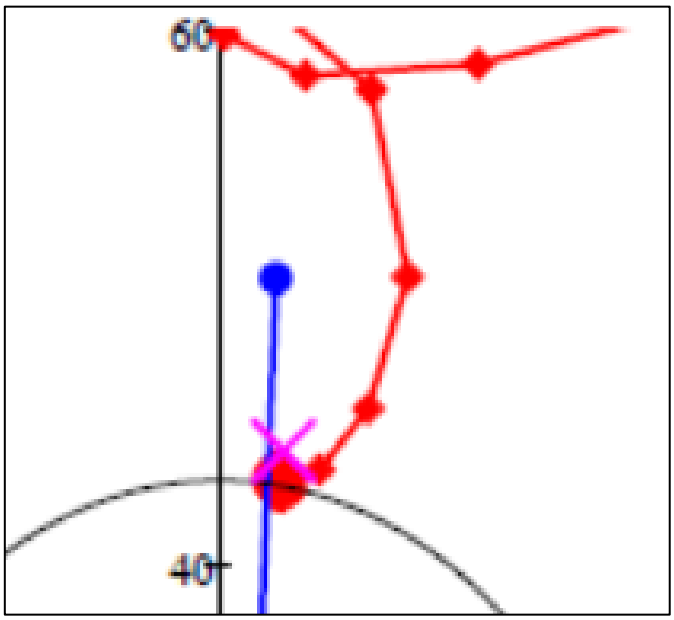

A.4. Impacts of STATCOMs on the Effective Impedance

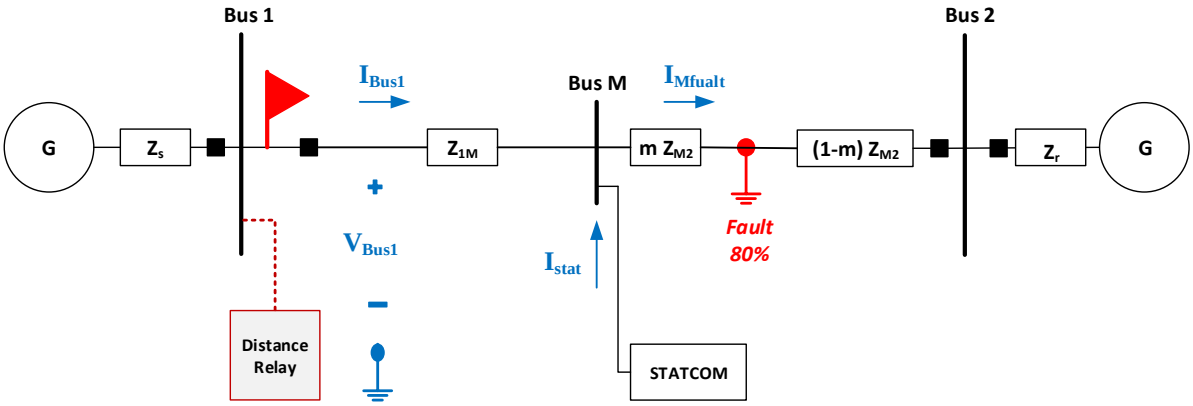

Figure A.3. STATCOMs effect causes impedance errors

When the STATCOM is disconnected and a bolted three phase fault is applied at 80% of the line, $I_{Mfault} = I_{Bus1}$ and $I_{stat} = 0$. The measured voltage at Bus 1 is:

$V_{Bus1} = (I_{Bus1} * Z_{1M}) + (m\ Z_{M2} * I_{Bus1})$

Z_{1M}: the impedance of the line from Bus 1 to Bus M

Z_{M2}: the impedance of the line from Bus M to Bus 2

m: the distance to the fault location in pu of Z_{M2}

The effective impedance seen by the relay is:

$Z_{Effective} = (V_{Bus1} / I_{Bus1}) = Z_{1M} + m\ Z_{M2}$

However, when the STATCOM is connected and a bolted three phase fault is applied at 80% of the line, $I_{Mfault} = I_{Bus1} + I_{stat}$ and the measured voltage at Bus 1 is affected. The voltage at Bus 1 seen by the relay is:

$V_{Bus1} = (I_{Bus1} * Z_{1M}) + m\, Z_{M2}\, (I_{Mfault} / I_{Bus1}))$

Or,

$V_{Bus1} = (I_{Bus1} * Z_{1M}) + m\, Z_{M2}\, (1 + (I_{stat} / I_{Bus1}))$

The effective impedance seen by the relay is:

$Z_{Effective} = (V_{Bus1} / I_{Bus1}) = Z_{1M} + m\, Z_{M2}\, (1 + (I_{stat} / I_{Bus1}))$

The distance relay will underreach when $(1 + (I_{stat} / I_{Bus1})) > 1$ because the effective impedance calculated by the relay is increased. This case is true when the STATCOM is suppling capacitive current.

$$I_{stat} = \left|I_{stat}\right| \cdot e^{j \cdot \theta_{stat}}$$

On the other hand, the distance relay will overreach when $(1 + (I_{stat} / I_{Bus1})) < 1$ because the effective impedance calculated by the relay is decreased. In this case, the STATCOM is absorbing reactive power.

$$I_{stat} = \left|I_{stat}\right| \cdot e^{-j \cdot \theta_{stat}}$$

Appendix B: Forming Microgrids in a Pacific Northwest City

B.1. Power System Parameters

- **Power Transformers Parameters:**

Step up transformer (13.8 kV to 115 kV) connected at Bus S1:

Z_{xfmr}= (0.022 + j 0.633) pu V_{baser}= 13.8 kV S_{base}= 100 MVA

Step up transformer (4.16 kV to 13.8 kV) connected at Bus G1:

Z_{xfmr}= (0.033 + j 0.564) pu V_{baser}= 4.16 kV S_{base}= 100 MVA

Step down transformer (115 kV to 13.2 kV) connected at Bus S1:

Z_{xfmr}= (0.023 + j 0.659) pu V_{baser}= 115 kV S_{base}= 100 MVA

Step down transformer (13.2 kV to 0.48 kV) connected at Bus H1:

Z_{xfmr}= (0.265 + j 0.075) pu V_{baser}= 13.2 kV S_{base}= 100 MVA

- **Transmission Lines Parameters:**

Transmission line from Bus S1 to Bus S2:

Z_{line1}= (0.00016 + j 0.00126) pu V_{baser}= 115 kV S_{base}= 100 MVA

Z_{line0}= (0.0004 + j 0.00315) pu

B_{line}= (j 0.00773) pu

Transmission line from Bus S1 to Bus R1:

Z_{line1}= (0.00017 + j 0.00142) pu V_{baser}= 115 kV S_{base}= 100 MVA

Z_{line0}= (0.000425 + j 0.00355) pu

B_{line}= (j 0.00612) pu

Transmission line from Bus S1 to Bus R2:

Z_{line1}= (0.00189 + j 0.00799) pu V_{baser}= 115 kV S_{base}= 100 MVA

Z_{line0}= (0.004725 + j 0.019975) pu

B_{line}= (j 0.00931) pu

B.2. ATP-EMTP Power System Model

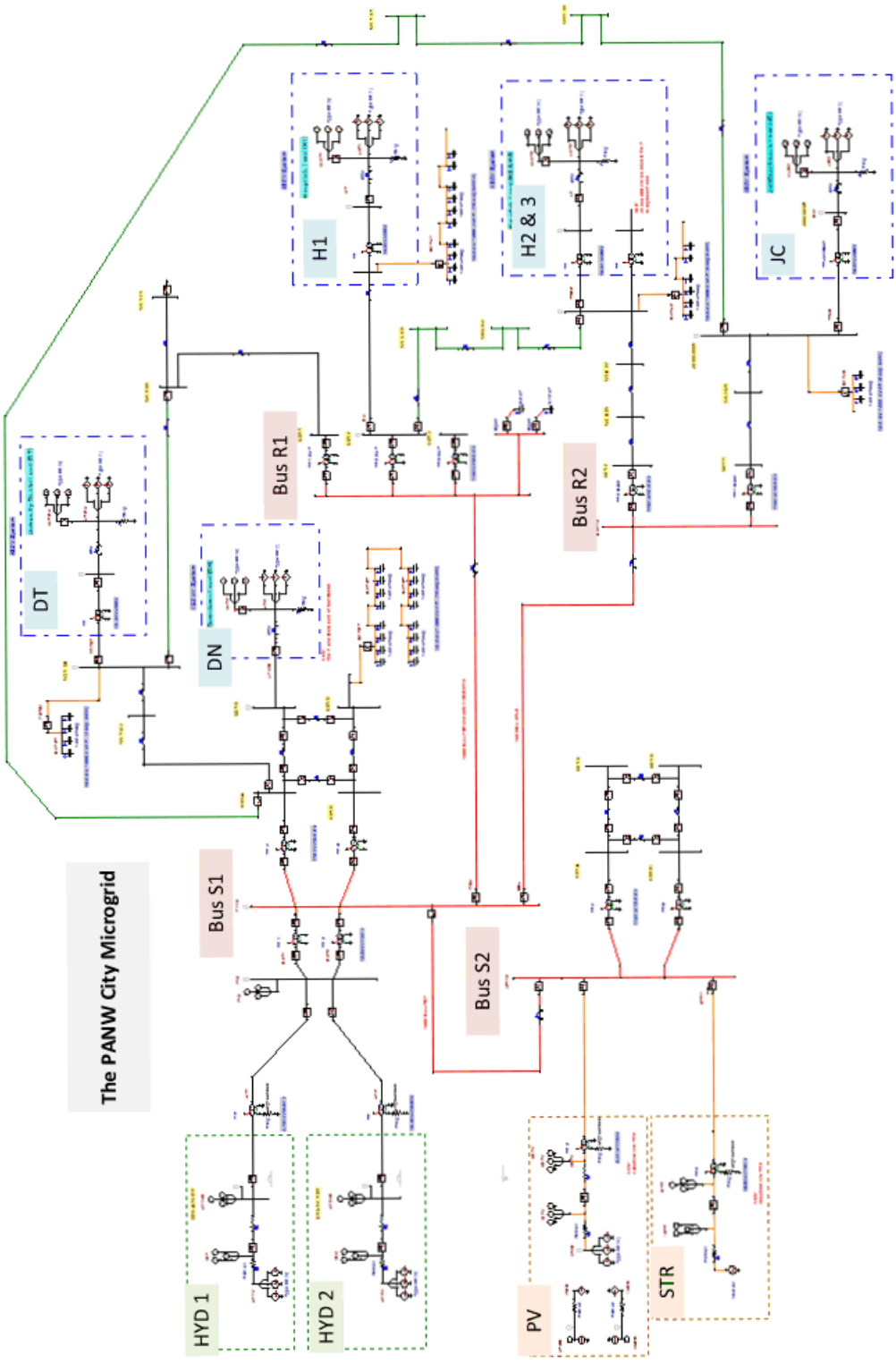

Figure B.1. ATP-EMTP power system model

B.3. ATP-EMTP Hydroelectric Power Circuit Model

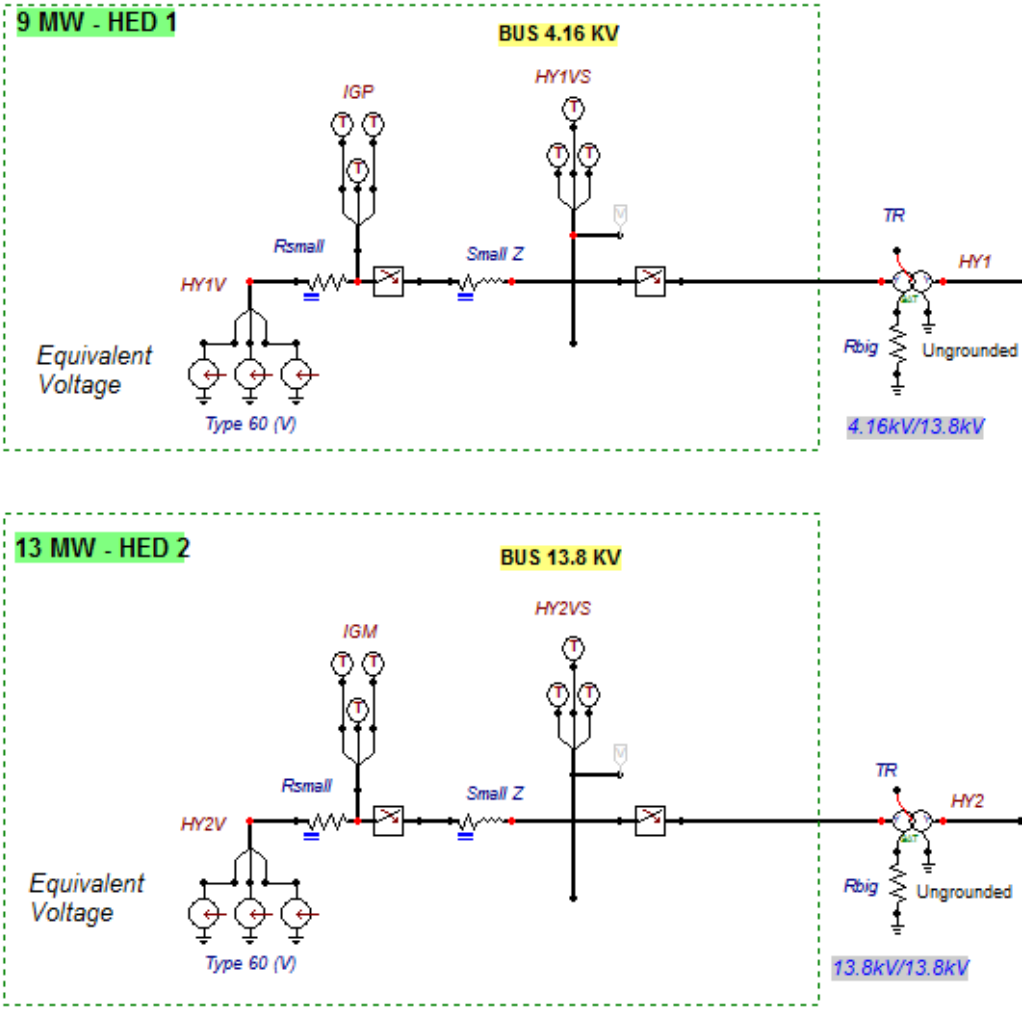

Figure B.2. ATP-EMTP HYD 1 and HYD 2 power circuit models

B.4. ATP-EMTP Hydroelectric Control System Model

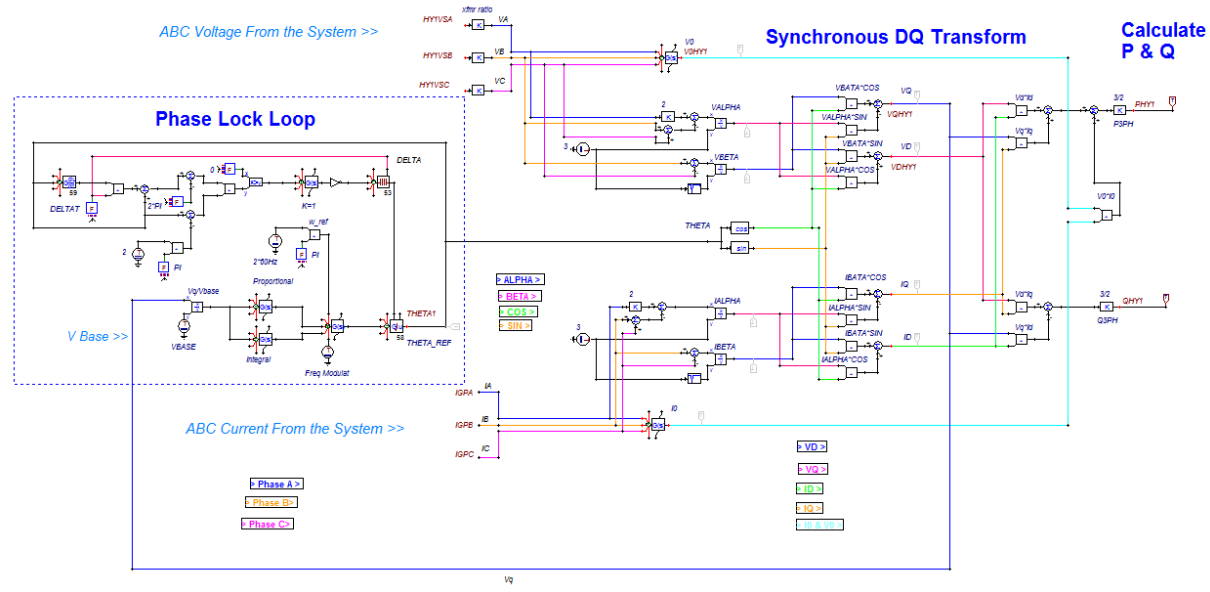

Figure B.3. PLL, DQ transformation, and P and Q calculation

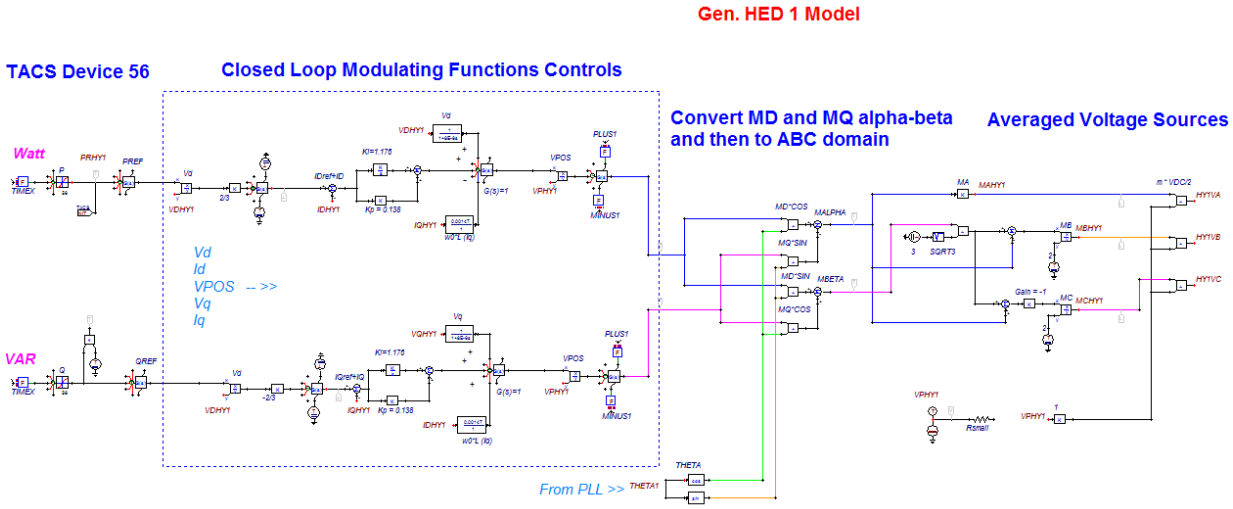

Figure B.4. ATP-EMTP HYD 1 control system models

B.5. ATP-EMTP PV System Converter Averaged Circuit Model

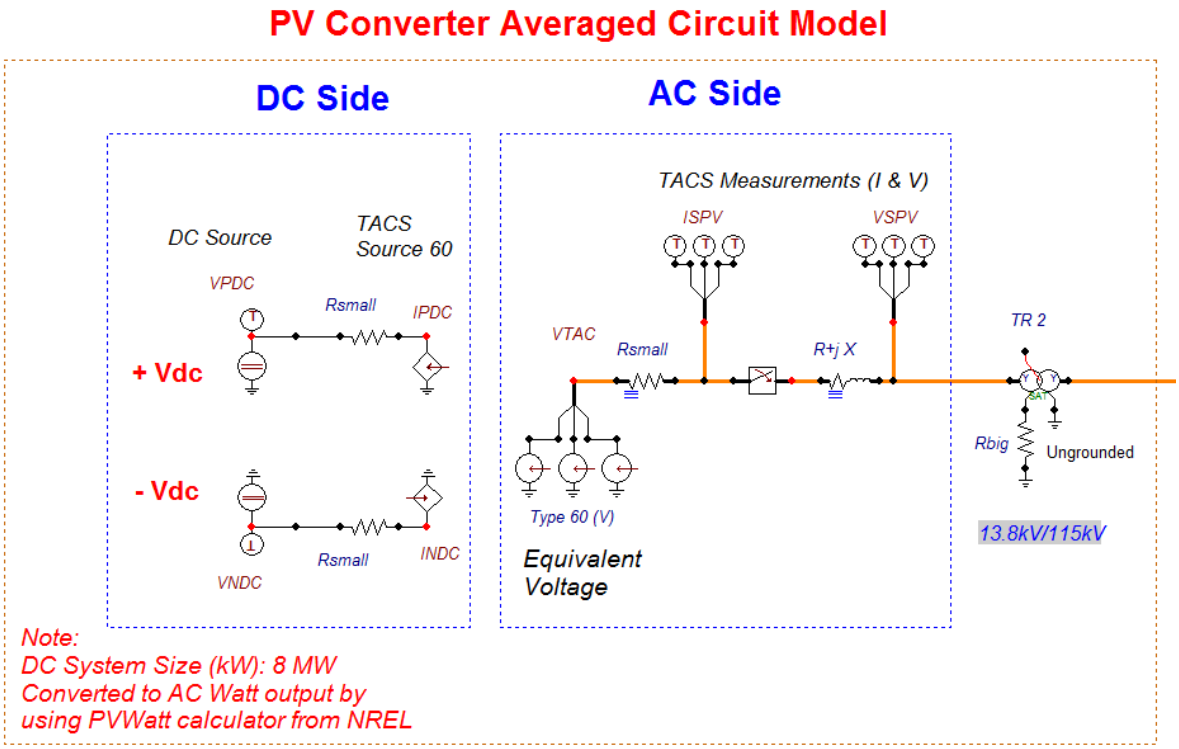

Figure B.5. ATP-EMTP PV converter averaged circuit model

B.6. ATP-EMTP PV Control System Model

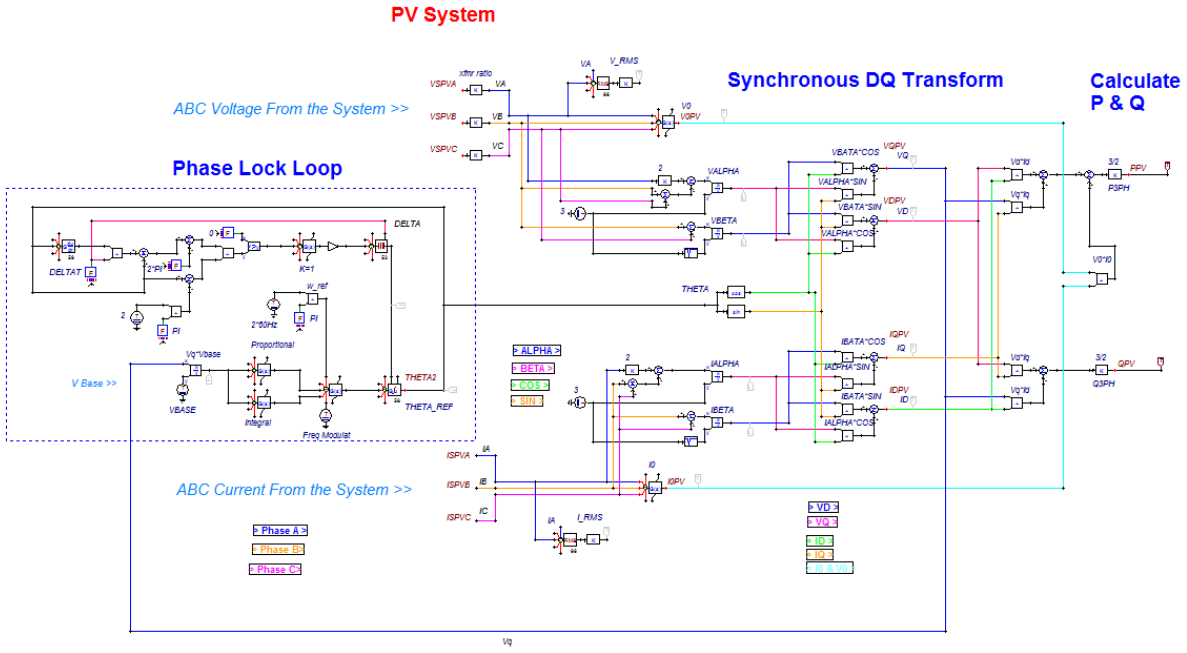

Figure B.6. PLL, DQ transformation, and P and Q calculation

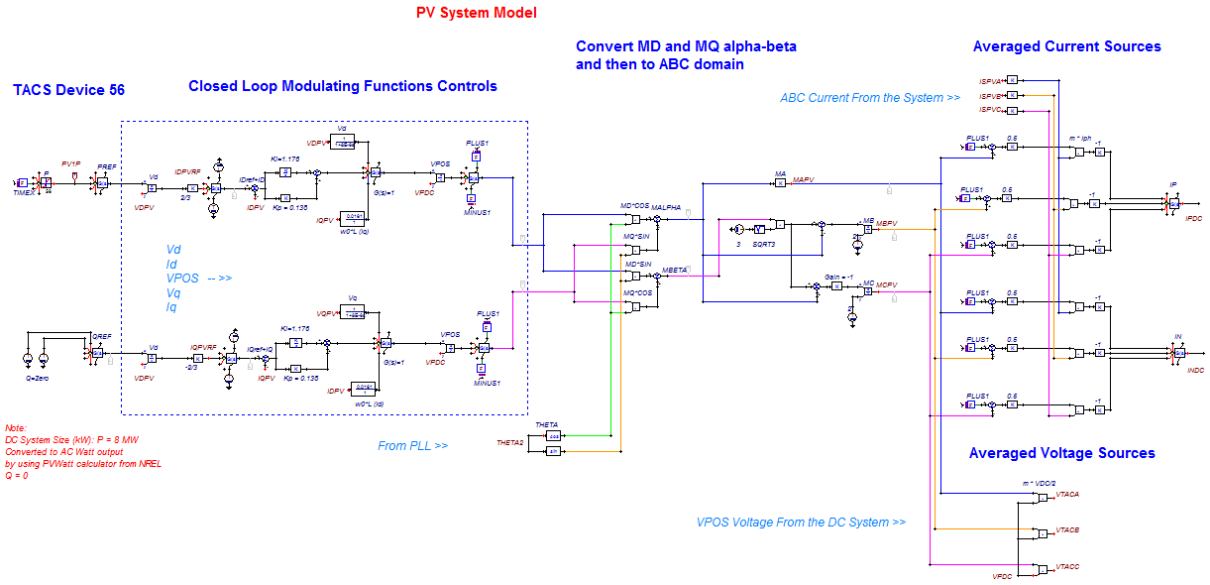

Figure B.7. ATP-EMTP PV control system models

B.7. ATP-EMTP Variable Load Model

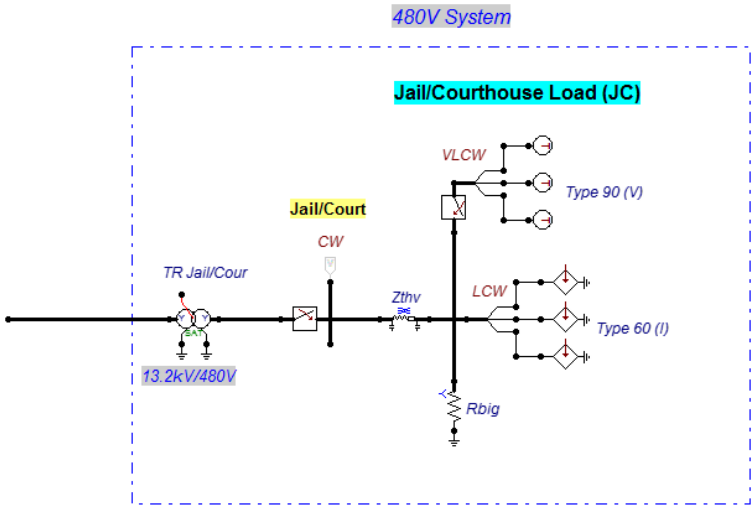

Figure B.8. ATP-EMTP load jail and courthouse (JC) power circuit model

B.8. ATP-EMTP Variable Load Control System Model

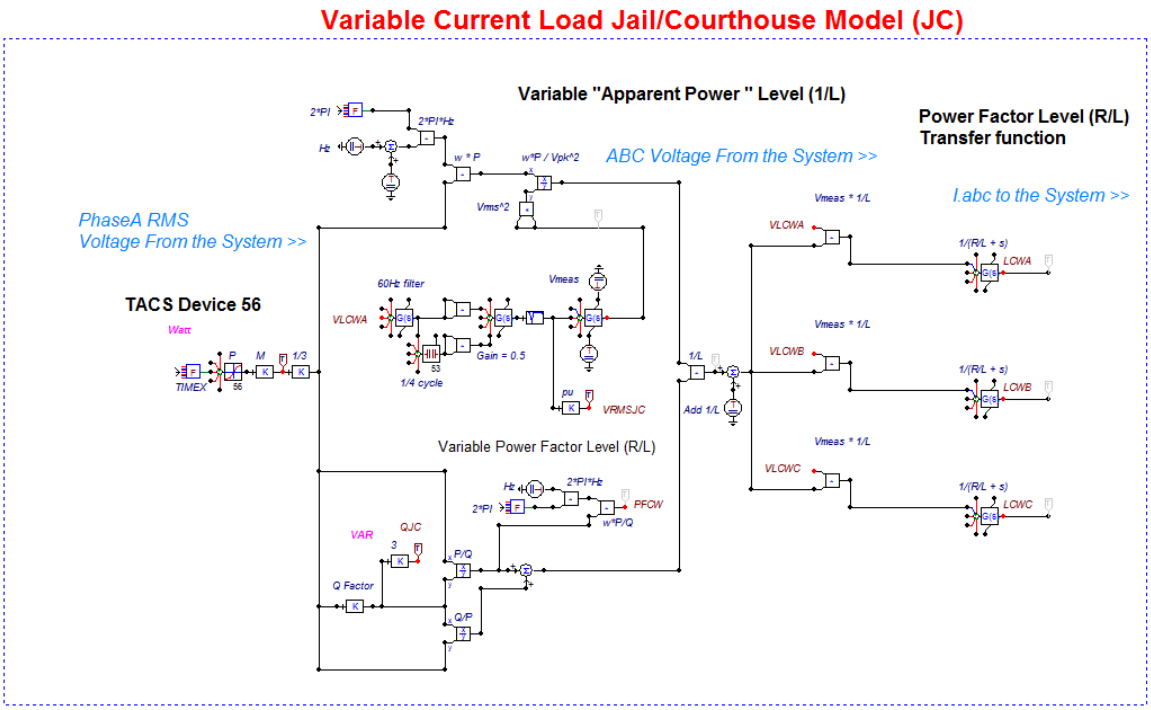

Figure B.9. ATP-EMTP load jail and courthouse (JC) control system model